Free convection flows in vertical channels with two rectangular obstructions on opposite walls
by Prasad Viswatmula

A thesis submitted in partial fulfillment of the requirements for the degree of Master of Science in Mechanical Engineering
Montana State University
© Copyright by Prasad Viswatmula (1993)

Abstract:
One of the engineering applications of natural convection flows is the cooling of electronic cabinets containing circuit cards which are aligned to form vertical channels. Of the many diverse flow configurations possible in electronic cooling applications, the vertical channel is a commonly used configuration. In many practical applications, obstructions due to electronic circuit cards are located inside the channel and these obstructions convert the governing parabolic equations into elliptic equations. The designer of electronic equipment benefits from the numerical solution of the two dimensional, steady-state laminar natural convection flow equations of a Newtonian fluid.

The present study involved the numerical analysis of coupled, non-linear, elliptic partial differential equations using NACHOS II, a general purpose finite element computer code. NACHOS II is designed to solve both transient and steady-state two-dimensional flows that are governed by Navier-Stokes equations including the effect of heat transfer.

Heat transfer and fluid flow inside the channel were studied for different values of the governing parameters such as Rayleigh number, channel aspect ratio, and obstruction location. The results of this study included average Nusselt numbers, plots of isotherms, streamlines at different Rayleigh numbers, and profile plots for temperature and velocity at the exit and inlet planes.

Average Nusselt numbers for the obstructed channels were less than those of the smooth channel. Regions of recirculating flow were formed above and below the obstructions. These regions of recirculating zones reduced the heat transfer even though the surface area was increased due to the presence of the obstructions. The final results of this study lead to an efficient design of the cooling system of electronic cabinets.

FREE CONVECTION FLOWS IN VERTICAL CHANNELS WITH TWO RECTANGULAR OBSTRUCTIONS ON OPPOSITE WALLS

by

Prasad Viswatmula

A thesis submitted in partial fulfillment
of the requirements for the degree

of

Master of Science

in

Mechanical Engineering

MONTANA STATE UNIVERSITY
Bozeman, Montana

March 1993

N378
V8294

APPROVAL

of a thesis submitted by

Prasad Viswatmula

This thesis has been read by each member of the thesis committee and has been found to be satisfactory regarding content, English usage, format, citations, bibliographic style, and consistency, and is ready for submission to the College of Graduate Studies.

14 April 1993
Date

Richard Amin
Chairperson, Graduate Committee

Approved for the Major Department

15 April 1993
Date

Byron J. Bennett
Head, Major Department

Approved for the College of Graduate Studies

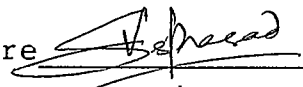
4/28/93
Date

R. L. Brown
Graduate Dean

STATEMENT OF PERMISSION TO USE

In presenting this thesis in partial fulfillment of the requirements for a master's degree at Montana State University, I agree that the Library shall make it available to borrowers under rules of the Library.

If I have indicated my intention to copyright this thesis by including a copyright notice page, copying is allowable only for scholarly purposes, consistent with "fair use" as prescribed in the U.S. Copyright Law. Requests for permission for extended quotation from or reproduction of this thesis in whole or in parts may be granted only by the copyright holder.

Signature 

Date 04/15/93

ACKNOWLEDGEMENTS

I would like to thank Dr. Ruhul Amin for his continuous guidance in my thesis work. My special thanks go to Dr. Alan George and Dr. Thomas Reihman for their support as the committee members.

I acknowledge my appreciation to the Department of Mechanical Engineering for providing me with financial assistance. I would also like to thank the graduate students and staff of the Department of Mechanical Engineering whose support made this project successful.

Finally, I deeply appreciate my parents, Mallikarjuna Rao and Annapurna for their encouragement during this graduate program.

TABLE OF CONTENTS

Page

LIST OF TABLES.....vii

LIST OF FIGURES.....viii

NOMENCLATURE.....xii

ABSTRACT.....xiv

1. INTRODUCTION.....1

Motivation for the Present Research.....1
Problem Description.....5
Literature Survey.....7
General References on Convection Heat Transfer...7
General References on Finite Element Method.....7
General References on Electronic Packaging.....8
Channels with Isothermal or Isoflux Walls.....8
Channels with Conducting or Heat Source Embedded Walls.....11
Channels with Major Emphasis on Optimization of Interplate Spacing.....12
Channels with Symmetric or Asymmetric Heating...13
Channels where Both the Walls are subjected to Different Boundary Conditions.....15
Channels with Mixed Convection.....16
Variable Property Effects in Channels.....16
Mixed Convection in Channels with Obstructions..17
Laminar Convection in Channels with Obstructions.....19

2. PROBLEM FORMULATION.....22

Introduction.....22
Modelling Assumptions.....22
Normalization of the Governing Equations.....25

3. NUMERICAL INVESTIGATION.....29

Introduction.....29
The Computational Matrix.....31
The Computational Grid.....35

TABLE OF CONTENTS-Continued

Page

4. RESULTS AND DISCUSSION....42

Introduction....42
Discussion of the Results for an Unobstructed Channel....44
Discussion of the Results for the Obstructed Channels....60
Results for Geometry I....60
Results for Geometry II....71
Results for Geometry III....86
Results for Geometry IV....94

5. CONCLUSIONS AND RECOMMENDATIONS....108

Conclusions....108
Recommendations....111

REFERENCES....112

APPENDICES....117

Appendix A - The Finite Element Algorithm for NACHOS II....118

Appendix B - Mathematical Definition of Nusselt Number....127

Appendix C - Chanel.for: Code to Calculate the Average Nusselt Number of the Smooth Channel....131

Appendix D - Obsnu.for: Code to Calculate the Average Nusselt Number of the Smooth Channel....139

LIST OF TABLES

Table

Page

1. Computational matrix for smooth channel.....32

2. Computational matrix for the obstructed channel..33

3. Number of elements used for the smooth channel.....40

4. Number of elements used for the obstructed channels.....40

LIST OF FIGURES

Figure — Page

1. A typical electronic system with vertical channel configuration, Aung et al. (1972).....2
2. Geometry of the obstructed channel.....6
3. Mesh generation for the smooth channel (Ar = 0.2).....37
4. Mesh generation for the obstructed channel (Ar = 0.2).....38
5. Mesh generation for the obstructed channel (Ar = 0.3).....39
6. Comparison of computed average Nusselt numbers for a square enclosure with the benchmark solution.....43
7. Computed streamlines and isotherms for smooth channel with $Ra = 10^2$, Ar = 0.2.....45
8. Computed streamlines and isotherms for smooth channel with $Ra = 5x10^3$, Ar = 0.2.....46
9. Computed streamlines and isotherms for smooth channel with $Ra = 10^4$, Ar = 0.2.....47
10. Computed streamlines and isotherms for smooth channel with $Ra = 5x10^4$, Ar = 0.2.....48
11. Computed streamlines and isotherms for smooth channel with $Ra = 5x10^3$, Ar = 0.3.....49
12. Computed streamlines and isotherms for smooth channel with $Ra = 5x10^4$, Ar = 0.3.....50
13. Transverse distribution of temperature at the exit for the smooth channel with $Ra = 10^3$, Ar = 0.2.....52

LIST OF FIGURES-Continued

Figure Page

14. Transverse distribution of temperature at the exit for the smooth channel with $Ra = 5x10^4$, Ar = 0.2.....53

15. Transverse distribution of inlet velocity for smooth channel with $Ra = 10^3$, Ar = 0.2.....54

16. Transverse distribution of exit velocity for smooth channel with $Ra = 10^3$, Ar = 0.2.....55

17. Transverse distribution of inlet velocity for smooth channel with $Ra = 5x10^4$, Ar = 0.2.....56

18. Transverse distribution of exit velocity for smooth channel with $Ra = 5x10^4$, Ar = 0.2.....57

19. Variation of local Nusselt number with elevation in the smooth channel.....59

20. Computed streamlines and isotherms for geometry I with $Ra = 10^2$, Ar = 0.2.....61

21. Computed streamlines and isotherms for geometry I with $Ra = 5x10^3$, Ar = 0.2.....62

22. Computed streamlines and isotherms for geometry I with $Ra = 10^4$, Ar = 0.2.....63

23. Computed streamlines and isotherms for geometry I with $Ra = 5x10^4$, Ar = 0.2.....64

24. Transverse distribution of inlet velocity for geometry I with $Ra = 5x10^4$, Ar = 0.2.....67

25. Transverse distribution of exit velocity for geometry I with $Ra = 5x10^4$, Ar = 0.2.....68

26. Transverse distribution of temperature at the exit for geometry I with $Ra = 5x10^4$, Ar = 0.2.....69

27. Variation of Nu (right wall) with the elevation for geometry I with $Ra = 10^4$, Ar = 0.2.....70

28. Variation of Nu (left wall) with the elevation for geometry I with $Ra = 10^4$, Ar = 0.2.....72

LIST OF FIGURES-Continued

Figure Page

29. Computed streamlines and isotherms for geometry II with Ra = 10^2, Ar = 0.2.....73

30. Computed streamlines and isotherms for geometry II with Ra = $5x10^3$, Ar = 0.2.....74

31. Computed streamlines and isotherms for geometry II with Ra = 10^4, Ar = 0.2.....75

32. Computed streamlines and isotherms for geometry II with Ra = $5x10^4$, Ar = 0.2.....76

33. Transverse distribution of inlet velocity for geometry II with Ra = $2x10^4$, Ar = 0.2.....77

34. Transverse distribution of exit velocity for geometry II with Ra = 2×10^4, Ar = 0.2.....78

35. Transverse distribution of temperature at the exit for geometry II with Ra = $2x10^4$, Ar = 0.2....79

36. Variation of Nu (right wall) with the elevation for geometry II with Ra = 10^4, Ar = 0.2.....81

37. Comparison of the computed average Nusselt numbers for the obstructed and unobstructed channel flows with Ar= 0.2.....83

38. Variation of ratio of Nusselt numbers with Rayleigh number (Ar = 0.2).....84

39. Computed streamlines and isotherms for geometry III with Ra = 10^2, Ar = 0.3.....87

40. Computed streamlines and isotherms for geometry III with Ra = $5x10^3$, Ar = 0.3.....88

41. Computed streamlines and isotherms for geometry III with Ra = 10^4, Ar = 0.3.....89

42. Computed streamlines and isotherms for geometry III with Ra = $5x10^4$, Ar = 0.3.....90

LIST OF FIGURES-Continued

Figure Page

43. Transverse distribution of inlet velocity for geometry III with Ra = $5x10^4$, Ar = 0.3.....91

44. Transverse distribution of exit velocity for geometry III with Ra = $5x10^4$, Ar = 0.3.....92

45. Transverse distribution of temperature at the exit for geometry III with Ra=$5x10^4$.....93

46. Computed streamlines and isotherms for geometry IV with Ra = 10^2, Ar = 0.3.....95

47. Computed streamlines and isotherms for geometry IV with Ra = $5x10^3$, Ar = 0.3.....96

48. Computed streamlines and isotherms for geometry IV with Ra = 10^4, Ar = 0.3.....97

49. Computed streamlines and isotherms for geometry IV with Ra = $5x10^4$, Ar = 0.3.....98

50. Transverse distribution of inlet velocity for geometry IV with Ra = $5x10^4$, Ar = 0.3.....99

51. Transverse distribution of exit velocity for geometry IV with Ra = $5x10^4$, Ar = 0.3.....100

52. Transverse distribution of temperature at the exit for geometry IV with Ra = $5x10^4$, Ar = 0.3..101

53. Comparison of the computed average Nusselt numbers for the obstructed and unobstructed channel flows with Ar = 0.3.....103

54. Variation of ratio of Nusselt numbers with Rayleigh number (Ar = 0.3).....104

55. Effect of aspect ratio on the rate of heat transfer.....106

56. Chanel.for.....129

57. Obsnu.for.....137

NOMENCLATURE

Ar	aspect ratio of the channel (=b/L)
b	channel width
C_p	specific heat of fluid
g	acceleration due to gravity
h	local heat transfer coefficient
k	fluid thermal conductivity
L	channel height
$\bar{L}_1$	height of the obstruction on the left wall from the channel entrance
$\bar{L}_2$	height of the obstruction on the right wall from the channel entrance
L_1	dimensionless height of the obstruction on the left wall from channel entrance, $\bar{L}_1/L$
L_2	dimensionless height of the obstruction on the right wall from channel entrance, $\bar{L}_2/L$
p	ambient pressure
p_∞	static pressure
$\bar{P}$	motion pressure, $p-p_\infty$
P	dimensionless pressure, $[p-p_\infty]/[g\beta\rho_\infty \Delta TL]$
Pr	Prandtl number
Ra	Rayleigh number, $g\beta\Delta Tb^3/\alpha\nu$
Ra	modified Rayleigh number, RaAr
$\bar{T}$	fluid temperature
T_w	wall temperature

NOMENCLATURE-Continued

T_∞	ambient temperature
T_f	average film temperature, $[T_w+T_\infty]/2$
ΔT	(T_w-T_∞)
$\bar{u}$	x-component of velocity, see Fig. 2
$\bar{v}$	y-component of velocity, see Fig. 2
u	dimensionless x-component of velocity, $\bar{u}b/\alpha$
v	dimensionless y-component of velocity, $\bar{v}b^2/\alpha L$
$\bar{x}$	cartesian x-coordinate
$\bar{y}$	cartesian y-coordinate
x	dimensionless x-coordinate, $\bar{x}/L$
y	dimensionless y-coordinate, $\bar{y}/L$

Greek symbols

α	thermal diffusivity
ß	thermal expansion coefficient of fluid
θ	dimensionless temperature for UWT, $[\bar{T}-T_\infty]/[T_w-T_\infty]$
μ	dynamic viscosity of fluid
ν	kinematic viscosity of fluid
ρ	density of fluid

Subscripts

w	wall value
∞	refers to the conditions at infinity

ABSTRACT

One of the engineering applications of natural convection flows is the cooling of electronic cabinets containing circuit cards which are aligned to form vertical channels. Of the many diverse flow configurations possible in electronic cooling applications, the vertical channel is a commonly used configuration. In many practical applications, obstructions due to electronic circuit cards are located inside the channel and these obstructions convert the governing parabolic equations into elliptic equations. The designer of electronic equipment benefits from the numerical solution of the two dimensional, steady-state laminar natural convection flow equations of a Newtonian fluid.

The present study involved the numerical analysis of coupled, non-linear, elliptic partial differential equations using NACHOS II, a general purpose finite element computer code. NACHOS II is designed to solve both transient and steady-state two-dimensional flows that are governed by Navier-Stokes equations including the effect of heat transfer.

Heat transfer and fluid flow inside the channel were studied for different values of the governing parameters such as Rayleigh number, channel aspect ratio, and obstruction location. The results of this study included average Nusselt numbers, plots of isotherms, streamlines at different Rayleigh numbers, and profile plots for temperature and velocity at the exit and inlet planes.

Average Nusselt numbers for the obstructed channels were less than those of the smooth channel. Regions of recirculating flow were formed above and below the obstructions. These regions of recirculating zones reduced the heat transfer even though the surface area was increased due to the presence of the obstructions. The final results of this study lead to an efficient design of the cooling system of electronic cabinets.

CHAPTER 1

INTRODUCTION

Motivation for the Present Research

Laminar free convection has many engineering applications. Some of these applications are the cooling of electronic equipment, solar collection systems, building energy systems, and fin-tube baseboard heaters. Among these applications, cooling of electronic equipment draws much attention because of the microminiaturization (which results in higher functional and power densities) and the use of semiconductor devices which require fairly close temperature control. Natural convection has a variety of advantages like inherently high reliability, low operating noise level, low cost, ease of maintenance and simplicity. Therefore, it is widely used in the cooling of communications and microelectronic equipment.

The vertical channel flow configuration is of primary interest in most electronic equipment applications. A typical electronic system with vertical channel configuration is shown in Figure 1 (taken from Aung et al. 1972a). The component cards are assembled in vertical or inclined arrays, with small

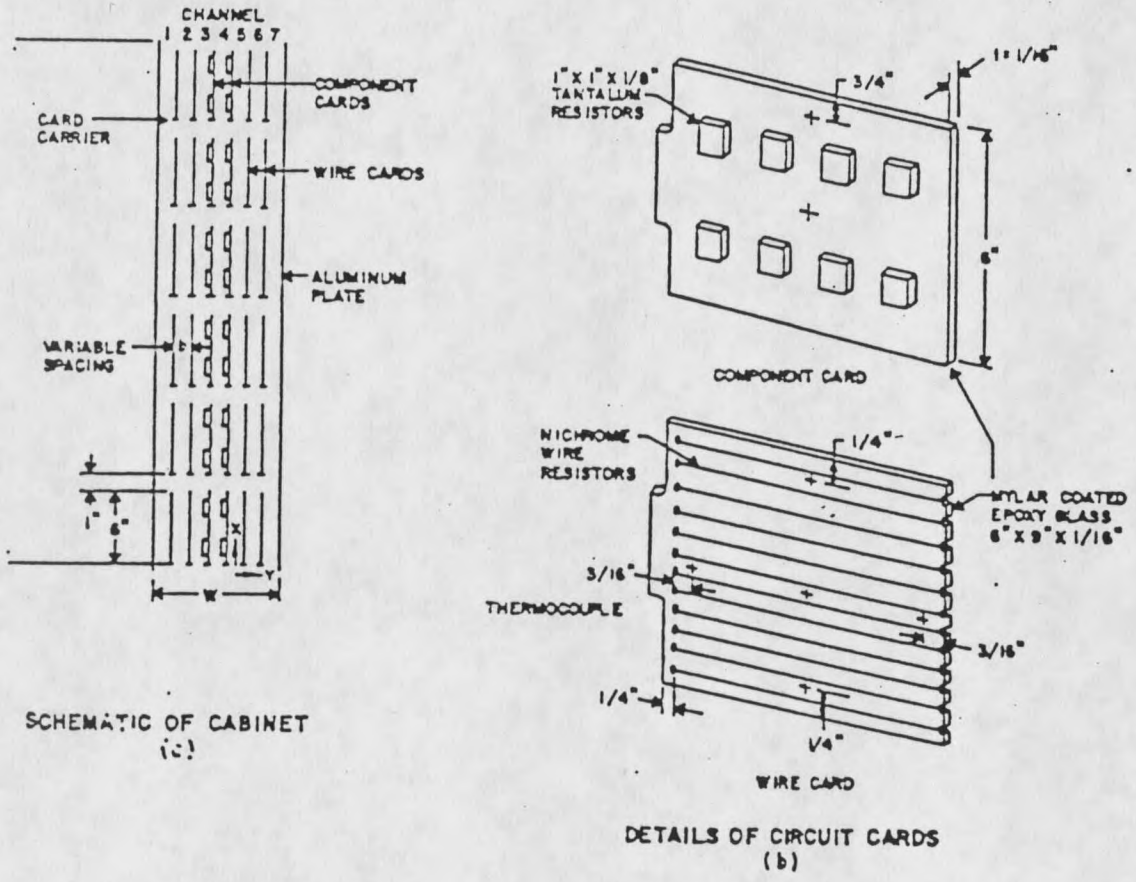


Figure 1. A typical electronic system with vertical channel configuration. Aung et al., (1972)

gaps or channels between each card. The inlet and exit of these channels are open to the ambient conditions.

Repeating cross-sectional protuberances or flow restrictions on the surface of a vertical channel is a common occurrence. Examples are the convective heat transfer applications such as those of surface cooling and heating in electronic packaging and heat exchangers. The flow found in blocked passages of vertical channels or ducts of small dimensions is in a developing regime. The effect of obstructions on heat transfer in such channels draws special attention. The flow governing equations are transformed from parabolic to elliptic due to the presence of these obstructions which are encountered in many practical applications. Complex free convection flows of this type have not been explored thoroughly in previous studies. Hence, the present study is concerned with the numerical investigation of the steady laminar natural convection flow of air (Pr=0.72) in a vertical channel with multiple obstructions of rectangular shape.

In the present study, a general purpose finite element code called NACHOS II (1978a, 1978b) was used to solve the coupled, non-linear, elliptic equations. Uniform wall temperature (UWT) type of boundary condition was employed for the walls of the vertical channel. The NACHOS code was used to solve the two-dimensional, incompressible fluid dynamics problems along with the effects of heat transfer.

The important features and capabilities of the code are presented here and the detailed description can be found in the Appendix[A]. This code was developed by Gartling of Sandia National Laboratories. This code is a general purpose program developed for the solution of two-dimensional, viscous, incompressible fluid dynamics problems. The Galerkin method of weighted residuals (GMWR) is used in the code to discretize the partial differential equations.

A wide range of problems can be solved using NACHOS II. For example, steady or transient analyses of isothermal, free convection, mixed convection, and conjugate heat transfer problems can be simulated using this code. For steady free convection problems, the false transient method can be used at high Rayleigh numbers.

Using NACHOS II, the problem domain can be discretized into isoparametric/subparametric triangular or quadrilateral elements. Of the four degrees of freedom (U,V,P, T), the velocity components and temperature are approximated using the biquadratic basis functions and the pressure is estimated using either a continuous, bilinear approximation or a discontinuous linear approximation. Iterative solution procedures are employed in code e.g., steady state problems are analyzed using the Picard or Newton's method and the transient analyses are done using the first-order Euler or second-order trapezoid rule.

Problem Description

Geometry of the problem analyzed in the present study is shown in Figure 2. Thermal boundary conditions considered are (i) the channel walls, including the obstructions, are maintained at a uniform wall temperature (UWT), T_w, (ii) the fluid (air, Pr=0.72) enters the channel at the ambient temperature, T_∞. (iii) thermal gradient in the axial direction, or heat transfer at the exit of the channel is zero. The hydrodynamic boundary conditions considered are (i) Prandtl boundary condition on the two channel walls and the obstructions, (ii) lateral velocity and normal stress are equal to zero at the entrance as well as the exit of the channel. As mentioned before, the effect of obstructions on heat transfer is of primary interest in the present study. This effect can be studied through a comparison of computed average Nusselt numbers of the obstructed channel to those of the smooth channel. The modelling assumptions and the governing equations for the geometry of Figure 2 are given in the following chapter. Numerical analysis for the present study was performed for various values of the parameters Ra, Ar, and for various locations of the obstructions. It will be shown later from the nondimensional governing equations that the average Nusselt number Nu due to free convection flow

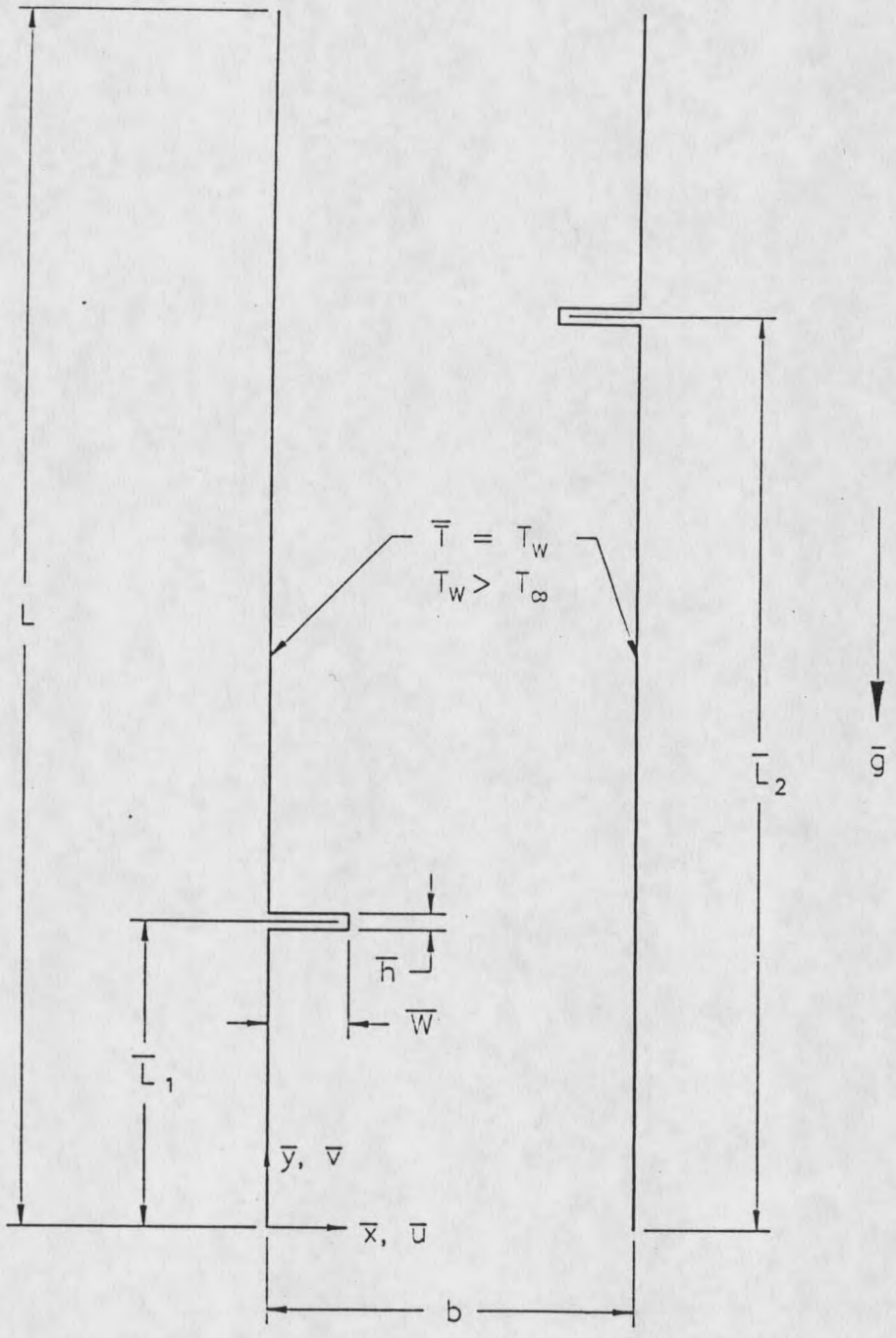


Figure 2. Geometry of the obstructed channel

in a vertical channel with obstruction is a function of Rayleigh number (Ra), Prandtl number (Pr), aspect ratio (Ar), and the location and size of the obstruction. The average Nusselt numbers at different values of these parameters were compared with the corresponding Nusselt numbers of the smooth (or unobstructed) vertical channel.

Literature Survey

General References on Convection Heat Transfer

The textbooks by Kays and Crawford (1980), Bejan (1984), Kakac and Yener (1984), and Eckert and Drake (1959) provide useful information in the area of natural convection heat transfer. The textbook by Patankar (1980) is a good reference for the numerical methods in heat transfer and fluid flow.

General References on Finite Element Method

The textbooks by Chung (1978) and Burnette (1988) are excellent sources of information on the subject of finite element analysis. For the numerical analysis, the present study uses the finite element program NACHOS II, developed by Sandia National Laboratories. Detailed description of the code is documented in Gartling (1978a, 1978b).

General References on Electronic Packaging

The textbooks by Scott (1974), and by Kraus and Bar-Cohen (1983) are good resources on packaging and cooling of electronic equipment. In addition to these books, the books by Seraphim et al. (1989) and Sloan (1985) were used as references for the cooling of electronic equipment by free convection.

Channels with Isothermal or Isoflux Walls

Elenbass (1942) conducted an experimental study of free convection between parallel plates. Elenbass determined the correlation for the functional dependence of average Nusselt number on aspect ratio and Rayleigh number. The maximum difference between the plate and ambient temperatures used in his experiments was 330 C (~600 F). This magnitude of plate-to-ambient temperature difference activates both variable property effects and thermal radiation. The Ra can be varied either by changing the channel width, b, or by changing the temperature difference, ΔT . Elenbass changed b in order to determine the functional dependence of average Nusselt number on the parameters Ra, Ar and Pr. In contrast, this dependence was determined in the present study by changing the

temperature difference. The disadvantage associated with changing b, to vary Ra, is that a finite element mesh is to be developed for each value of b.

Bodoia and Osterle (1962) investigated the development of free convection between heated vertical plates. They solved the basic flow governing equations numerically using a finite difference scheme. The fluid was assumed to enter the channel with ambient temperature and a flat velocity profile. Their results were obtained for the variations of velocity, temperature and pressure throughout the flow field. The authors also studied the flow and heat transfer characteristics of the channel and established a development height.

Churchill (1977) developed a general correlating equation for the mean rate of heat transfer in laminar, buoyancy-driven flow through vertical channels. He used the theoretical and experimental results of a number of authors to develop this correlation. The correlation provided a satisfactory representation for the available experimental data and computed values for buoyancy-induced convection in vertical channels.

Bar-Cohen and Rohsenow (1984) studied analytically, the optimization based on maximizing total heat transfer per unit volume or unit primary area. In order to study this analytic optimization, they developed composite relations for the variation of the heat transfer coefficient along the plate

surfaces which can be symmetrically or asymmetrically isothermal or isoflux surfaces. These results were aimed at thermal optimization of electronic packages with vertical parallel plate arrays.

Starner and McManus (1963) performed an experimental investigation of free-convection heat transfer from rectangular-fin arrays. They used three different test positions for each set of fins with the base of the fins being vertical, 45-degrees, and horizontal. The experimental results indicated that heat transfer coefficients for all their cases were less than those for similarly placed parallel plates.

Sparrow and Bahrami (1980) conducted experiments on natural convection from vertical parallel plates using naphthalene sublimation technique. Their experiments were based on mass transfer rather than on heat transfer. The advantage of using mass transfer technique is that the results obtained are unaffected by thermal radiation, variable property effects and extraneous heat losses. These experiments encompassed three types of hydrodynamic boundary conditions along the lateral edges: (i) fully open to ambient, (ii) blockage of one of the edge gaps, (iii) blockage along both of the edge gaps.

Their results can be summarized as: (i) blockage of fluid flow along one lateral edge gap generally has only a modest effect on the transfer coefficients and no effect for $Ra' > 4$,

(ii) blockage of fluid flow along both edges reduces the transfer coefficients by 30 percent (or more) at lower Ra' and no effect for Ra' > 10.

Aung et al. (1972a) studied experimentally and numerically the natural convection cooling of electronic cabinets containing arrays of vertical circuit cards. The authors' primary emphasis was on the electronic equipment in which the cards are aligned to form vertical channels or ducts. Their results include (i) nomograms for rapid estimation of card temperatures, (ii) nomograms for choosing the optimum card spacings, (iii) the effects of channel flow restrictions, staggered cards and baffles, and (iv) parametric effects of card spacing, heat dissipation, and channel height on maximum card temperature. Figure 1 which shows a typical electronic system with vertical channel configuration is taken from this reference.

Channels with Conducting or Heat Source Embedded Walls

Kim et al. (1989) studied numerically the laminar free convective heat transfer in channels formed between a series of vertical parallel plates with embedded line heat sources. The results indicate that the channels subjected to a repeated boundary condition (e.g., line heat source) approach that of a symmetrically heated channel subjected to UWT conditions at $K \geq 100$, where K is the ratio of thermal conductivity of the

solid wall to the thermal conductivity of air.

Again, Kim et al. (1990) studied the effect of wall conduction on laminar free convection between asymmetrically heated vertical plates. The parameters of interest in this study are the Grashof number, the conductivity ratio (ratio of thermal conductivity of solid to air, K) and the wall thickness to channel width ratios (t/B). The results of this study can be summarized as: (i) a maximum increase of 30% increase in mass flow rate of air for symmetric heating (ii) a maximum decrease of 22% in average Nusselt number due to wall conduction, (iii) the increase in mass flow rate is greater for asymmetric heating.

Channels with Major Emphasis on Optimization of Interplate Spacing

Anand et al. (1990) studied numerically the effect of plate spacing on free convection between vertical parallel plates. In their study, they calculated the optimum plate spacing $(b/L)_{opt}$ for a wide range of Grashof numbers and asymmetric heating parameters. The plate spacing is declared to be optimum when the average Nusselt number based on the channel height is maximum. These optimum spacings are reported to be more accurate than the ones in the literature and are believed to be of value to the design engineers in the field of electronic packaging.

Levy (1971) derived the optimum plate spacings for

laminar natural convection heat transfer from parallel vertical isothermal flat plates. The result of this study is a criterion which can be used to determine the maximum spacing between vertical isothermal parallel flat plates required for a minimum difference in temperature between the plates and the fluid.

Experimental verification of this optimum plate spacing was done by Levy et al. (1975) in another study. The results of this experiment confirmed the optimum plate spacings derived by Levy (1971).

Channels with Symmetric or Asymmetric Heating

Wirtz and Stutzman (1982) studied experimentally the free convection of air between parallel plates with symmetric heating and developed a correlation that allows for the calculation of the maximum temperature variation of the plates for a given input heat flux and plate geometry. They collected data over a range of heat fluxes and geometric parameters where the flow was in the developing temperature field regime.

Aung (1972b) analyzed and presented, in closed forms, the fully developed solutions for laminar free convection in a vertical, parallel plate channel with asymmetric heating. He considered both the UHF and UWT boundary conditions.

Aung et al. (1972c) investigated numerically as well as experimentally the developing laminar free convection between

vertical flat plates with asymmetric heating. Both UHF and UWT types of thermal boundary conditions were used for the flat plates. The results of this investigation show that (i) for fully developed flow, numerical solutions approach the closed form solution asymptotically (ii) for UHF, the difference between the maximum temperatures on the two walls diminishes as fully developed flow is achieved.

Webb and Hill (1989) conducted experiments on high Rayleigh number laminar natural convection in an asymmetrically heated vertical channel. UHF and thermal insulation boundary conditions were used for the walls. They collected local temperature data for both the walls for a wide range of heating rates and channel wall spacings corresponding to the high modified Rayleigh number regime.

Carpenter et al. (1976) investigated numerically the interaction of radiation and free convection between vertical flat plates with asymmetric heating. They developed a unique iterative-marching technique to solve the governing non-linear partial differential field equations and the integrodifferential radiant constraint equations. According to the authors, the nonradiation fully developed flow solution could not be obtained with radiation present. Experimental verification was done for all the numerical results.

Channels where Both the Walls are Subjected to Different Boundary Conditions

Miyatake and Fujii (1972) analyzed numerically the natural convection between two parallel plates where one plate was subjected to an isothermal heating boundary condition and the other to a thermally insulated boundary condition. Numerical results were obtained for the variations of flow rate, fluid temperature, fluid pressure, and local and mean Nusselt numbers. Their results indicated that the inlet velocity profile has no effect upon average Nusselt number.

Miyatake and Fujii (1973) analyzed numerically and experimentally the above problem again with different boundary conditions, one plate with a UHF and the other thermally insulated. The numerical results included the variations of velocity, temperature, pressure, induced flow rate, and local Nusselt number for fluids having Prandtl numbers 0.7 and 10. Their experimental measurements with water over a wide range of Rayleigh numbers yielded local Nusselt numbers which were in close agreement with their numerical solution.

Cha et al. (1989) utilized a finite difference numerical method to simulate natural convection between two vertical parallel plates where one plate was subjected to oscillating surface temperature boundary condition. Their results indicate that heat transfer enhancement by the oscillating

surface temperature has an upper limit for a specific Rayleigh number.

Channels with Mixed Convection

Rheault and Bilgen (1990) studied numerically the steady laminar mixed convection in vertical and inclined parallel channels with asymmetric isothermal boundary conditions. The results of this study show that the flow reversal near the colder wall and/or in the center of the channel becomes more pronounced when the nondimensional group, Gr/Re^2 increases where Re = Reynolds number based on the channel inlet velocity and the channel width.

Variable Property Effects in Channels

Zhong et al. (1985) studied the variable property effects in laminar natural convection in a square enclosure. The specific issues addressed in this study are the limits of the Boussinesq approximation, the proper use of a reference temperature, variable property correlation of the heat transfer rate and the limits of conduction-dominated regions. Their study indicated that (i) the Boussinesq approximation is generally valid for $\Theta_0 \leq 0.1$, where $\Theta_0 = (T_H - T_C)/T_C$, and T_H, T_C are the absolute temperatures of hot and cold walls respectively, and (ii) the heat transfer data for the whole

range of Θ_0 can be correlated by using a specific reference temperature (which is closer to T_C).

Mixed Convection in Channels with Obstructions

Kim and Boehm (1990) investigated numerically the combined free and forced convective heat transfer from multiple rectangular wall blocks in vertical channels. Thermal boundary conditions considered were for asymmetric heating, where one plate with blocks is heated, and the other plate is smooth and adiabatic. The parameter representative of mixed flow, Gr/Re^2 is varied between 0.04 and 12 and Re between 25 and 250. It was found from this study that (i) velocity distribution is unaffected by Rayleigh number (ii) temperature distribution is primarily affected by the Reynolds number variation with only a minor influence from the Rayleigh number range. It was observed by the authors that (i) maximum heat flux from each block occurs at the leading edge on the top (ii) the heat flux generally decreases over each successive block (iii) local Nusselt number reaches its peak as the fluid turns around the corner at the front edge of each block. This is attributed to the presence of a secondary boundary layer started at the leading edge of each top surface of the blocks.

Habchi and Acharya (1986) investigated numerically the laminar mixed convection of air in a vertical channel

containing a partial rectangular blockage on one channel wall. Both symmetric heating (two heated plates) and asymmetric heating (blocked plate heated and the other insulated) type of thermal boundary conditions were used for the walls of the channel. Gr/Re^2 was varied between 0.1 and 5 and Ra was assigned the values 10^3, 10^5, and 10^6. Negative velocities were observed beyond the blockage due to a recirculating eddy. The recirculating region was smaller at higher Gr/Re^2 values. The computed Nusselt numbers for the blocked channel for both thermal boundary conditions were less than the corresponding smooth channel Nusselt numbers. The Nusselt number attained a maximum value near the channel inlet as the surface near the entrance was washed by cold fluid of zero dimensionless temperature. Then, the Nusselt number decreased as the fluid flowed along the hot surface, and the fluid temperature increased. The same behavior was observed along the vertical surface of the blockage. Beyond the blockage, the Nusselt number increased up to the point of reattachment and then decreased gradually towards the exit of the channel. Nusselt number distribution along the right wall for the symmetrically heated channel followed the trend explained above. However, the local Nusselt number magnitudes were lower by about 10%.

Laminar Convection in Channels with Obstructions

Scarce research has been done on laminar natural convection in vertical channels with obstructions. Said and Krane (1990) performed an experimental and numerical investigation of laminar natural convection flow of air in a vertical channel with a single semi-circular obstruction. They analyzed both the UWT and UHF thermal boundary conditions. They studied the effects of the aspect ratio of the obstructed channel and the location of the obstruction on the rate of heat transfer. Regions of recirculating flow were observed above and below the obstruction. In the isotherm plots, the limiting case of an isolated single vertical flat plate was obtained at high Ra values. The results for UWT boundary conditions indicated that the presence of an obstruction reduces the average Nusselt number by 5% at a Ra of 10^4 to about 40% at a Ra of 10. It was also observed that moving the obstruction away from the entrance towards the exit reduces the average heat transfer rate for the channel. For UHF boundary conditions, it was noted that maximum temperature is only 4% higher than the maximum temperature for an unobstructed channel (occurs at the exit of the channel). For the obstructed channel, the maximum temperature occurred at the intersection of the top edge of the obstruction and the

wall. Their experimental results agreed well with their numerical results. The average deviation was 5% and the maximum deviation was 6.25%. A Mach-Zehnder interferometer (MZI) was used to record the interferograms which produce different fringe patterns. These fringe patterns can be used to represent isotherms, temperature distribution etc. A Wallaston prism interferometer was used in their study to measure the local heat flux on the walls.

Said and Muhanna (1990) studied numerically the natural convection of air in a vertical channel with a single square obstruction for Rayleigh numbers up to 10^4. The effects of the parameters like Rayleigh number, aspect ratio, height of the obstruction (from the channel entrance) on the average Nusselt number of the channel were studied. The results concerning the effect of aspect ratio on Nu indicated that the effect of Ar decreases as Ra increases. The range for this effect of Ar on Nu was found to be from about 10% at large Ra to about 33% at small Ra. This was attributed to the fact that the flow approaches a fully developed channel flow for lower Ra. The results pertaining to the effect of the dimensionless obstruction length, L_2, showed that the average Nusselt number decreases as L_2 increases, due to the decrease in the flow area. They compared the average Nusselt numbers of the square obstruction channel to those of the semi-circular obstruction (same surface area as the square one) channel of the previous study by Said and Krane (1990). The

authors concluded that obstructions with different shapes but with same surface areas have the same effect on the values of the average Nusselt number. It was also mentioned that the average Nusselt number (which is a function of temperature gradient) decreases as the dimensionless height, L_1 increases (i.e., the obstruction is moved away from the entrance towards the exit). This was due to the decrease in the temperature gradient (the boundary layer thickness at the channel entrance increases and temperature gradient decreases as L_1 increases) at the wall.

Acharya and Mehrotra (1993) conducted an experimental study of natural convection heat transfer in smooth and ribbed UWT and UHF vertical channels. It was observed by them that the ribbed duct heat transfer was lower than the smooth duct heat transfer. The authors developed the correlating equations for the average Nusselt number based on the experimental data.

There is a necessity to numerically study the compound effect of (i) multiple obstructions (e.g., more than one obstruction) (ii) obstructions on both walls of the channel (iii) aspect ratio of channel (iv) location of the obstruction. The present numerical study is aimed at studying the effect of the aforesaid factors on the rate of heat transfer.

CHAPTER 2

PROBLEM FORMULATION

Introduction

The governing equations for the flow in a vertical channel are parabolic in nature. But the presence of obstructions make these governing equations elliptic. Also, the momentum and energy equations are coupled and hence need to be solved simultaneously. In addition to being elliptic and coupled, the partial differential equations are also non-linear. These equations along with their boundary conditions are presented below, in terms of the physical variables. Then, the equations and boundary conditions are rewritten in terms of the non-dimensional variables.

Modelling Assumptions

In the present study, the free convection flows of interest for a Newtonian fluid with no internal heat generation are assumed to be laminar, steady-state, two-dimensional and with constant properties. In the present numerical model, the fluid is assumed to be incompressible,

with one exception. This exception is to account for the effect of variable density in buoyancy force (known as, the Boussinesq approximation). Other valid assumptions made are that the viscous dissipation, compressible work, and radiative transport are negligibly small. Geometry of the obstructed channel is shown in Figure 2. With these assumptions, the basic conservation equations can be written in terms of their physical variables as follows:

Conservation of mass:

$$\frac{\partial \overline{u}}{\partial \overline{x}} + \frac{\partial \overline{v}}{\partial \overline{y}} = 0 \qquad (1)$$

Conservation of momentum:

x - momentum:

$$\overline{u}\frac{\partial \overline{u}}{\partial \overline{x}} + \overline{v}\frac{\partial \overline{u}}{\partial \overline{y}} = -\frac{1}{\rho}\frac{\partial \overline{P}}{\partial \overline{x}} + \nu\left(\frac{\partial^2 \overline{u}}{\partial \overline{x}^2} + \frac{\partial^2 \overline{u}}{\partial \overline{y}^2}\right) \qquad (2)$$

$\overline{y}$ - momentum:

$$\overline{u}\frac{\partial \overline{v}}{\partial \overline{x}} + \overline{v}\frac{\partial \overline{v}}{\partial \overline{y}} = -\frac{1}{\rho}\frac{\partial \overline{P}}{\partial \overline{y}} + \nu\left(\frac{\partial^2 \overline{v}}{\partial \overline{x}^2} + \frac{\partial^2 \overline{v}}{\partial \overline{y}^2}\right) + g\beta\left(\overline{T} - T_\infty\right) \qquad (3)$$

Conservation of energy

$$\overline{u}\frac{\partial \overline{T}}{\partial \overline{x}} + \overline{v}\frac{\partial \overline{T}}{\partial \overline{y}} = \alpha\left(\frac{\partial^2 \overline{T}}{\partial \overline{x}^2} + \frac{\partial^2 \overline{T}}{\partial \overline{y}^2}\right) \qquad (4)$$

The boundary conditions for these equations are given by

$$\bar{u} = \bar{v} = 0 \text{ and } \bar{T} = T_w \quad \text{for} \quad \left\{ \begin{array}{c} \bar{x} = 0 \text{ and } \quad 0 \le \bar{y} \le (\bar{L}_1 - \frac{\bar{h}}{2}) \\ 0 \le \bar{x} \le \bar{W} \text{ and } \quad \bar{y} = (\bar{L}_1 - \frac{\bar{h}}{2}) \\ \bar{x} = \bar{W} \quad \text{and } (\bar{L}_1 - \frac{\bar{h}}{2}) \le \bar{y} \le (\bar{L}_1 + \frac{\bar{h}}{2}) \\ 0 \le \bar{x} \le \bar{W} \text{ and } \quad \bar{y} = (\bar{L}_1 + \frac{\bar{h}}{2}) \\ \bar{x} = 0 \quad \text{and } (\bar{L}_1 + \frac{\bar{h}}{2}) \le \bar{y} \le L \end{array} \right\} \quad (5)$$

$$\bar{u} = \bar{v} = 0 \text{ and } \bar{T} = T_w \text{ for} \left\{ \begin{array}{c} \bar{x} = b \text{ and } \quad 0 \le \bar{y} \le (\bar{L}_2 - \frac{\bar{h}}{2}) \\ b - \bar{W} \le \bar{x} \le \bar{b} \text{ and } \quad \bar{y} = (\bar{L}_2 - \frac{\bar{h}}{2}) \\ \bar{x} = b - \bar{W} \quad \text{and } (\bar{L}_2 - \frac{\bar{h}}{2}) \le \bar{y} \le (\bar{L}_2 + \frac{\bar{h}}{2}) \\ b - \bar{W} \le \bar{x} \le b \text{ and } \quad \bar{y} = (\bar{L}_2 + \frac{\bar{h}}{2}) \\ \bar{x} = b \quad \text{and } (\bar{L}_2 + \frac{\bar{h}}{2}) \le \bar{y} \le L \end{array} \right\} \quad (6)$$

$$\left\{ \begin{array}{l} \bar{u} = 0 \\ \tau_{yn} = 0 \\ \dfrac{\partial \bar{T}}{\partial \bar{y}} = 0 \end{array} \right\} \quad \text{for} \quad 0 \le \bar{x} \le b \quad \text{and} \quad \bar{y} = L \qquad (7)$$

$$\left\{ \begin{array}{l} \bar{u} = 0 \\ \tau_{yn} = 0 \\ \bar{T} = T_\infty \end{array} \right\} \quad \text{for} \quad 0 \le \bar{x} \le b \quad \text{and} \quad \bar{y} = 0 \qquad (8)$$

where, $\tau_{yn} = -\bar{P} + \mu \dfrac{\partial \bar{v}}{\partial \bar{y}}$

Normalization of the Governing Equations

The different dimensionless variables and parameters are given by

$$x=\frac{\bar{x}}{b},\quad y=\frac{\bar{y}}{L},\quad u=\frac{\bar{u}b}{\alpha},\quad v=\frac{\bar{v}b^2}{\alpha L}\ \text{and}$$

$$L_1=\frac{\bar{L}_1}{L},\quad L_2=\frac{\bar{L}_2}{L}$$

Also,

$$\theta=\frac{\bar{T}-T_\infty}{T_w-T_\infty},\quad P=\frac{\bar{P}}{g\beta\rho_\infty(T_w-T_\infty)L} \tag{9}$$

By substituting these dimensionless quantities in the above governing equations which are expressed in terms of the physical variables, the normalized equations can be obtained as follows:

Conservation of mass:

$$\frac{\partial u}{\partial x}+\frac{\partial v}{\partial y}=0 \tag{10}$$

Conservation of momentum:

x - momentum:

$$\left(\frac{Ar^2}{Pr}\right)\left[u\frac{\partial u}{\partial x}+v\frac{\partial u}{\partial y}\right]=-(RaAr)\frac{\partial P}{\partial x}+Ar^2\left[\frac{\partial^2 u}{\partial x^2}+Ar^2\frac{\partial^2 u}{\partial y^2}\right] \tag{11}$$

y - momentum:

$$\left(\frac{1}{Pr}\right)\left[u\frac{\partial v}{\partial x}+v\frac{\partial v}{\partial y}\right]=(RaAr)\left(\theta-\frac{\partial P}{\partial y}\right)+\left[\frac{\partial^2 v}{\partial x^2}+Ar^2\frac{\partial^2 v}{\partial y^2}\right] \qquad (12)$$

Conservation of energy:

$$u\frac{\partial \theta}{\partial x}+v\frac{\partial \theta}{\partial y}=\frac{\partial^2 \theta}{\partial x^2}+Ar^2\frac{\partial^2 \theta}{\partial y^2} \qquad (13)$$

where Ra = Rayleigh number = $\dfrac{g\beta\,(T_w-T_\infty)\,b^3}{\alpha\nu}$,

Ar = Aspect ratio = $\dfrac{b}{L}$,

Pr = Prandtl number = $\dfrac{\nu}{\alpha}$.

Then, the normalized boundary conditions for the above equations can be expressed as:

$$u = v = 0 \text{ and } \theta = 1 \text{ for } \left\{\begin{array}{l} x = 0 \text{ and } \quad 0 \le y \le \left(L_1-\frac{h}{2}\right) \\ 0 \le x \le W \text{ and } \quad y = \left(L_1-\frac{h}{2}\right) \\ x = W \quad \text{and } \left(L_1-\frac{h}{2}\right) \le y \le \left(L_1+\frac{h}{2}\right) \\ 0 \le x \le W \text{ and } \quad y = \left(L_1+\frac{h}{2}\right) \\ x = 0 \quad \text{and } \left(L_1+\frac{h}{2}\right) \le y \le 1 \end{array}\right\} \qquad (14)$$

$$u=v=0 \text{ and } \theta=1 \text{ for } \left\{ \begin{array}{c} x=1 \text{ and } 0 \le y \le (L_2-\frac{h}{2}) \\ (1-W) \le x \le 1 \text{ and } y = (L_2-\frac{h}{2}) \\ x = (1-W) \text{ and } (L_2-\frac{h}{2}) \le y \le (L_2+\frac{h}{2}) \\ (1-W) \le x \le 1 \text{ and } y = (L_2+\frac{h}{2}) \\ x=1 \text{ and } (L_2+\frac{h}{2}) \le y \le 1 \end{array} \right\} \quad (15)$$

$$\left\{ \begin{array}{c} u = 0 \\ -P+(\frac{Ar}{Ra})\frac{\partial v}{\partial y} = 0 \\ \frac{\partial \theta}{\partial y} = 0 \end{array} \right\} \quad \text{for} \quad 0 \le x \le 1 \quad \text{and} \quad y = 1 \qquad (16)$$

$$\left\{ \begin{array}{c} u = 0 \\ -P+(\frac{Ar}{Ra})\frac{\partial v}{\partial y} = 0 \\ \theta = 0 \end{array} \right\} \quad \text{for} \quad 0 \le x \le 1 \quad \text{and} \quad y = 0 \qquad (17)$$

It is worth mentioning here that the elemental surface integrals in the Galerkin method of weighted residuals vanish. For present study, the two natural (or Neumann) boundary conditions i.e., the total stress normal to the boundary and the heat flux normal to the boundary are naturally enforced through the elemental surface integrals. This enforcement of Neumann boundary conditions through surface integrals is known as 'weak enforcement'.

The above normalized equations and the boundary conditions indicate that the parametric study of the present problem involves the parameters Ra, Ar, $\overline{L}_1/L(=L_1)$, $\overline{L}_2/L(=L_2)$, $\overline{W}/L(=W)$, and $\overline{h}/L(=h)$.

CHAPTER 3

NUMERICAL INVESTIGATION

Introduction

The objective of the present numerical study is to solve the boundary value problem formulated in the previous chapter. The set of coupled, nonlinear, elliptic equations (equations 1 through 4 of the previous chapter) along with the boundary conditions (equations 5 through 8 of the previous chapter) are too difficult for an analytic solution. Hence a numerical technique is to be adopted to solve these equations. Different techniques like a finite difference method, or a finite element method can be used to solve the governing nonlinear partial differential equations. Apart from the numerical aspects, two features of any natural convection problem that must be paid attention are:

(i) validity limits of the Boussinesq approximation, and

(ii) selection of a reference temperature to take care of the variable property effects.

The Boussinesq approximation is used to simplify the intractable natural convection equations. Initially, Boussinesq's approximation was defined to comprise three

parts, namely,

(i) density is constant except when it directly leads to buoyancy force

(ii) constant fluid properties

(iii) negligible viscous dissipation.

Later, Gray and Giorgini (1976) modified the second part of the above approximation such that fluid properties can be functions of pressure and temperature. As suggested by Zhong et al. (1985), the difference between the wall and ambient temperature was chosen so that $[T_w-T_\infty]/T_\infty \leq 0.1$ (or the driving force, $\beta \Delta T \leq 0.1$).

The results of any fluid flow problem (with the fluid properties being temperature dependent) depend on the selection of a proper reference temperature. Sparrow and Gregg (1958) analyzed the variable fluid property for laminar free convection on an isothermal vertical flat plate. Their study involved liquid-mercury, and gases whose properties vary according to a power law, Sutherland type formula etc. According to them, the film temperature (with ß = $1/T_\infty$ for gases) serves as an adequate reference temperature for most of the applications. Film temperature is the average of wall and ambient temperatures. This reference temperature with ß = $1/T_\infty$ was used in the present study.

The Computational Matrix

From the nondimensional governing equations and boundary conditions of the present study, it can be seen that the average Nusselt number (Nu) for the channel has the following functional dependencies:

$$Nu=Nu(Ra,Pr,Ar) \quad \text{(for smooth channel)} \tag{18}$$

$$Nu=Nu(Ra,Pr,Ar,L_1,L_2,W,h) \quad \text{(for obstructed channel)} \tag{19}$$

Where Ra is the Rayleigh number based on the channel width, Pr is the Prandtl number of the fluid, and Ar is the aspect ratio of the channel (=b/L). L_1 (= $\overline{L_1}/L$) and L_2 (= $\overline{L_1}/L$) are the dimensionless heights of the obstructions on the left wall and right wall from channel entrance respectively. W (= $\overline{W}/L$) and h (= $\overline{h}/L$) are the dimensionless width and height of the obstruction, respectively. Based on the above functional dependence, a total of 30 cases corresponding to two aspect ratios (Ar=0.2, 0.3) were run for the smooth channel. The computational matrix for these cases is shown in Table 1. Average Nusselt numbers were calculated for all these cases so that they could be used as the standard of comparison for the obstructed channels.

Table 1: Computational Matrix for the Smooth Channel

Ra	Ar
10^2	0.2 0.3
$5x10^2$	0.2 0.3
10^3	0.2 0.3
$5x10^3$	0.2 0.3
$7.5x10^3$	0.2 0.3
10^4	0.2 0.3
$1.5x10^4$	0.2 0.3
$2x10^4$	0.2 0.3
$2.5x10^4$	0.2 0.3
$3x10^4$	0.2 0.3
$3.5x10^4$	0.2 0.3
$4x10^4$	0.2 0.3
$4.5x10^4$	0.2 0.3
$5x10^4$	0.2 0.3

For the cases with obstructed channel, W and h (define the size of the obstruction) were kept constant with the values of W=0.0667, h=0.01334. This was done to minimize the

number of parameters varied and as such reduce the size of the computational matrix. Based on these criteria, a total of 54 cases were run for the channel with obstruction. The effect of the multiple obstructions on the rate of heat transfer in the channel was determined by comparing the average Nusselt numbers of the obstructed channel to those of the smooth channel. The computational matrix of the obstructed channels is shown in Table 2. To achieve faster convergence and to limit the numerical instabilities that arise at higher Rayleigh numbers, the solution for one case was used as the initial condition for the next case.

Table 2: Computational matrix for the obstructed channel

Ra	Ar	L_1	L_2
10^2	0.2	0.25 0.5	0.75 0.5
	0.3	0.25 0.5	0.75 0.5
$5x10^2$	0.2	0.25 0.5	0.75 0.5
	0.3	0.25 0.5	0.75 0.5
10^3	0.2	0.25 0.5	0.75 0.5
	0.3	0.25 0.5	0.75 0.5
$2.5x10^3$	0.2	0.25 0.5	0.75 0.5
	0.3	0.25 0.5	0.75 0.5

Table 2: Continued

Ra	Ar	L_1	L_2
$5x10^3$	0.2	0.25 0.5	0.75 0.5
	0.3	0.25 0.5	0.75 0.5
$7.5x10^3$	0.2	0.25 0.5	0.75 0.5
	0.3	0.25 0.5	0.75 0.5
10^4	0.2	0.25 0.5	0.75 0.5
	0.3	0.25 0.5	0.75 0.5
$1.5x10^4$	0.2	0.25 0.5	0.75 0.5
	0.3	0.25 0.5	0.75 0.5
$2x10^4$	0.2	0.25 0.5	0.75 0.5
	0.3	0.25 0.5	0.75 0.5
$2.5x10^4$	0.2	0.25 0.5	0.75 0.5
	0.3	0.25 0.5	0.75 0.5
$3x10^4$	0.2	0.25 0.5	0.75 0.5
	0.3	0.25 0.5	0.75 0.5
$3.5x10^4$	0.2	0.25 0.5	0.75 0.5
	0.3	0.25 0.5	0.75 0.5

Table 2: Continued

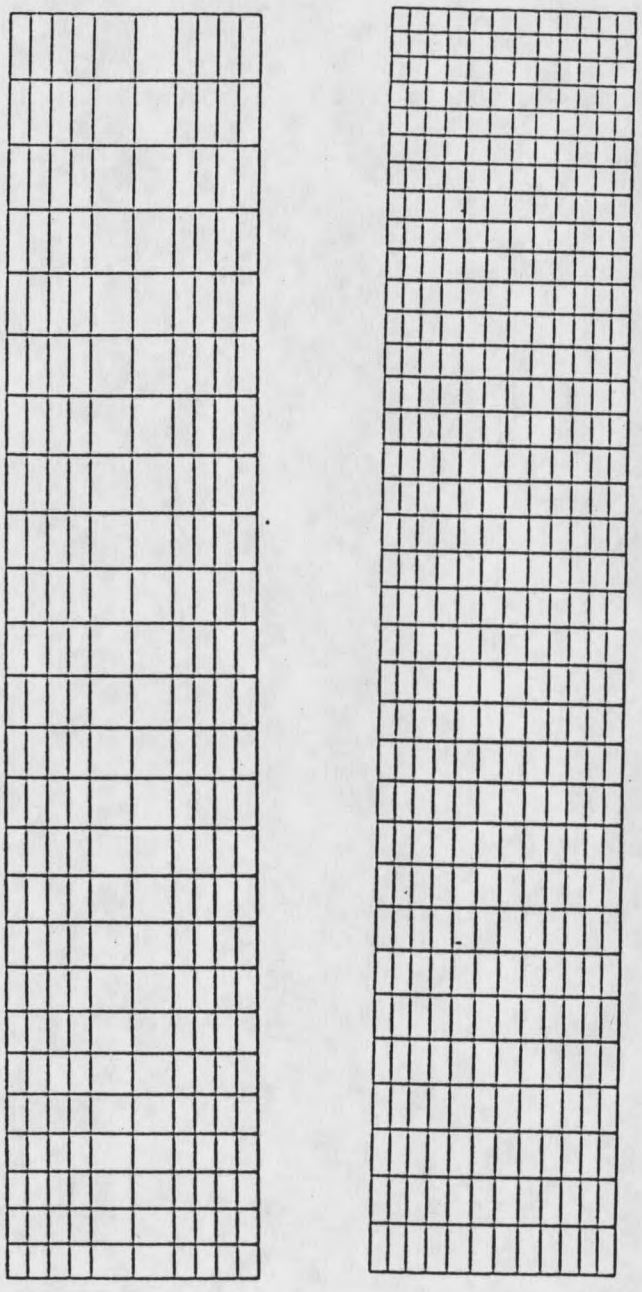
Ra	Ar	L_1	L_2
$4x10^4$	0.2	0.25 0.5	0.75 0.5
	0.3	0.25 0.5	0.75 0.5
$4.5x10^4$	0.2	0.25 0.5	0.75 0.5
	0.3	0.25 0.5	0.75 0.5
$5x10^4$	0.2	0.25 0.5	0.75 0.5
	0.3	0.25 0.5	0.75 0.5

The Computational Grid

For the smooth as well as the obstructed channel, different aspect ratios were obtained by changing the distance, b, between channel walls. A new mesh was developed for each aspect ratio of the channel. Aspect ratios of 0.2 and 0.3 were used for both the smooth and obstructed channels. More elements were packed in the regions of large temperature and/or velocity gradients as compared to the regions of less gradients. This yielded non-uniform mesh in all the cases. This use of a non-uniform mesh is based on the popular theory that denser packing of elements in particularly chosen locations leads to an improved accuracy, provided that the consequent coarse distribution elsewhere does not corrupt the accuracy of the solution.

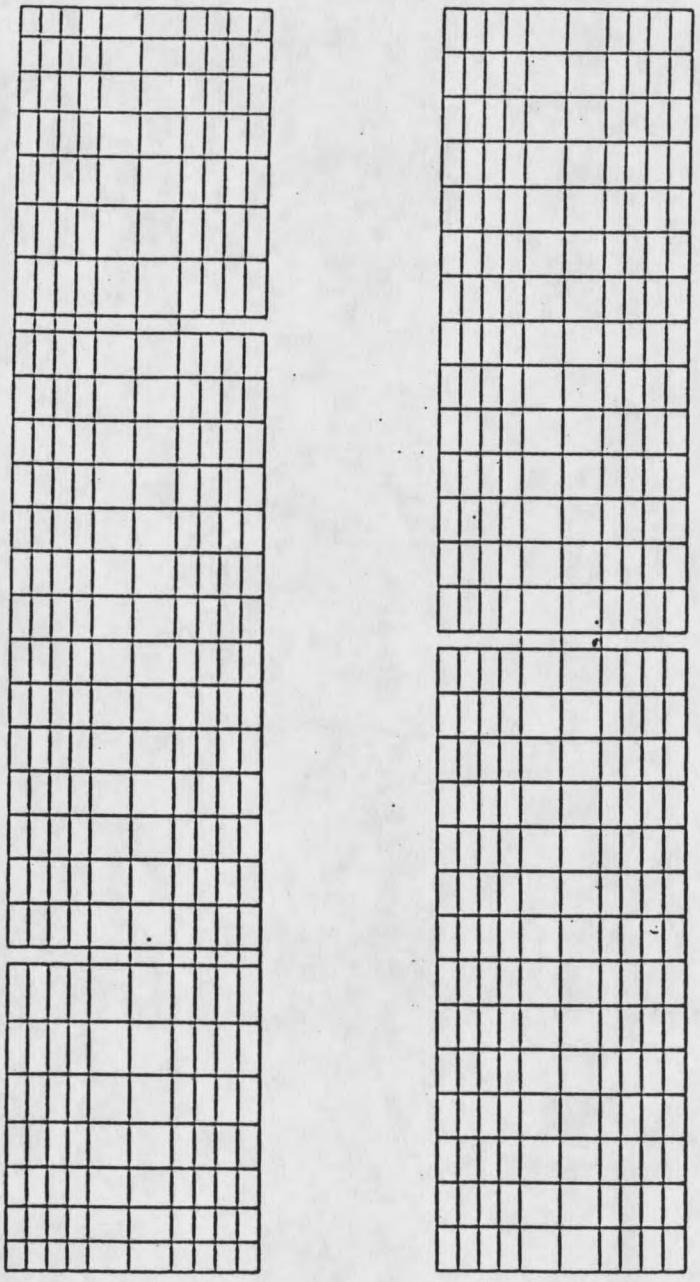
To test the grid-independency, two different nonuniform meshes were used for the smooth channel with Ar=0.2. Initially, a mesh of 250 subparametric, 9 node, quadrilateral elements was used and then the number of elements was increased to 420 (an increase of 68%). These two meshes are shown in Figure 3. The computed average Nusselt numbers in both the cases agreed very well with each other, with a maximum difference of 2% . Based on this comparison and the fact that the central processing unit (C.P.U) time required to run a particular case is in direct proportion to the number of elements in the mesh, a grid size of 250 elements was used. NACHOS calculates the maximum elemental mass balance error for the numerical grid and it was observed that this error was of the order of 10^{-6} for all the cases. In addition, mass conservation was verified numerically by considering the inlet and the exit of the channel and it was found to be satisfied within a percentage difference of 1% .

The results of the grid independency test for the smooth channel were used as a base to decide the grid size for the obstructed channels. That is, the grid spacing for all the subsequent cases was chosen such that it was proportional to the grid spacing of the base case of the smooth channel. This was necessary to ensure the numerical accuracy of the present study. For the obstructed channel, two meshes were developed for each aspect ratio (Ar = 0.2 and 0.3). The two meshes corresponding to an aspect ratio of 0.2 are shown in Figure 4



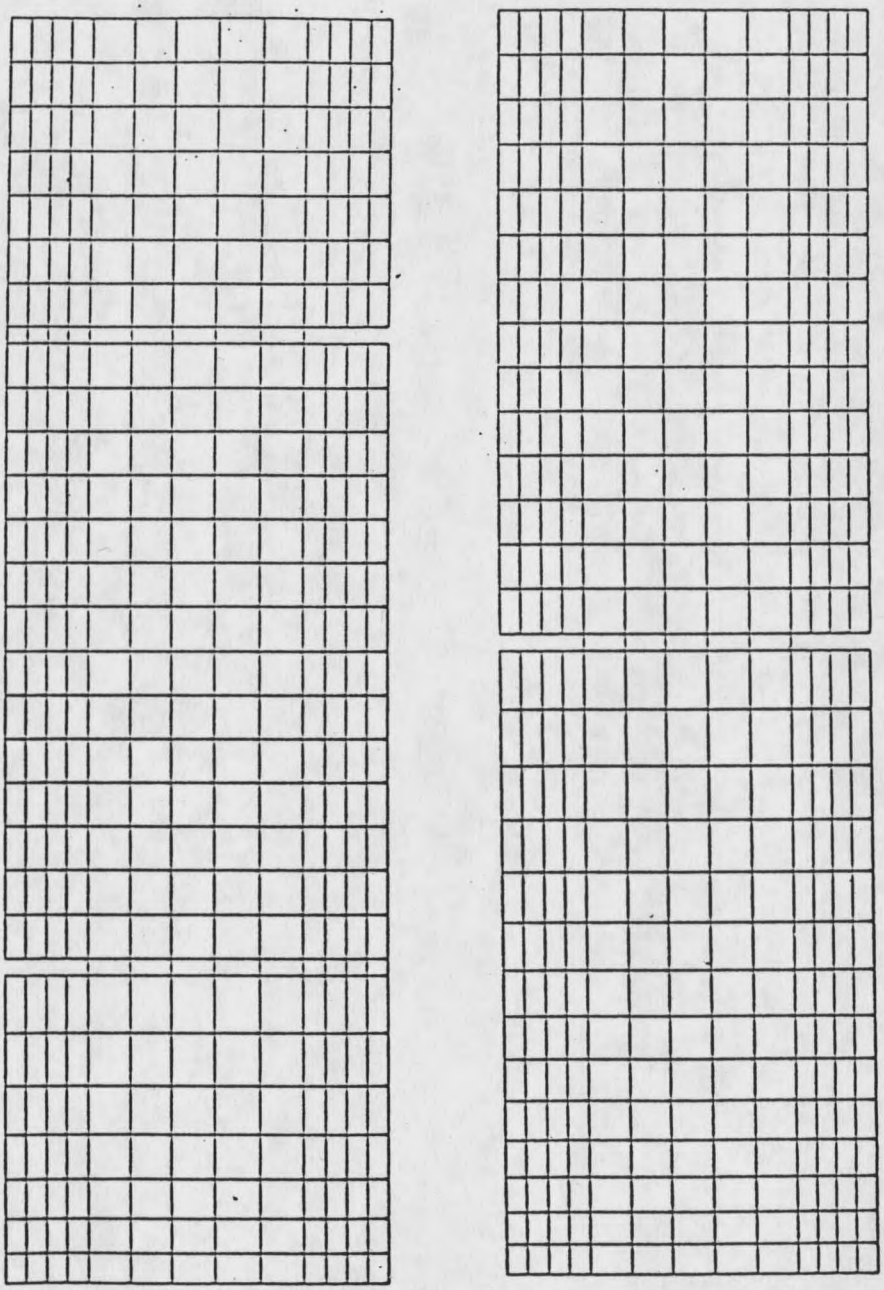
(a) 250 elements (b) 420 elements

Figure 3. Mesh generation for the smooth channel (Ar = 0.2)



(a) $L_1 = 0.25$, $L_2 = 0.75$ (b) $L_1 = 0.5$, $L_2 = 0.5$

Figure 4. Mesh generation for the obstructed channel (Ar = 0.2)



(a) $L_1 = 0.25$, $L_2 = 0.75$ (b) $L_1 = 0.5$, $L_2 = 0.5$

Figure 5. Mesh generation for the obstructed channel (Ar = 0.3)

and the two meshes corresponding to an aspect ratio of 0.3 are shown in Figure 5. Each of these meshes in turn, corresponds to a set of values for the obstruction locations. The two sets of values used were

(i) $L_1 = 0.25$, $L_2 = 0.75$, (ii) $L_1 = 0.5$, $L_2 = 0.5$.

The maximum aspect ratio used was limited to 0.3 All the computations were done on VAX 6500. All the cases were run using a steady state Newton-Raphson iteration scheme. A solution was defined to have reached the convergence when the norm of the product of the velocity components and the norm of temperature were less than 0.1%. The Entire analysis was done in terms of the primitive variables (PV) as required by NACHOS.

The following tables list the number of elements used for the different geometries investigated in this research.

Table 3: Number of elements used for smooth channels.

Ar (=b/L)	No. of elements
0.2	250 420
0.3	325

Table 4: Number of elements used for the obstructed channels

Ar	L_1	L_2	No. of elements
0.2	0.25 0.5	0.75 0.5	292 (geometry I) 282 (geometry II)
0.3	0.25 0.5	0.75 0.5	382 (geometry III) 369 (geometry IV)

In the following chapters, the obstructed channel with parameters Ar = 0.2, L_1 = 0.25, L_2 = 0.75 is referred to as geometry I, the channel with Ar = 0.2, L_1 = 0.5, L_2 = 0.5 as geometry II, the channel with Ar = 0.3, L_1 = 0.25, L_2 = 0.75 as geometry III, and finally the channel with Ar = 0.3, L_1 = 0.5, L_2 = 0.5 as geometry IV.

CHAPTER 4

RESULTS AND DISCUSSION

Introduction

To get familiar with the code, the benchmark problem of natural convection flow of air (Pr=0.72) in a square enclosure was solved using the code. The flow was analyzed within the context of Boussinesq approximation. UWT boundary condition was used for the two vertical walls and an adiabatic boundary condition was used for the two horizontal walls of the enclosure. This problem was solved by De Vahl Davis and Jones (1983) in the context of a benchmark solution. As can be seen from Figure 6, the computed average Nusselt numbers at various Rayleigh numbers were in excellent agreement with the benchmark Nusselt number values.

As mentioned in the previous chapter, the effect of multiple obstructions on the rate of heat transfer was studied by comparing the average Nusselt numbers of the unobstructed or smooth channels with those of the corresponding obstructed channels. The detailed mathematical definition of Nusselt number used in this study is shown in Appendix[B]. Two FORTRAN-77 codes called CHANEL and OBSNU were developed to

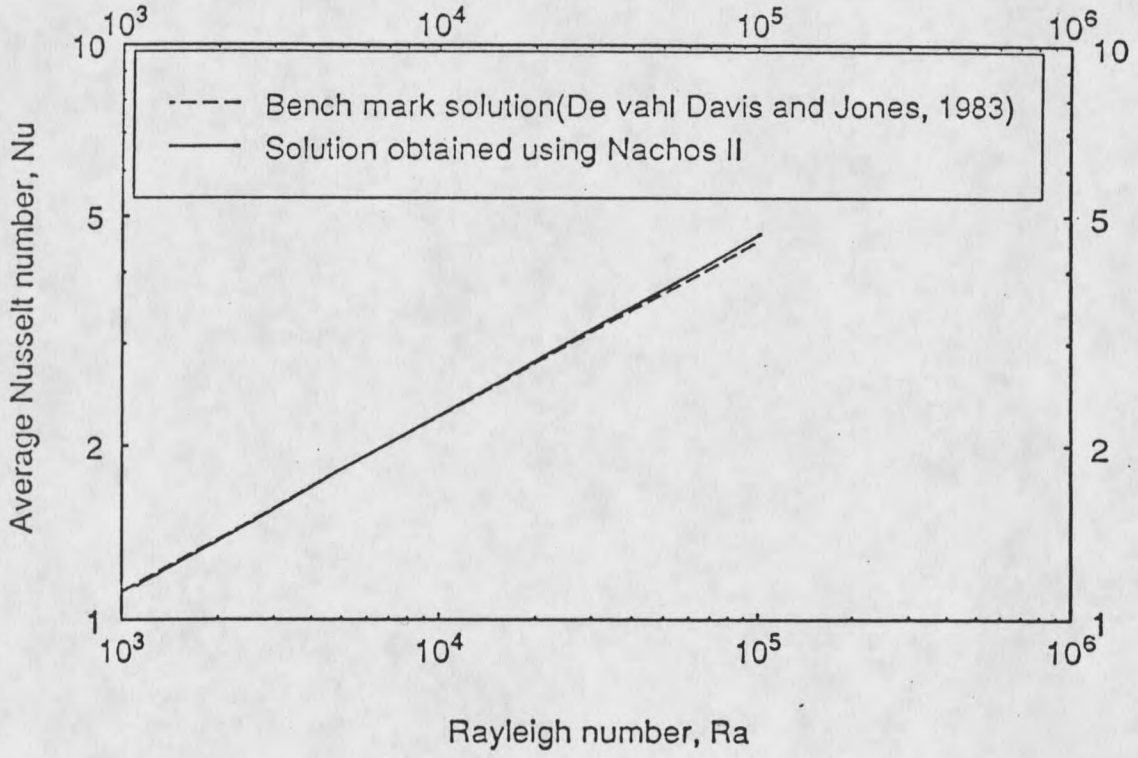


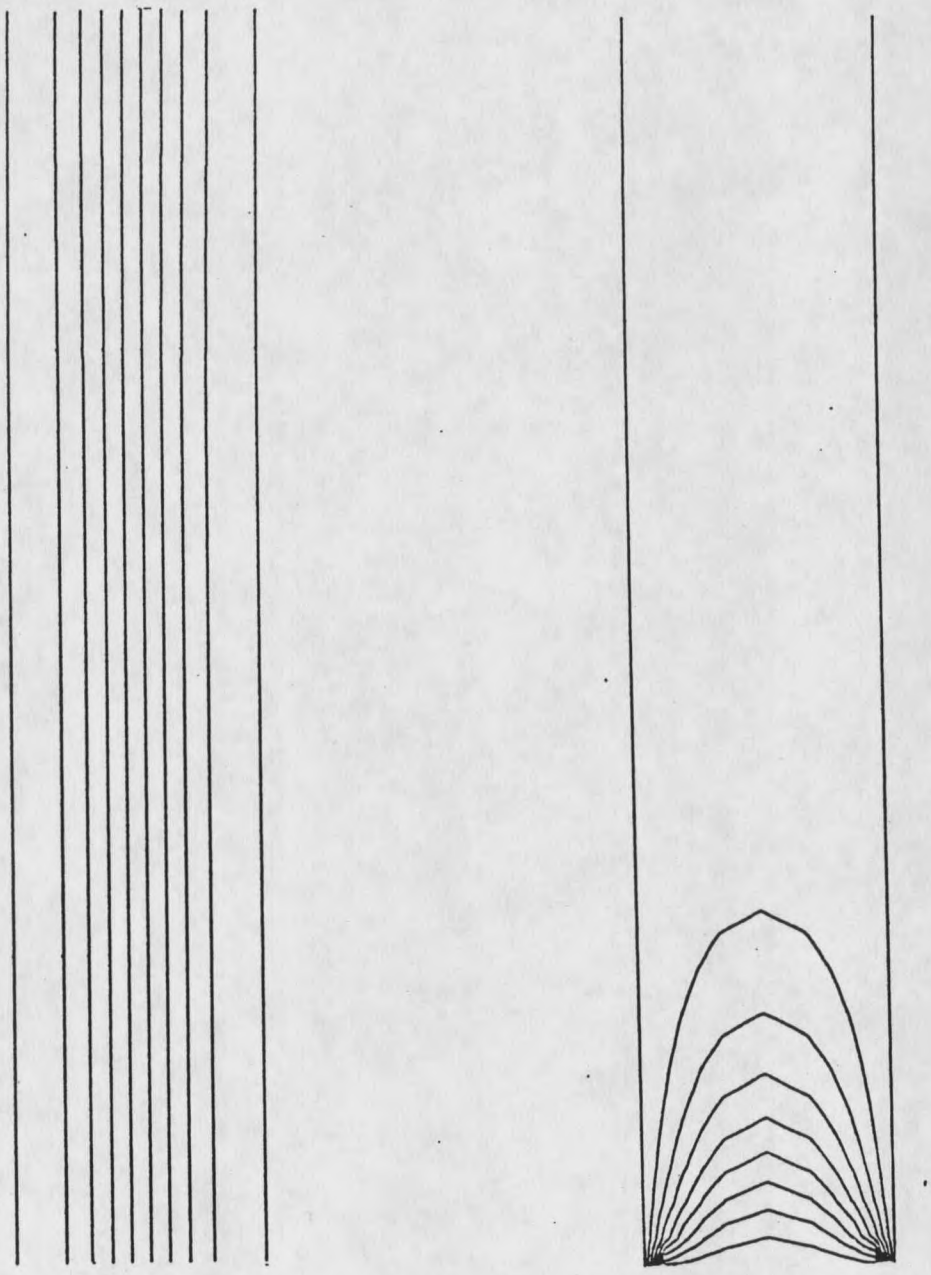
Figure 6. Comparison of computed average Nusselt numbers for a square enclosure with the benchmark solution.

compute the local heat transfer coefficients, local Nusselt numbers and average Nusselt numbers of the smooth and obstructed channels respectively. These codes were used for post processing operation after a solution was obtained by using NACHOS II. These two codes are provided in the Appendices C and D respectively.

Apart from the numerical results for the primitive variables or otherwise known as Degrees of freedom, the following results were also obtained for each case:
(i) the heat flux distribution along the channel walls in order to calculate the Nusselt numbers, (ii) maximum and minimum values of the stream function for the flow field, (iii) contour plots of stream functions and temperatures (Isotherms) for the flow field, (iv) vector plots of the velocity and heat flux, (v) profile plots of the vertical velocity at the entrance and exit of the channel and temperature plots at the exit of the channel.

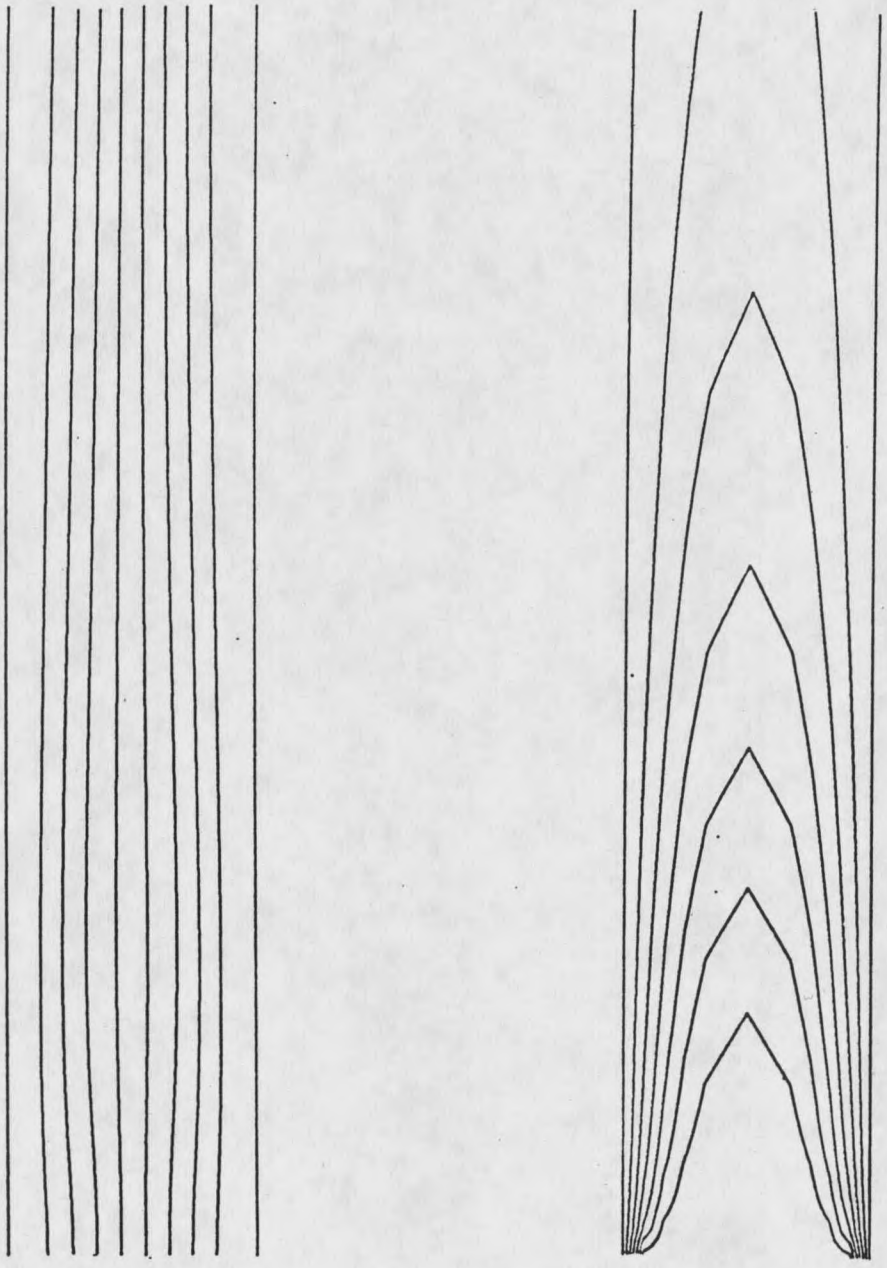
Discussion of the Results for an Unobstructed Channel

Numerical investigation was performed for the Unobstructed channel cases in the range $10^2 \leq Ra \leq 5 \times 10^4$. Plots of streamlines, and isotherms (at different Rayleigh numbers) for the smooth channel with Ar = 0.2 are shown in Figures 7 through 10. The streamline and isotherm plots at two Rayleigh numbers for the smooth channel with Ar = 0.3 are also presented in Figures 11 and 12. Direction of the fluid



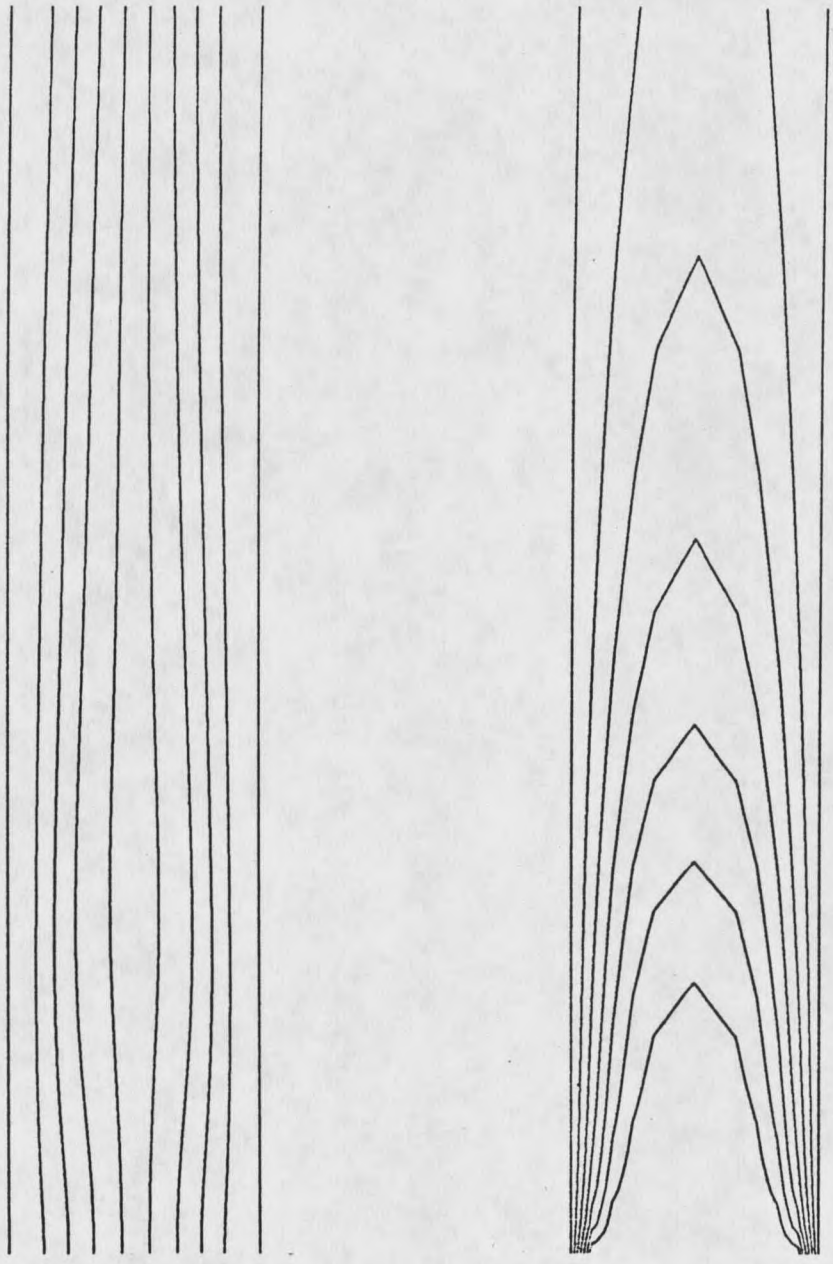
(a) Streamlines (b) Isotherms

Figure 7. Computed streamlines and isotherms for smooth channel with Ra = 10^2, Ar = 0.2



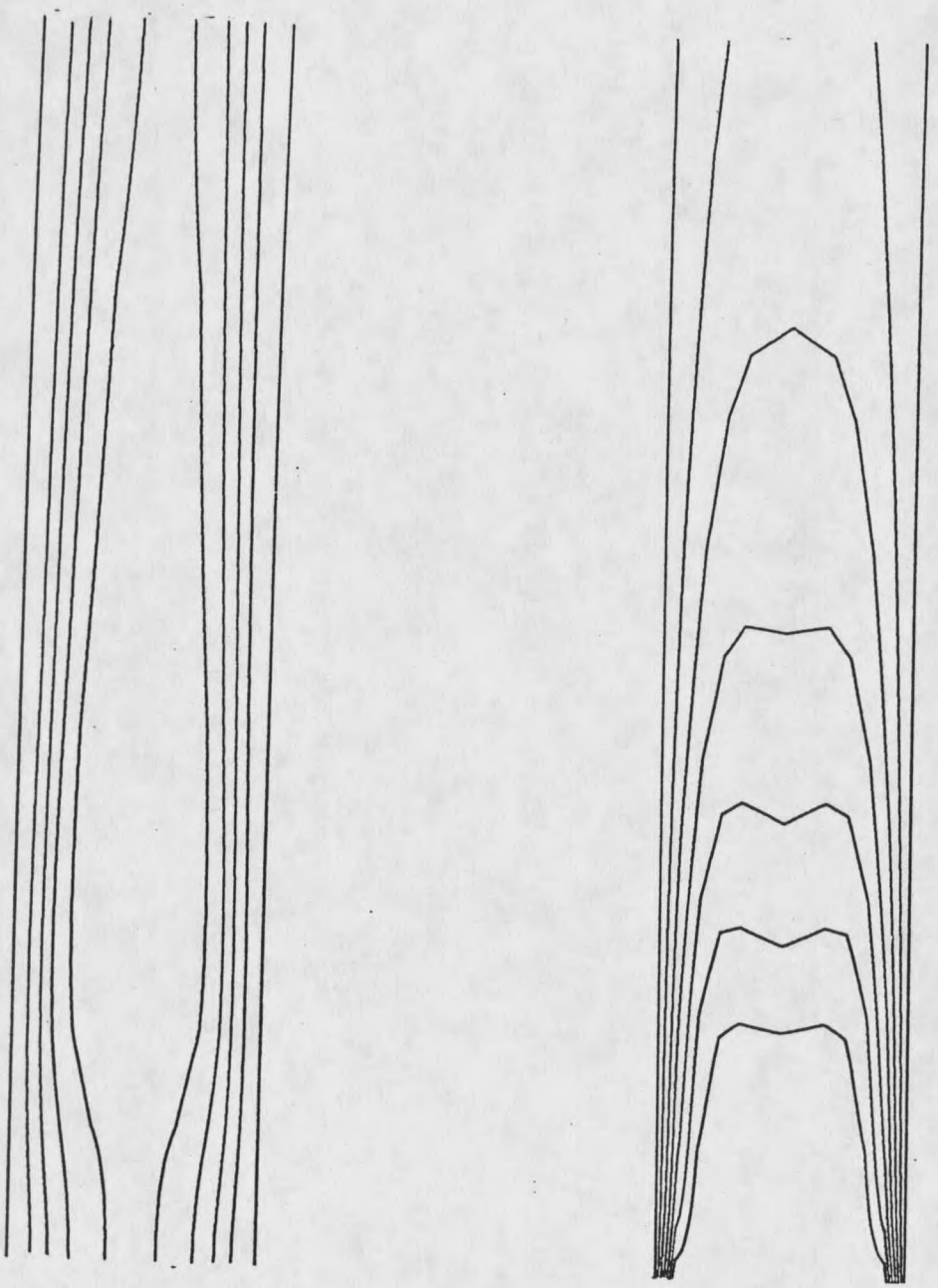
(a) Streamlines (b) Isotherms

Figure 8. Computed streamlines and isotherms for smooth channel with Ra = 5×10^3, Ar = 0.2



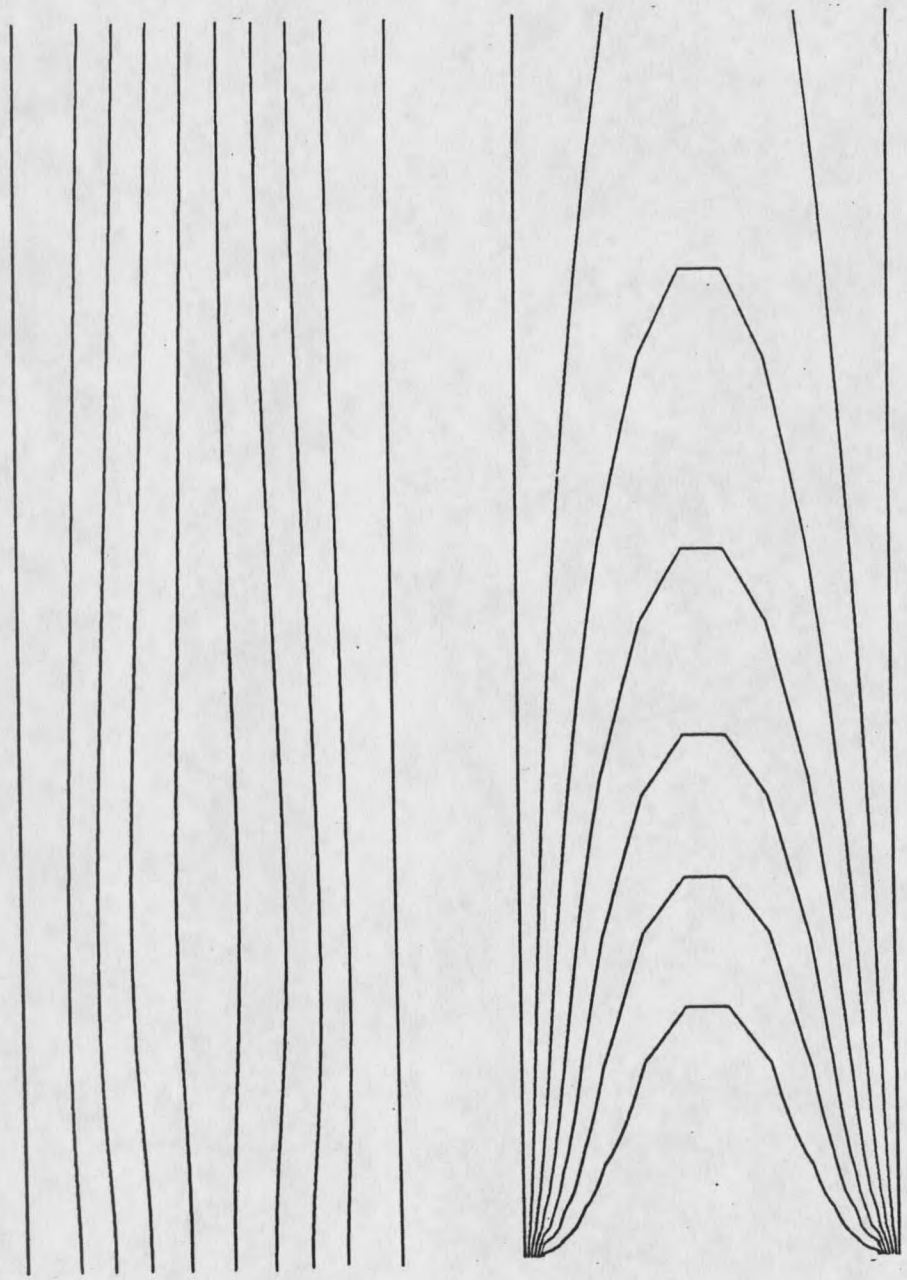
(a) Streamlines (b) Isotherms

Figure 9. Computed streamlines and isotherms for smooth channel with Ra = 10^4, Ar = 0.2



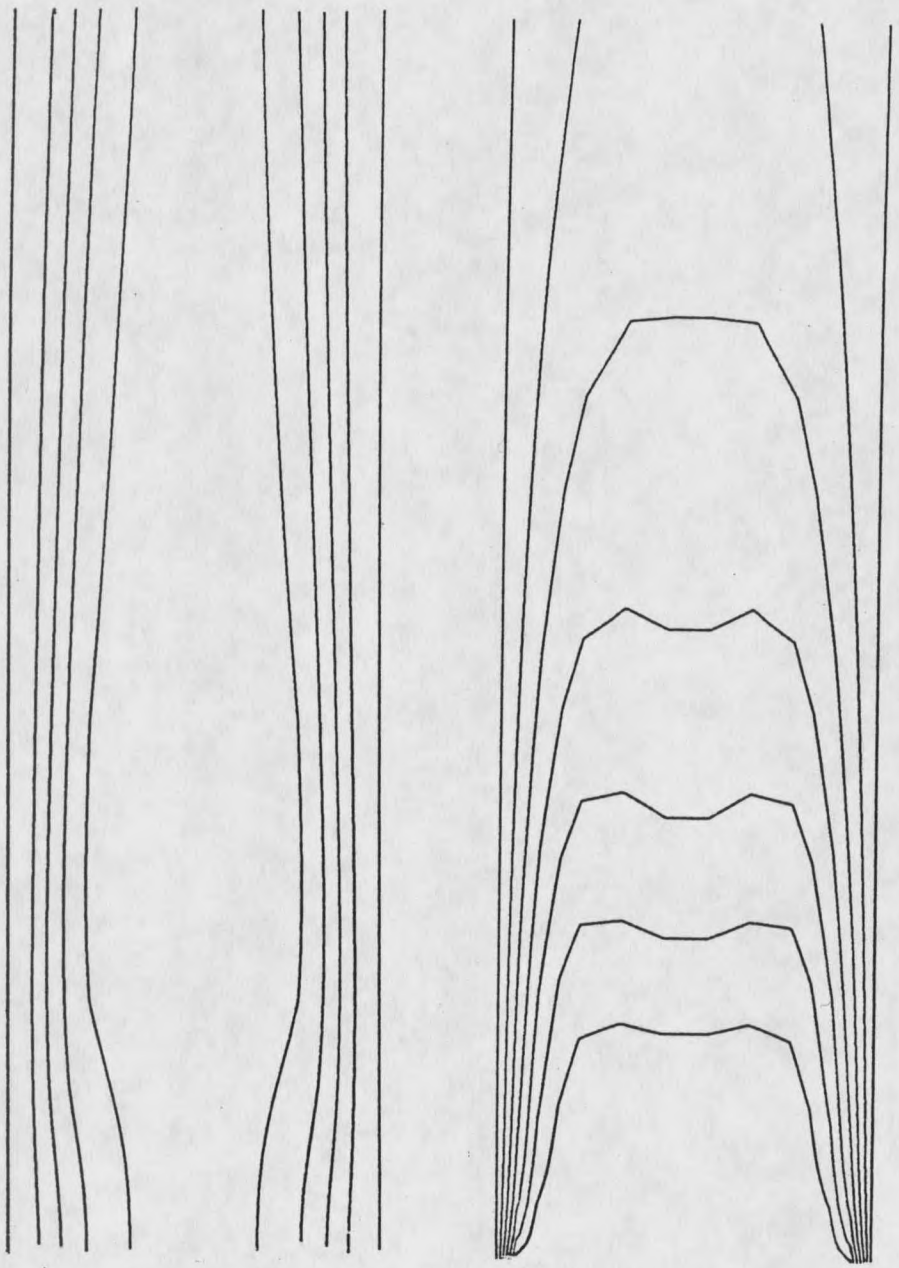
(a) Streamlines (b) Isotherms

Figure 10. Computed streamline and isotherms for smooth channel with Ra=5 x 10^4, Ar=0.2



(a) Streamlines (b) Isotherms

Figure 11. Computed streamlines and isotherms for smooth channel with Ra = 5×10^3, Ar = 0.3



(a) Streamlines (b) Isotherms

Figure 12. Computed streamlines and isotherms for smooth channel with Ra = 5×10^4, Ar = 0.3

flow, regions of higher velocity gradients in the flow field, can be interpreted from the streamline plots. Isotherms represent primarily the temperature gradients and thereby the heat fluxes at different locations in the channel. Comparison of the streamline, isotherm plots at Ar = 0.2 and 0.3 showed that the channel walls become independent of each other, as the aspect ratio increases. It can be predicted from the streamline and isotherm plots that, in the limiting case of a very high Ra, the flow on each channel wall approaches the flow on an isolated single vertical flat plate. In this limiting case, a separate boundary layer is formed on each channel wall. Also, the center line temperature remains at the ambient temperature or in other words, the dimensionless temperature $\Theta = 0$.

Figures 13 and 14 show the transverse distribution of temperature at the exit of the smooth channel for two Rayleigh numbers (Ar = 0.2). From the temperature distribution plots and also from the symmetry of the channel, it is observed that the minimum temperatures occur on the center line of the channel irrespective of the elevation in the channel. Also, the maximum center line temperature which occurs at the exit plane decreases as the Rayleigh number increases. This can be attributed to the fact that the thermal boundary layer thickness decreases as Rayleigh number increases.

Figures 15 through 18 show the transverse distribution of velocity at the inlet and the exit of the channel at two

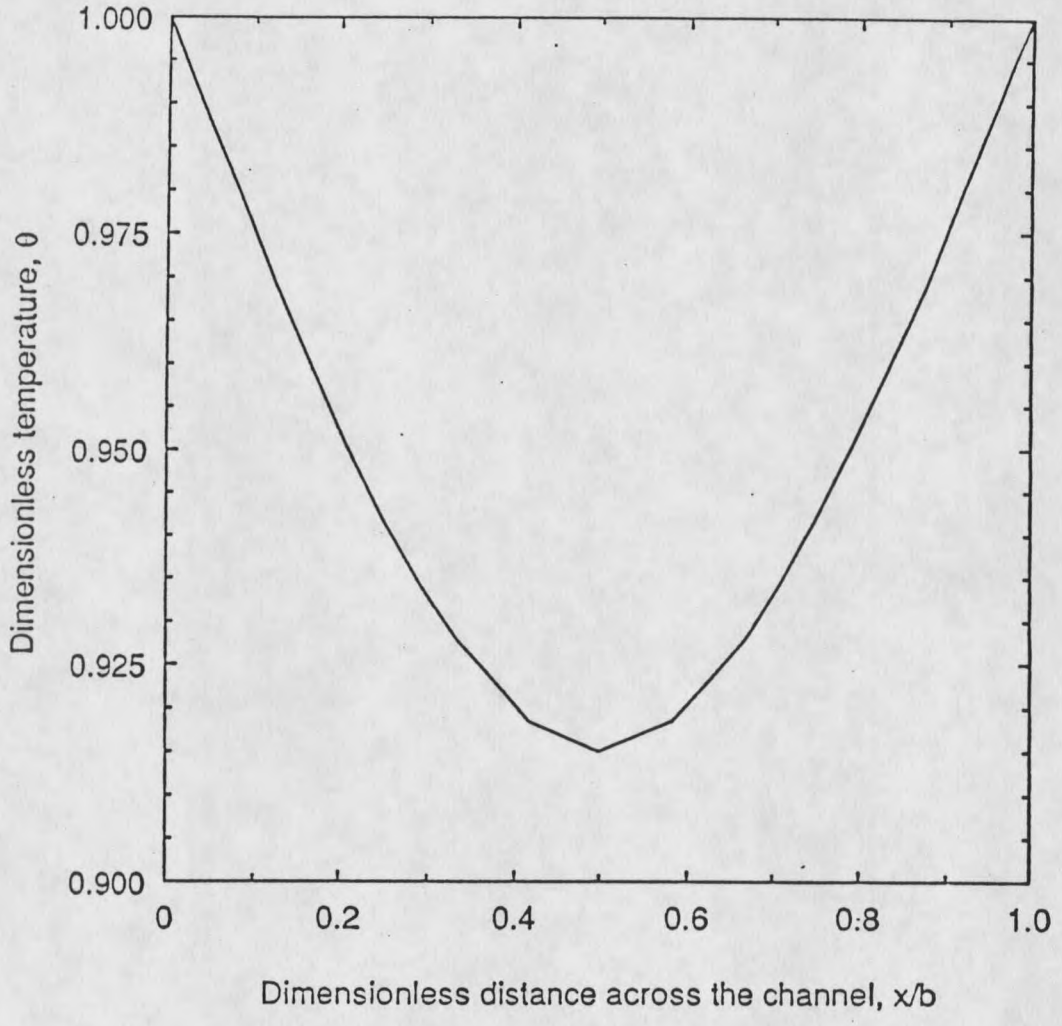


Figure 13. Transverse distribution of temperature at the exit plane for the smooth channel with $Ra=10^3$, Ar = 0.2

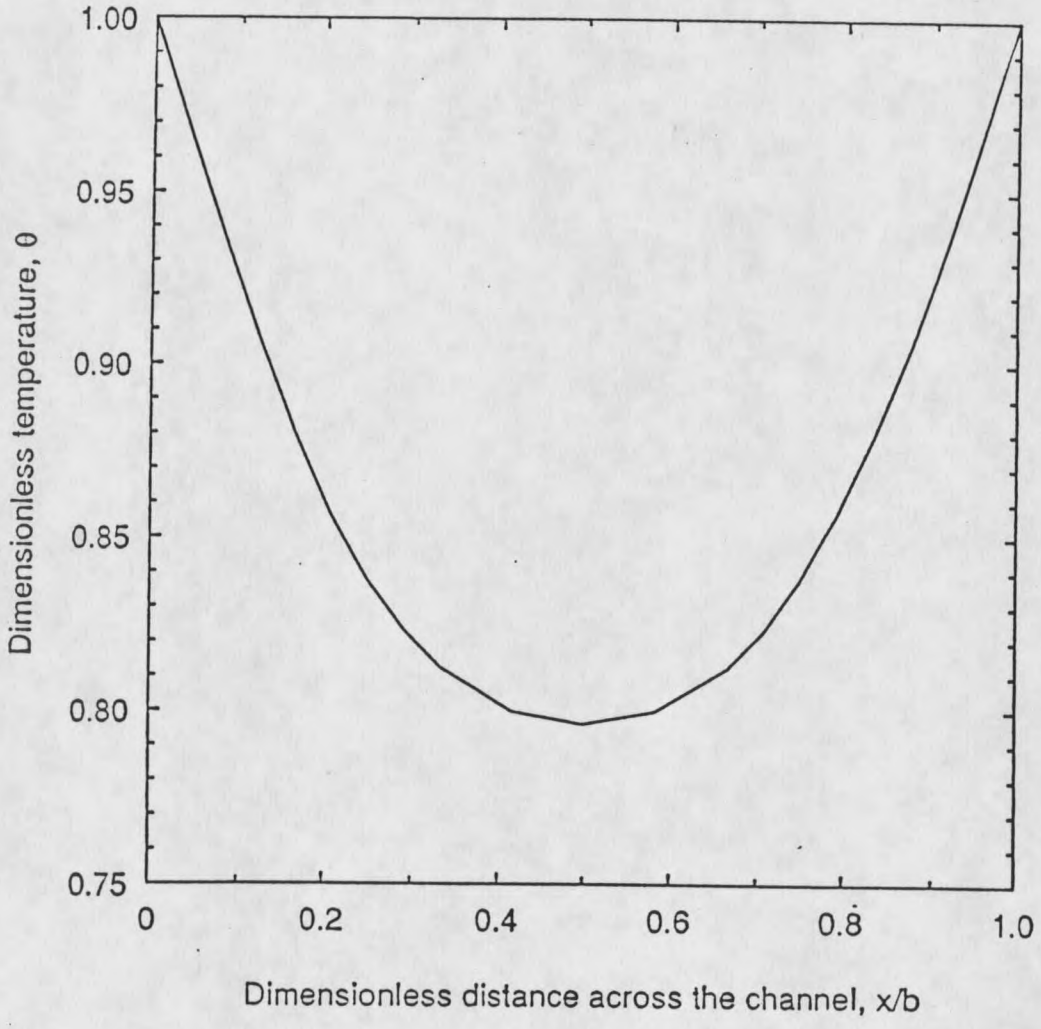


Figure 14. Transverse distribution of temperature at the exit plane for the smooth channel with $Ra=5x10^4$, Ar=0.2

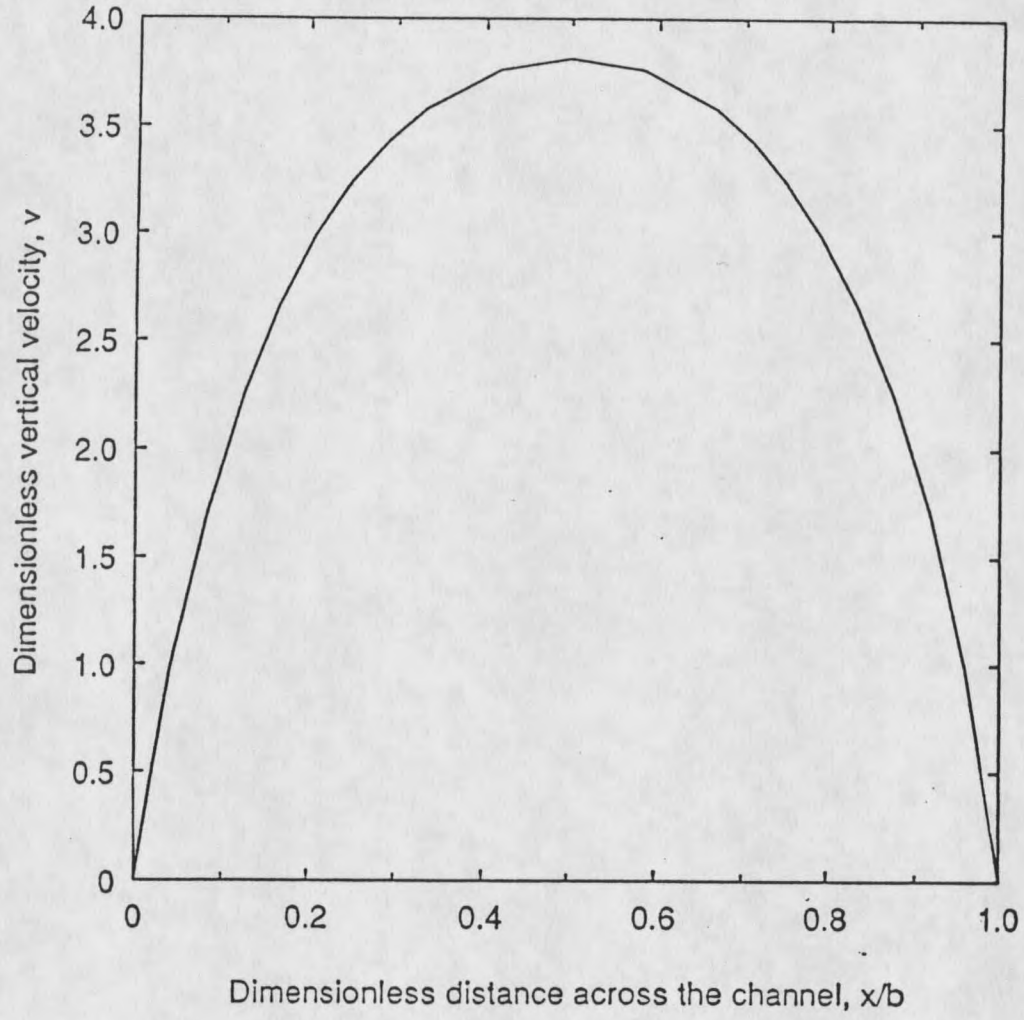


Figure 15. Transverse distribution of inlet velocity for smooth channel with Ra = 10^3, Ar = 0.2

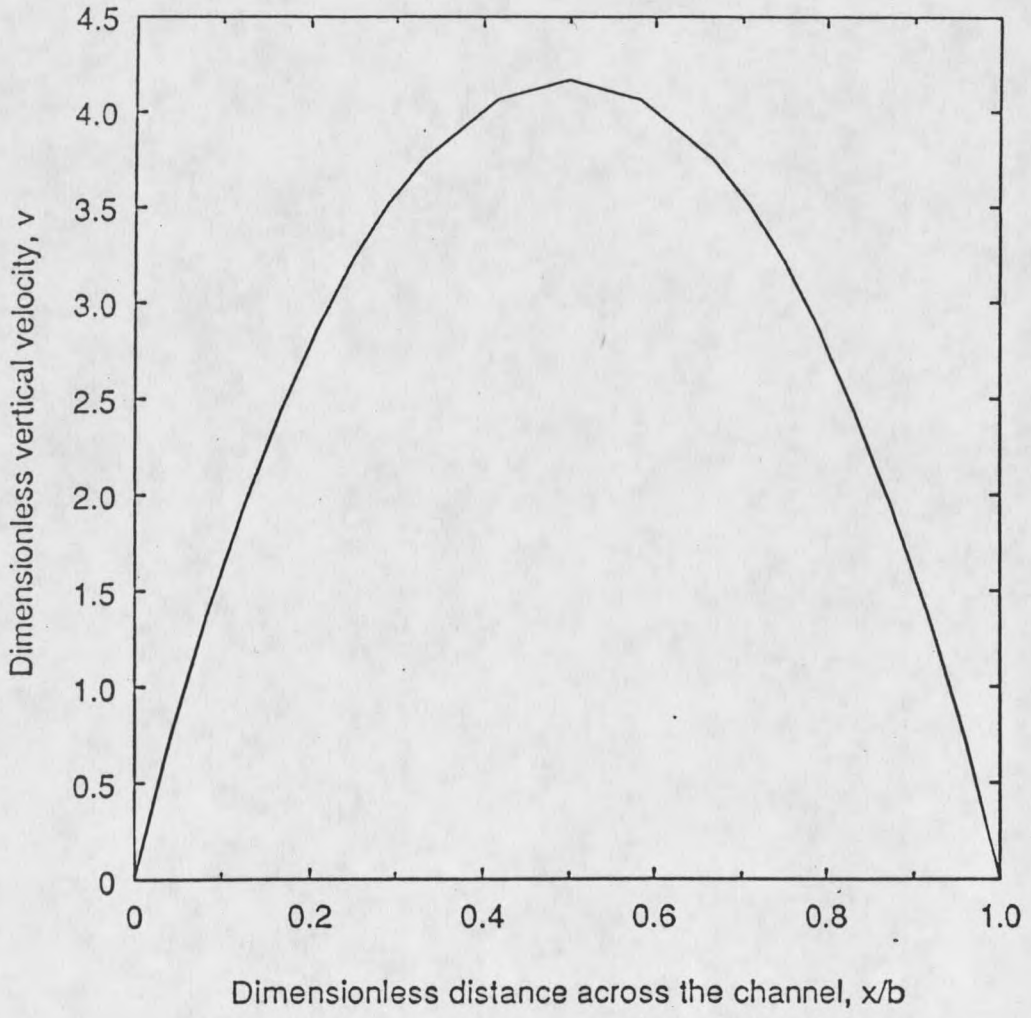


Figure 16. Transverse distribution of exit velocity for smooth channel with Ra = 10^3, Ar = 0.2

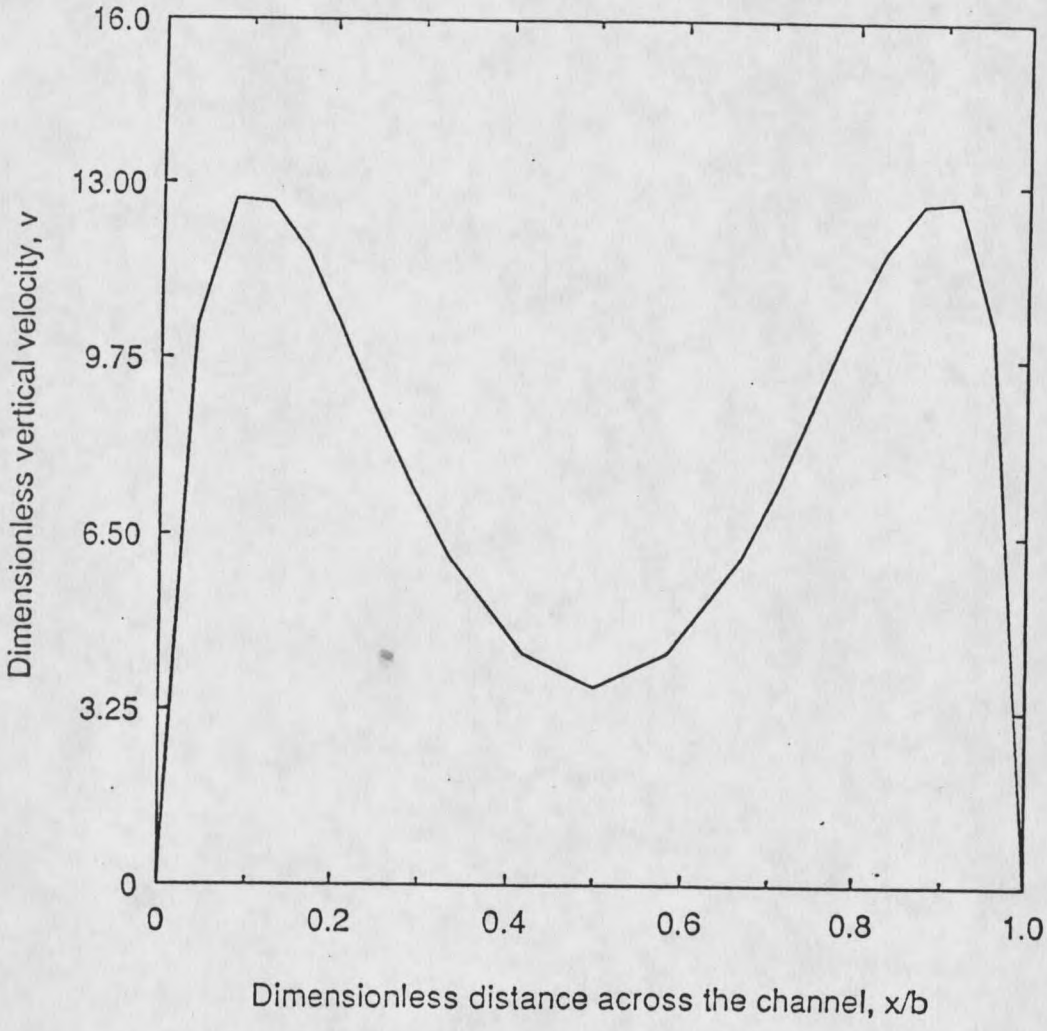


Figure 17. Transverse distribution of inlet velocity for smooth channel with $Ra=5x10^4$, Ar=0.2

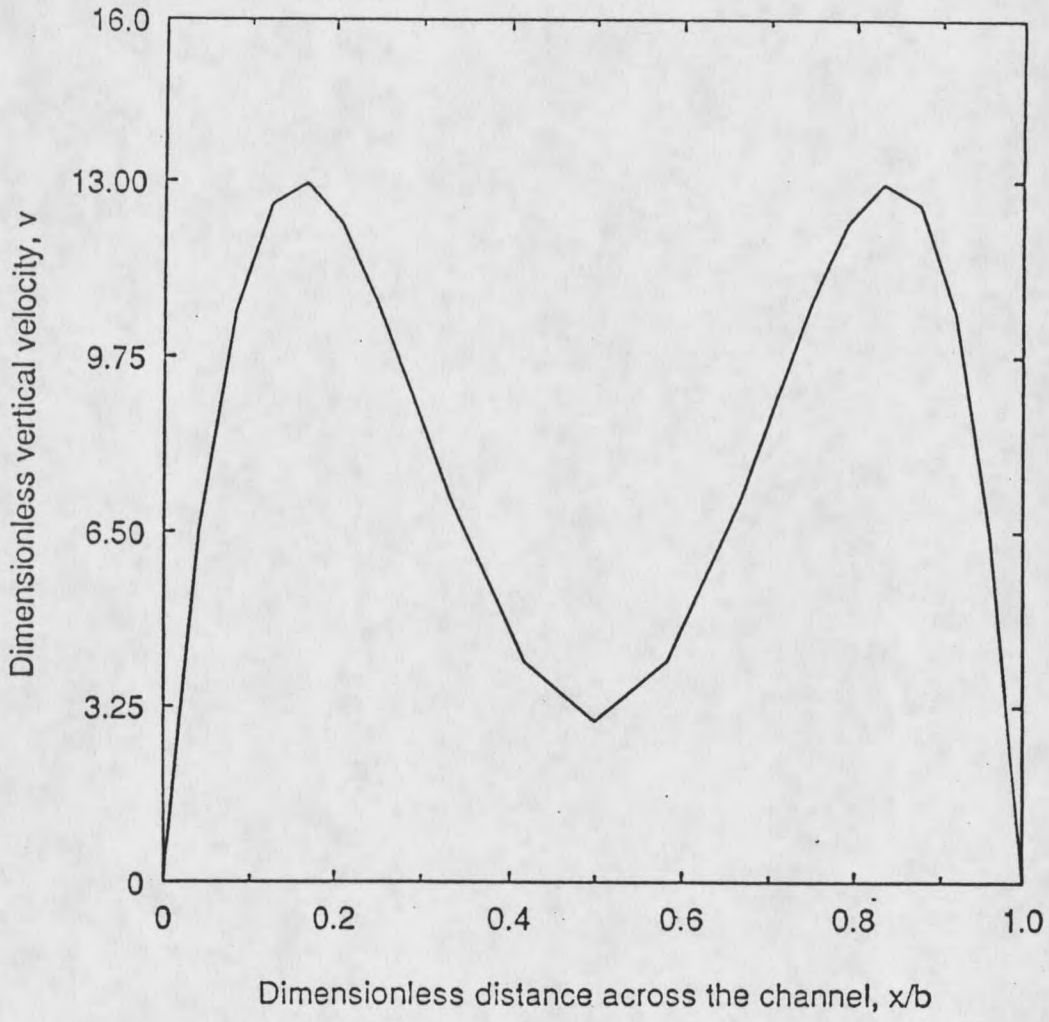


Figure 18. Transverse distribution of exit velocity for smooth channel with Ra=5x10^4, Ar=0.2

Rayleigh numbers. The entrance velocity distribution was determined by applying the natural boundary condition and was observed to be parabolic as shown by Figure 15. It was observed from Figures 16 and 18 that the exit velocity increases as the Rayleigh number increases.

Figure 19 represents the distribution of local Nusselt number along the channel wall for two aspect ratios (0.2, 0.3) at Ra = 10^4. From this figure it can be stated that the local Nusselt number Nu_y, decreases with increasing elevation along the channel wall and increases with increasing aspect ratio. Nusselt number is linearly proportional to the channel width, b. Therefore, as the aspect ratio (=b/L) is increased by increasing b, the Nusselt number also increases. It is also evident from the computed average Nusselt numbers (Nu), that Nu increases with increasing Ra.

From the above observations, it can be summarized that for the smooth channel, as Ra increases, the large induced vertical velocity causes an increase in the energy transport by convection (indicated by the increasing Nu). Also, at high Ra values, because of the large induced vertical velocity, the fluid does not remain long enough in the channel to be heated up to a temperature nearing the wall temperature (indicated by the decreasing center line temperature at the exit plane).

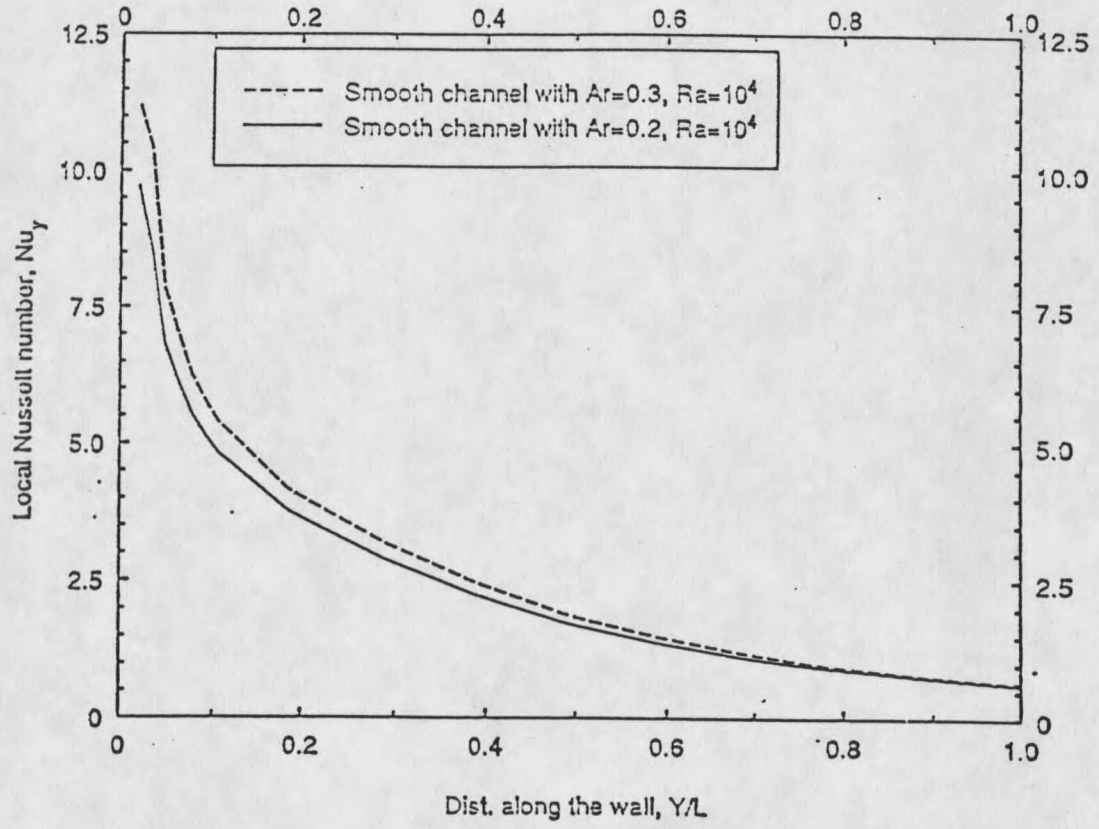


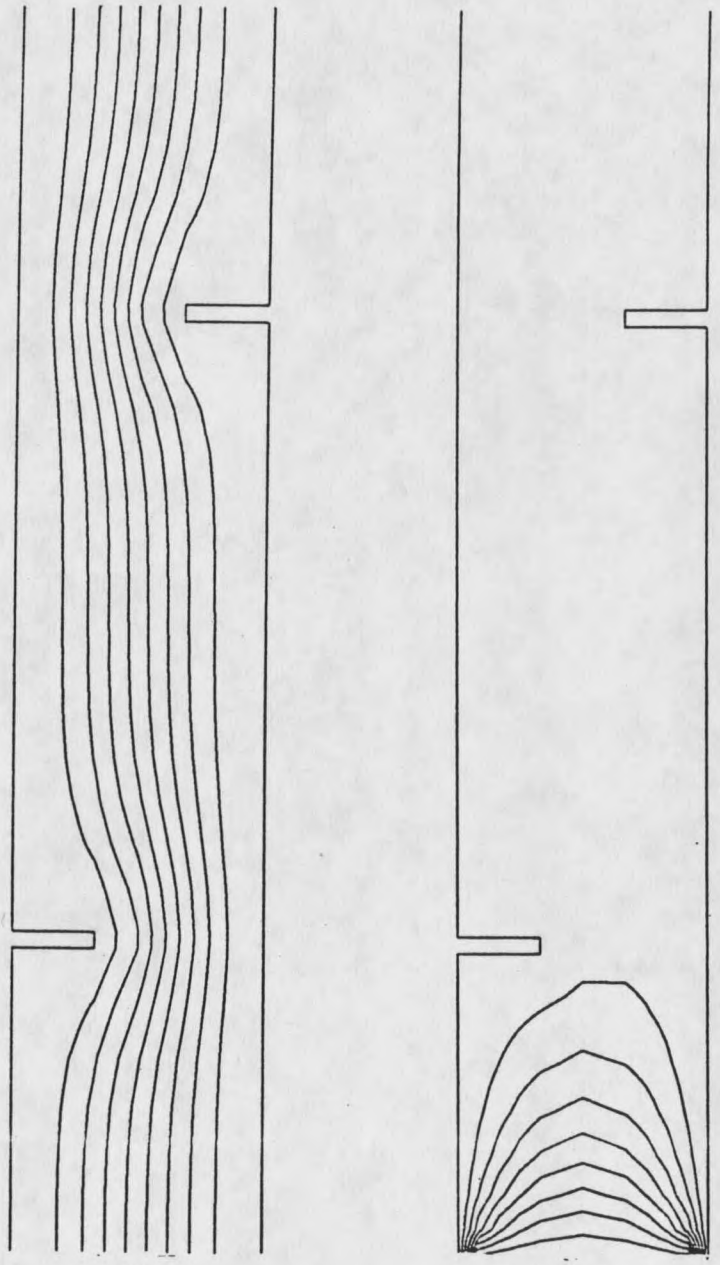
Figure 19. Variation of local Nusselt number with elevation in the smooth channel

Discussion of the Results for the Obstructed Channels

A total of four geometries were employed for the obstructed channel configuration. As mentioned in the previous chapter, these are referred to as geometry I, geometry II, geometry III, and geometry IV. These cases are discussed below in the numerical order. In order to enable the comparison between the smooth and obstructed channels, the streamlines and isotherms are computed for the smooth and obstructed channels at the same Ra values.

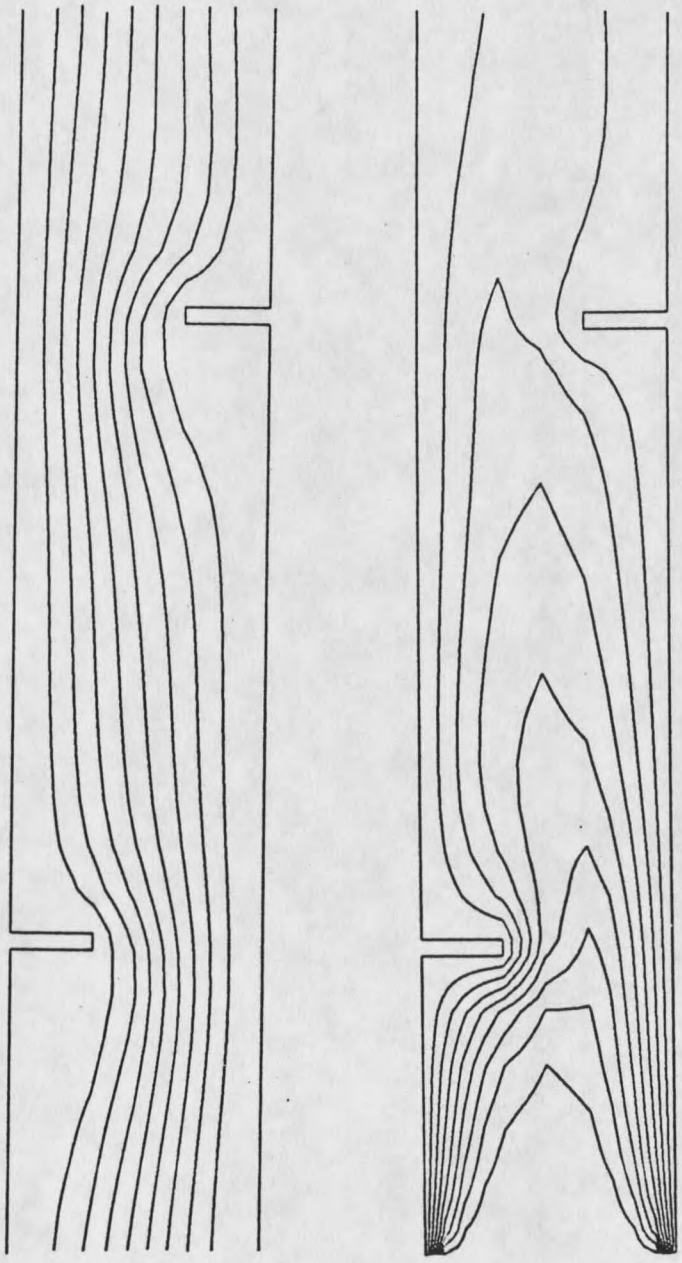
Results for Geometry I

Figures 20 through 23 show the computed streamlines and isotherms for geometry I. The following observations can be made from these figures. (a) From the isotherm plots, it can be observed that at low Rayleigh numbers (e.g., $Ra = 10^2$), all the heat transfer takes place near the entrance region of the channel. In other words, beyond the channel entrance, the fluid temperature approaches that of the wall temperature and as such no heat transfer. In contrast, at high Rayleigh numbers (e.g., $Ra \geq 5 \times 10^3$), the heat transfer takes place throughout the channel length. (b) It can also be observed that large temperature gradients exist near the tip of the lower obstruction ($L_1 = 0.25$) as compared to the upper



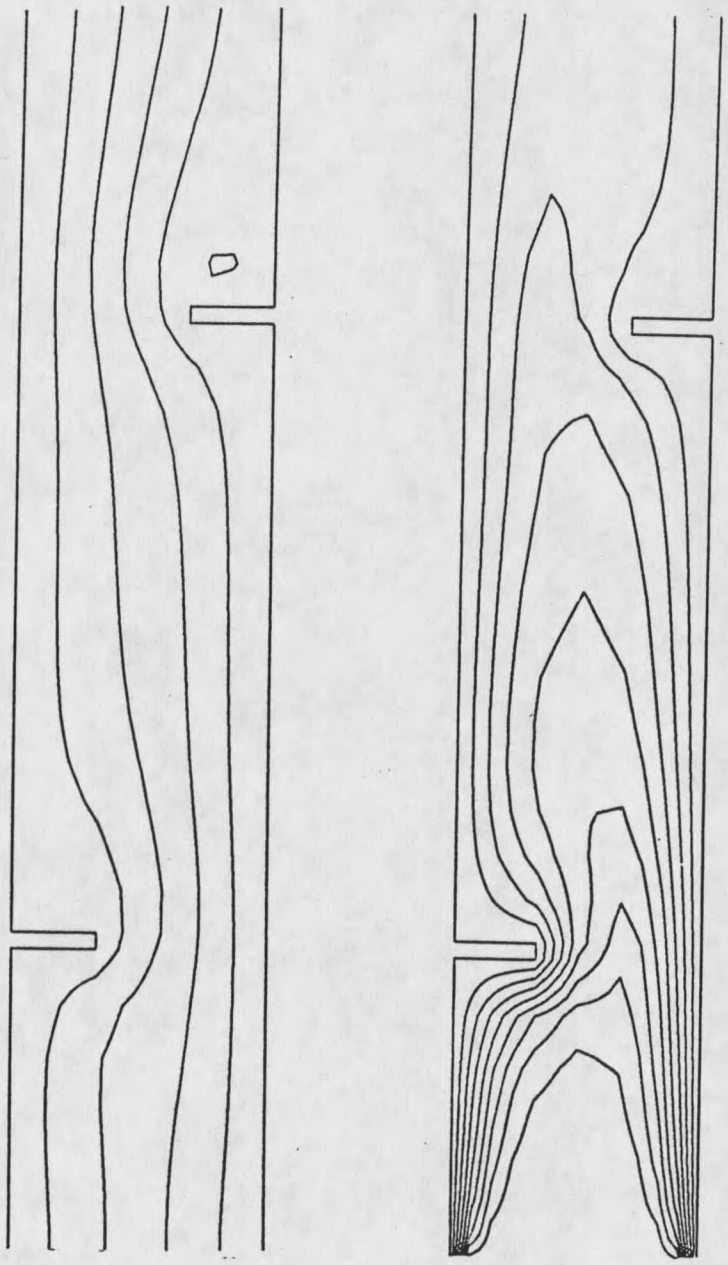
(a) Streamlines (b) Isotherms

Figure 20. Computed streamlines and isotherms for geometry I with $Ra=10^2$, Ar=0.2



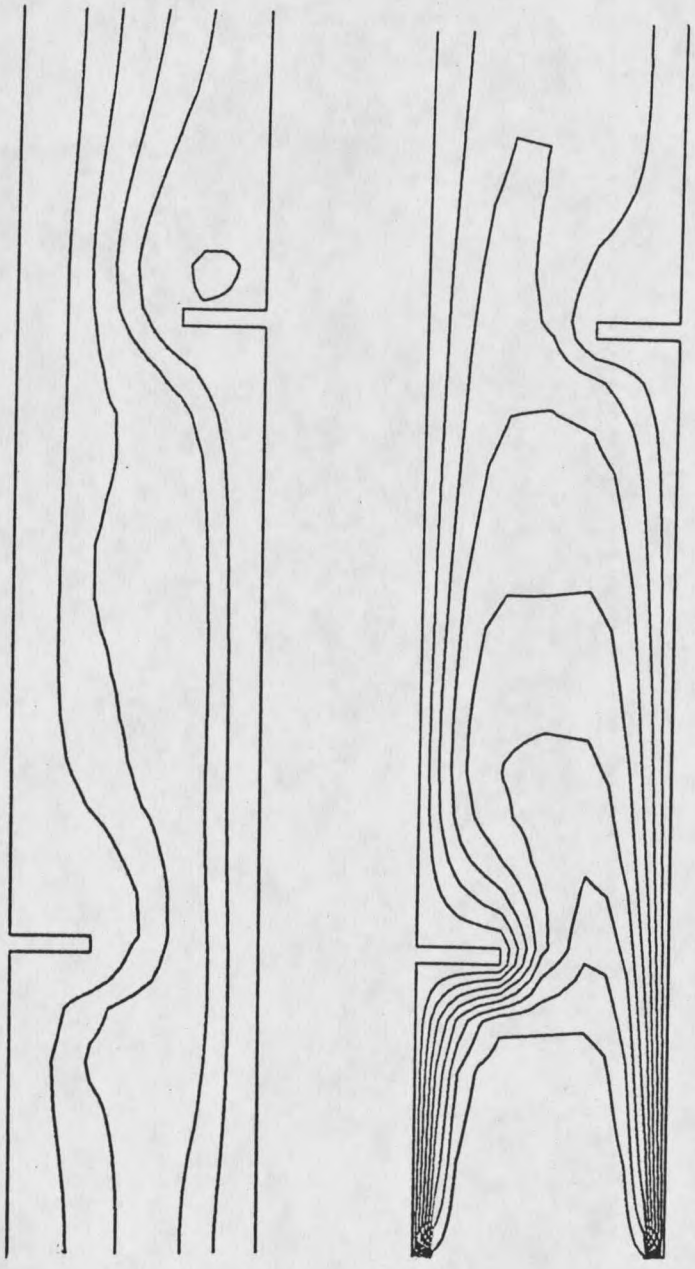
(a) Streamlines (b) Isotherms

Figure 21. Computed streamlines and isotherms for geometry I with $Ra=5x10^3$, Ar=0.2



(a) Streamlines (b) Isotherms

Figure 22. Computed streamlines and isotherms for geometry I with $Ra=10^4$, Ar=0.2



(a) Streamlines (b) Isotherms

Figure 23. Computed streamlines and isotherms for geometry I with $Ra=5x10^4$, Ar=0.2

obstruction (L_2 = 0.75).

(c) For the range of Rayleigh numbers investigated, it can be observed that the streamline pattern around the obstructions is qualitatively similar i.e., denser streamline distribution near the tip of the obstruction (d) From the streamlines, it can be observed that the density of the streamlines increases (i.e., the fluid velocity increases) in the regions around the tips of the obstructions. This is due to (i) reduction in the cross-sectional area of the channel around the tips of the obstructions, (ii) velocity magnitude is proportional to the stream function gradient, and also (iii) the boundary layer thickness is relatively small in the frontal side and particularly around the lower, outside corner of the obstruction.

(e) As the fluid approaches and passes over the obstructions, it undergoes a sequence of deceleration and acceleration. The boundary layer thickness is affected by this series of low and high velocity regions. The boundary layer thickens considerably in the regions above and below the obstruction and this leads to the recirculating zones above and below the obstructions. (f) The recirculating zones below the obstructions are usually quite small and difficult to plot. However, a small recirculating zone above the upper obstruction was detected at higher values of Ra, and is shown in Figure 22 and 23.

Figures 24 and 25 indicate the computed velocity profiles

at y/L = 0, 1 respectively. The profile at y/L = 0 is observed to be symmetric about the channel axis even though the geometry of the channel is not symmetric about the channel axis. From the profile at y/L = 1, the effect of the upper obstruction on the vertical velocity at the exit can be easily seen. Figure 26 shows a typical temperature profile at y/L = 1 and it can be observed that the minimum temperature occurs again on the center line of the channel as in the case of the smooth channel. It was also observed by comparing the temperature profiles at different Rayleigh numbers that this minimum temperature decreases as the Rayleigh number increases.

In order to study the effect of the obstruction on the rate of heat transfer, local Nusselt number of the right wall is plotted against the elevation in the channel (i.e., y/L). It is shown in Figure 27. It is seen from this figure that the lowest local Nusselt numbers are at the two intersections between the obstruction and the wall. The peak local nusselt number (Nu_y) takes place at the lower, outside corner (or tip, e.g., point 3 in figure) of the obstruction. As mentioned earlier, the velocity of the fluid increases in the vicinity of the tip of the obstruction and leads to an increase in the local heat transfer coefficient to a maximum value. The reduction in heat transfer rates at points 2 and 5 in the figure is due to the presence of stagnant fluid and recirculation flow. Figure 28 shows the variation of Nu_y with

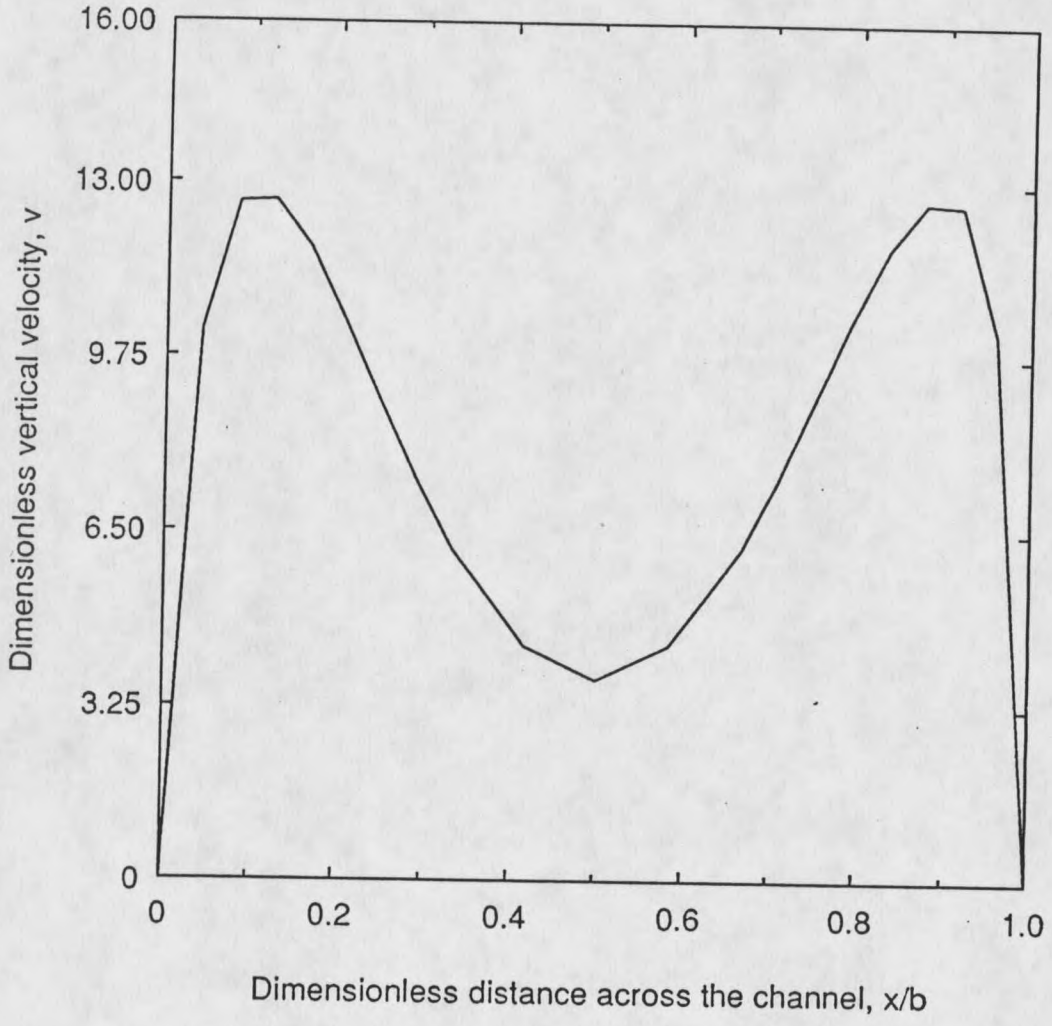


Figure 24. Transverse distribution of inlet velocity for geometry I with Ra = 5 x 10^4, Ar=0.2

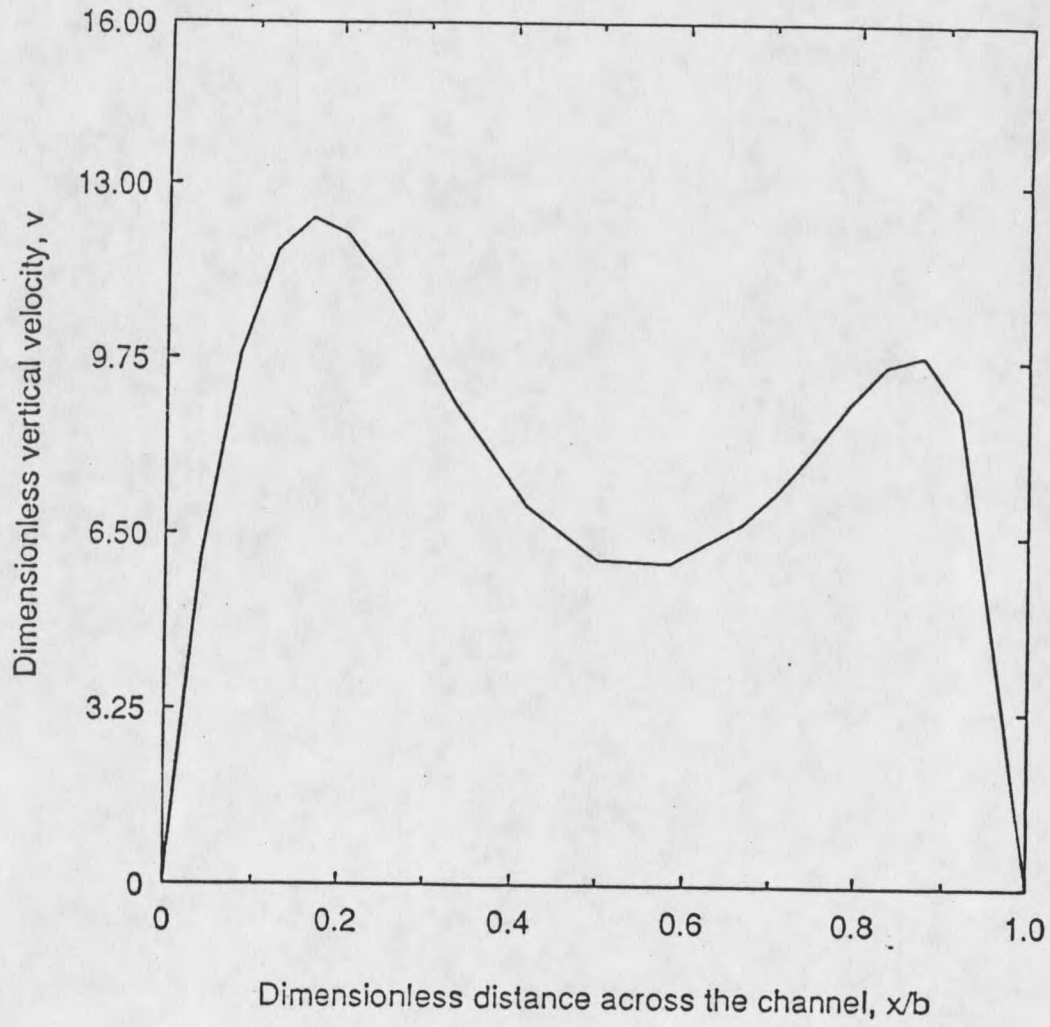


Figure 25. Transverse distribution of exit velocity for geometry I with $Ra=5x10^4$, Ar=0.2

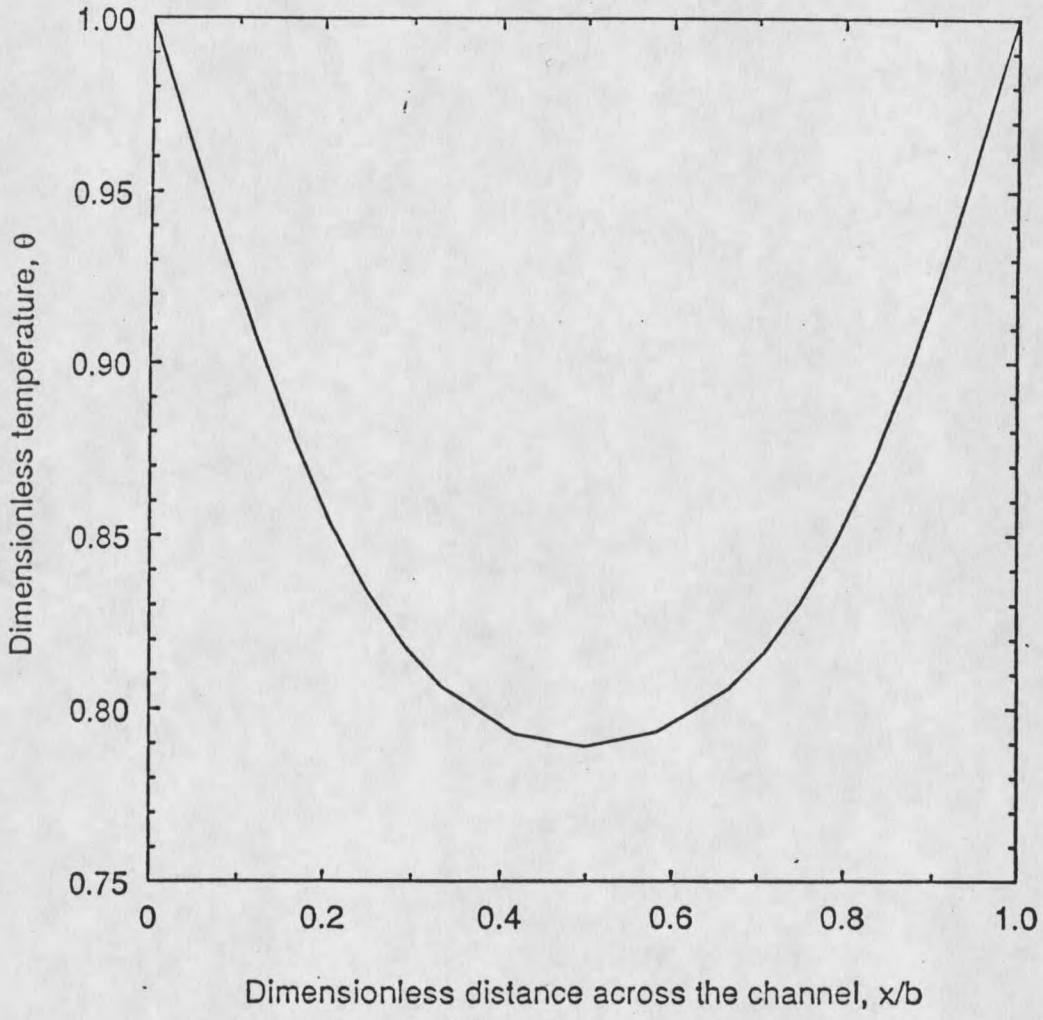


Figure 26. Transverse distribution of temperature at the exit for geometry I with Ra=5x10^4, Ar=0.2

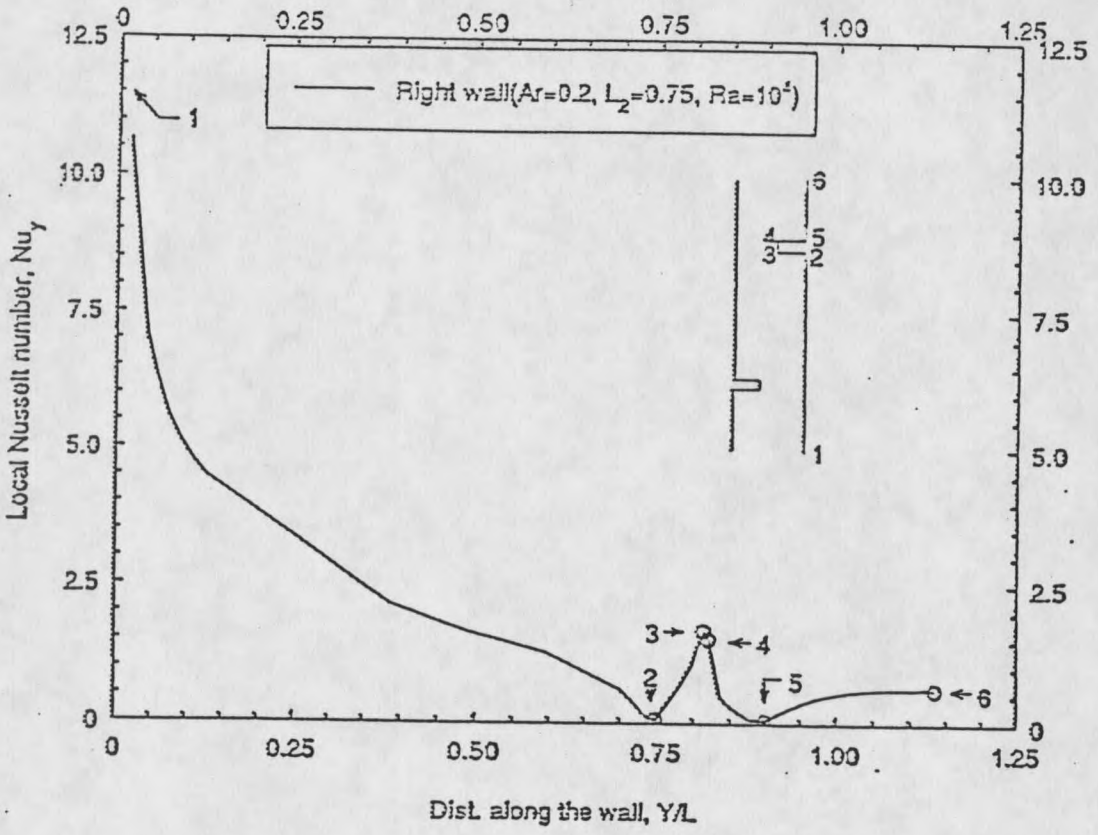


Figure 27. Variation of Nu (right wall) with elevation for geometry I with Ra=10^4, Ar=0.2

the elevation, for the left channel wall. Local Nusselt number attained the maximum and minimum values at the same locations as those for the right channel wall (e.g., maximum at point 3 and minimum at points 2 and 5 in figure).

Results for Geometry II

Figures 29 through 32 show the computed streamlines and isotherms which are symmetric about the vertical axis of the channel. The observations a, c, d, e and f for the previous geometry are also true for this geometry. In this geometry, two relatively large recirculation zones can be observed just above the obstructions at higher values of Rayleigh number. The effect of these recirculating zones on heat transfer is discussed later. The two obstructions for this geometry are facing each other and this reduced the flow cross-sectional area by nearly 67%. This leads to an increased velocity for heat transfer in this region.

Figures 33 and 34 show the computed velocity profiles for geometry II with $Ra = 5 \times 10^4$ at $y/L = 0$ and 1 respectively. The profile at $y/L = 0$ is observed to be symmetric again. The computed temperature profile with $Ra = 5 \times 10^4$ at $y/L = 1$ is shown in Figure 35. Like before, minimum temperature occurred on the center line of the channel and this minimum temperature decreased as Ra increased.

The variation of local Nusselt number along the channel

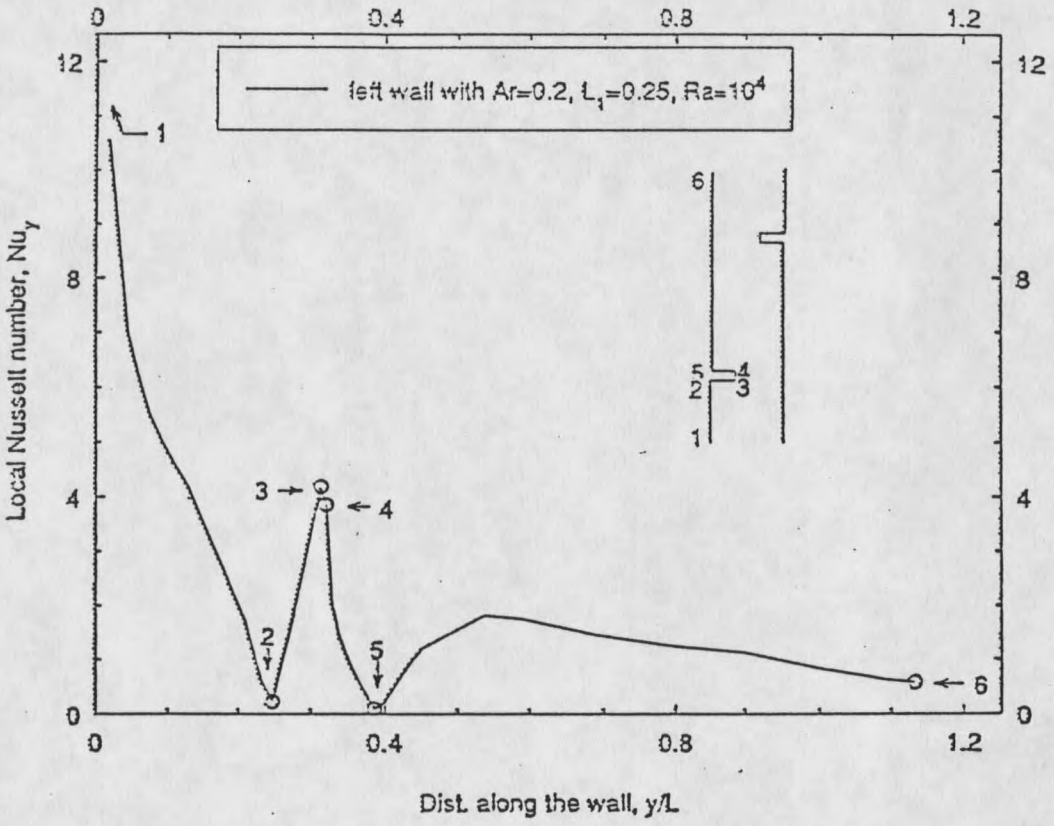
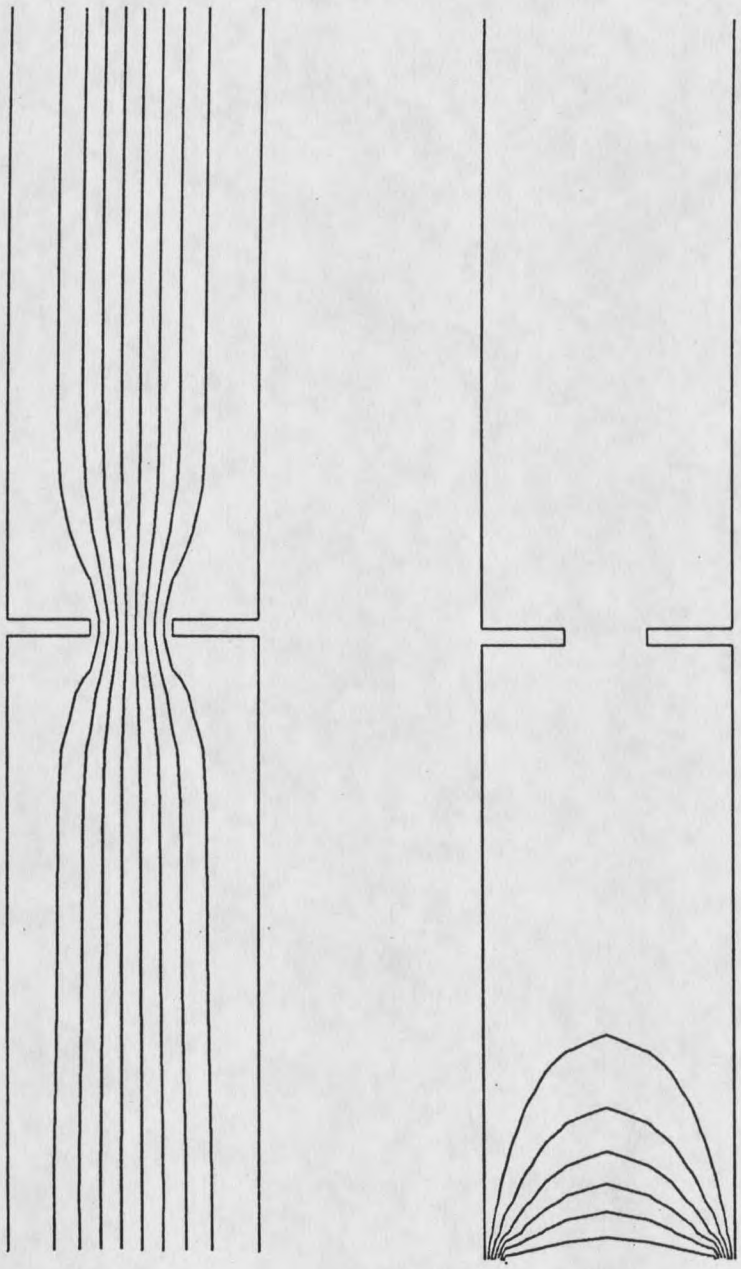
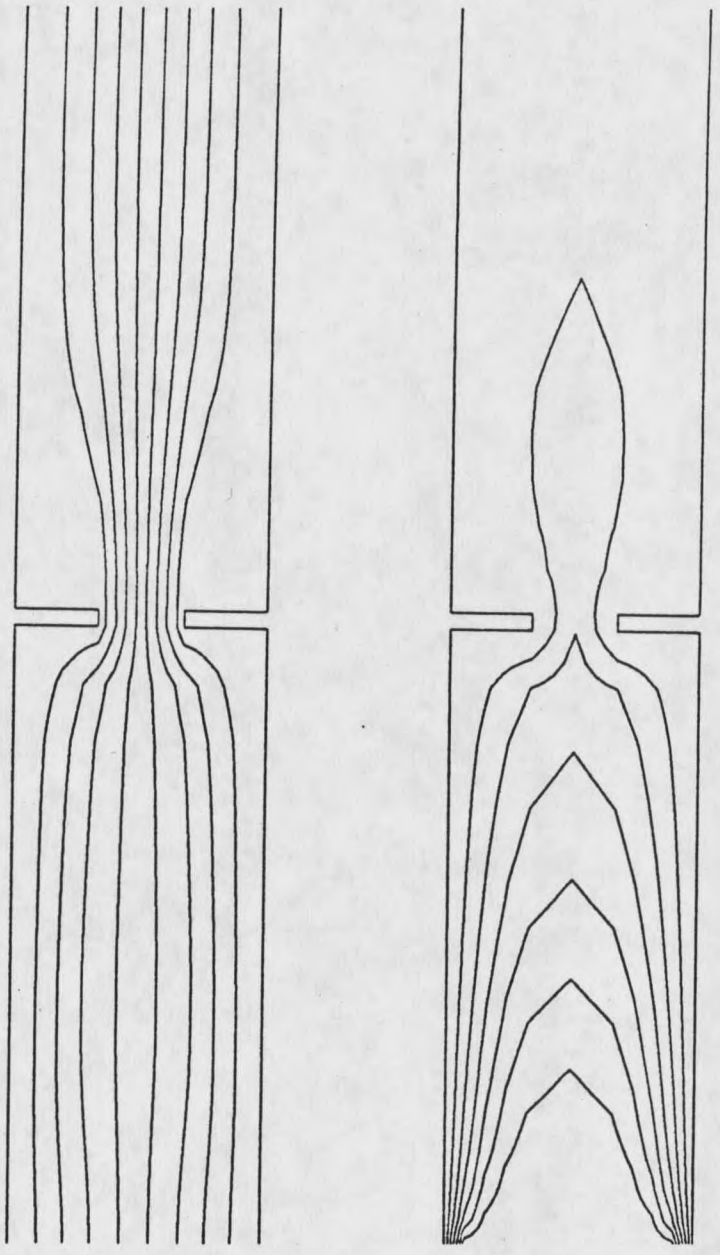


Figure 28. Variation of Nu (left wall) with elevation for geometry I with Ra = 10^4, Ar=0.2



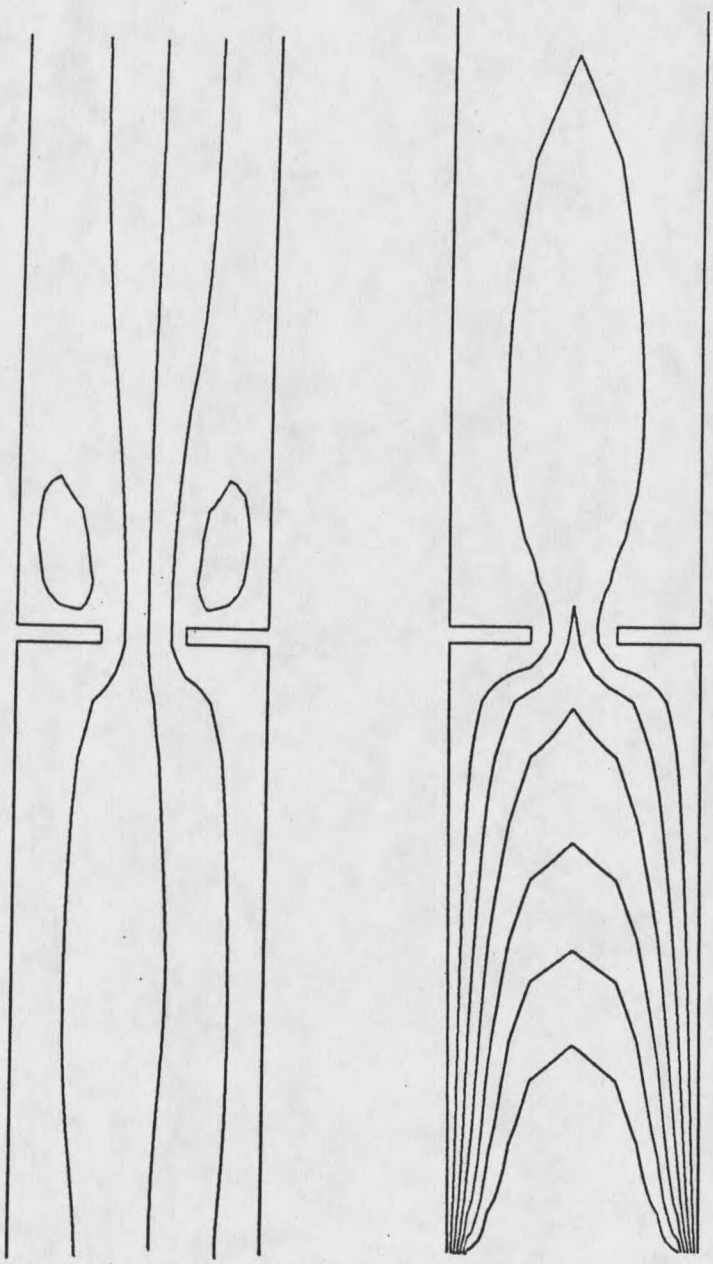
(a)Streamlines (b) Isotherms

Figure 29. Computed streamlines and isotherms for geometry II with Ra = 10^2, Ar=0.2



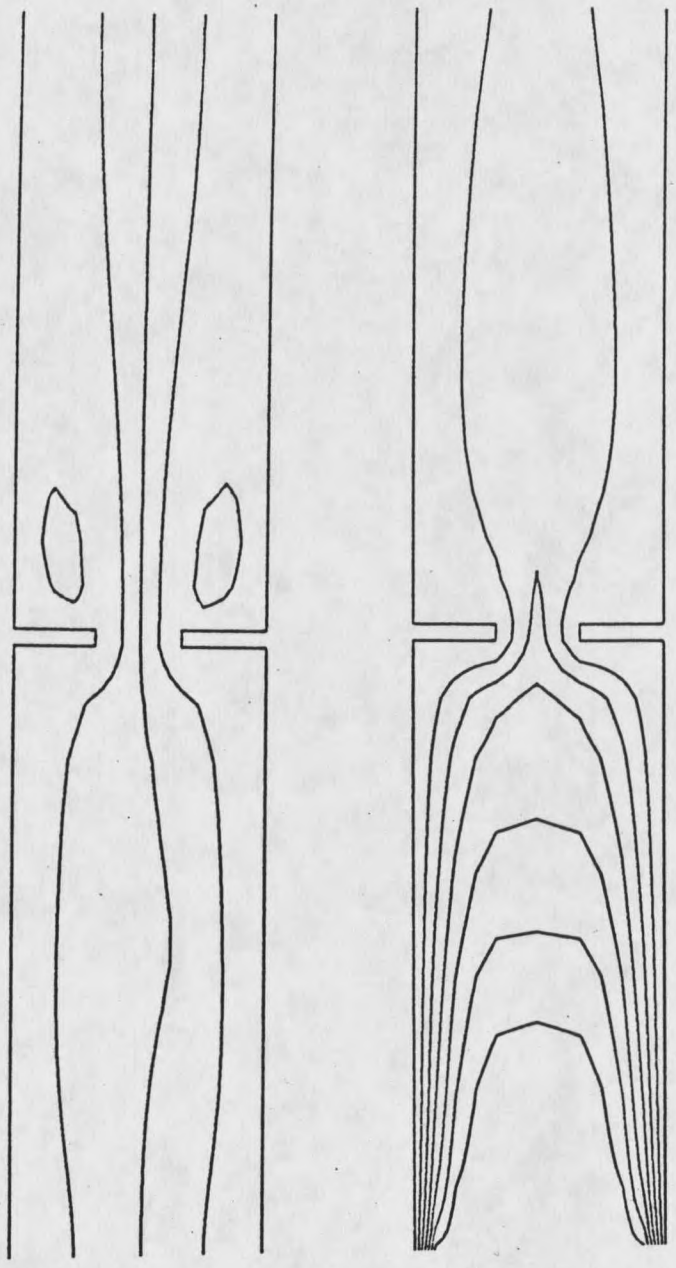
(a) Streamlines (b) Isotherms

Figure 30. Computed streamlines and isotherms for geometry II with $Ra=5x10^3$, Ar=0.2



(a) Streamlines (b) Isotherms

Figure 31. Computed streamlines and isotherms for geometry II with $Ra=10^4$, Ar=0.2



(a) Streamlines (b) Isotherms

Figure 32. Computed streamlines and isotherms for geometry II with $Ra=5x10^4$, Ar=0.2

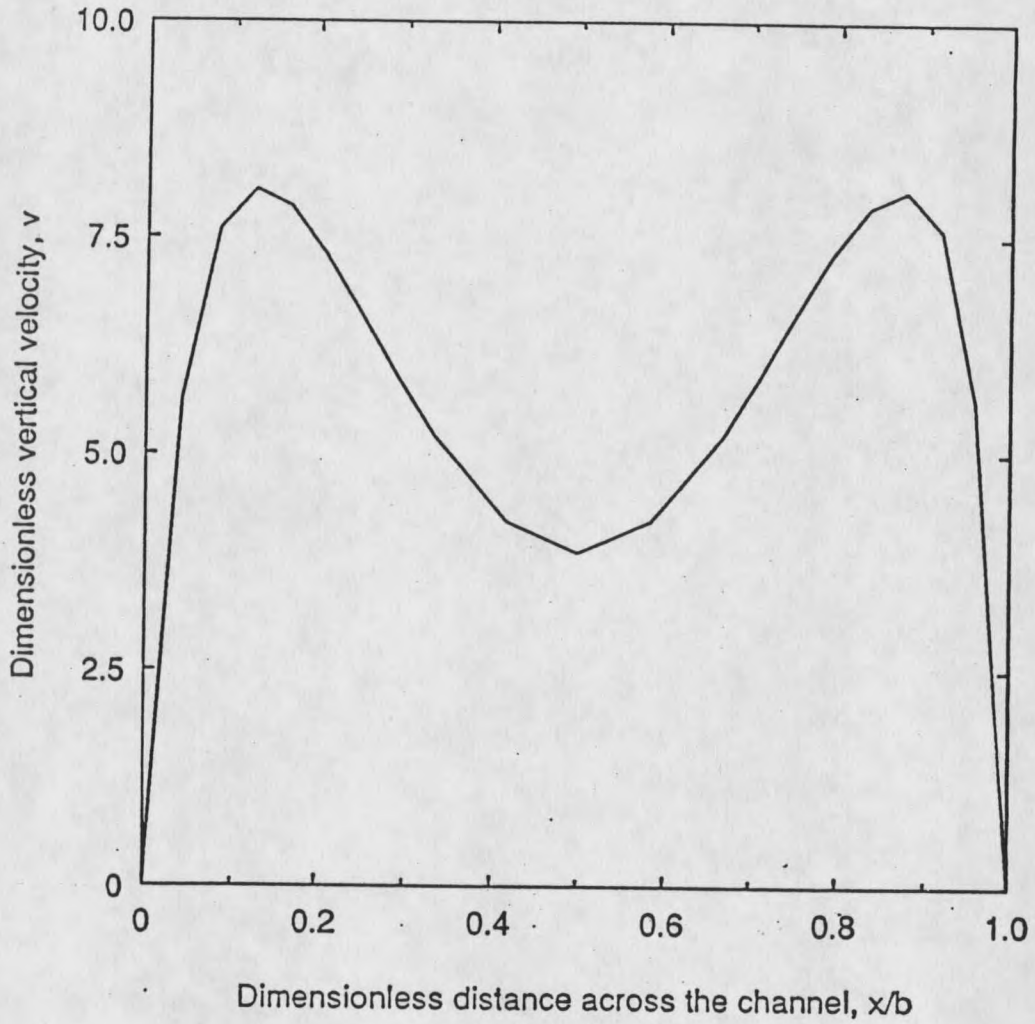


Figure 33. Transverse distribution of inlet velocity for geometry II with $Ra=2x10^4$, Ar=0.2

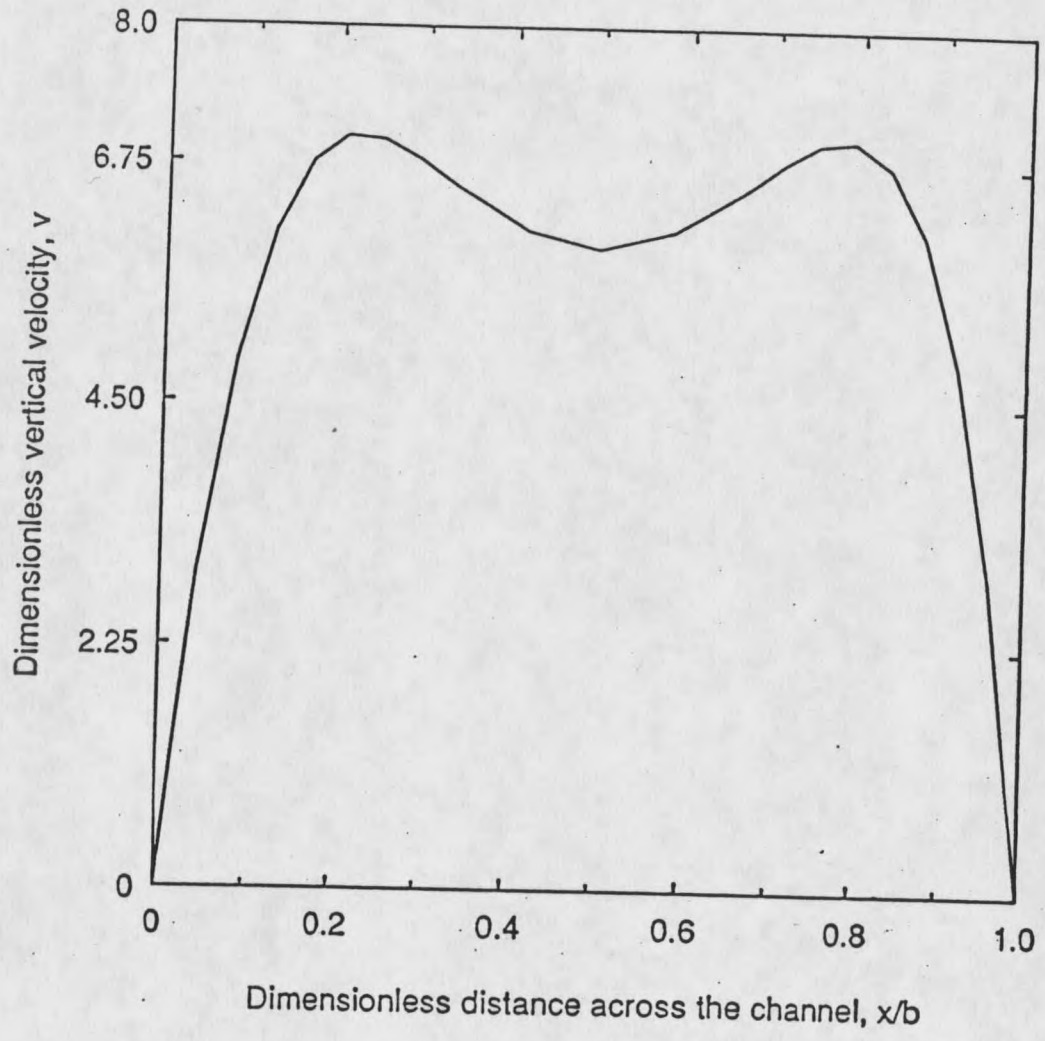


Figure 34. Transverse distribution of exit velocity for geometry II with $Ra=2x10^4$, Ar=0.2

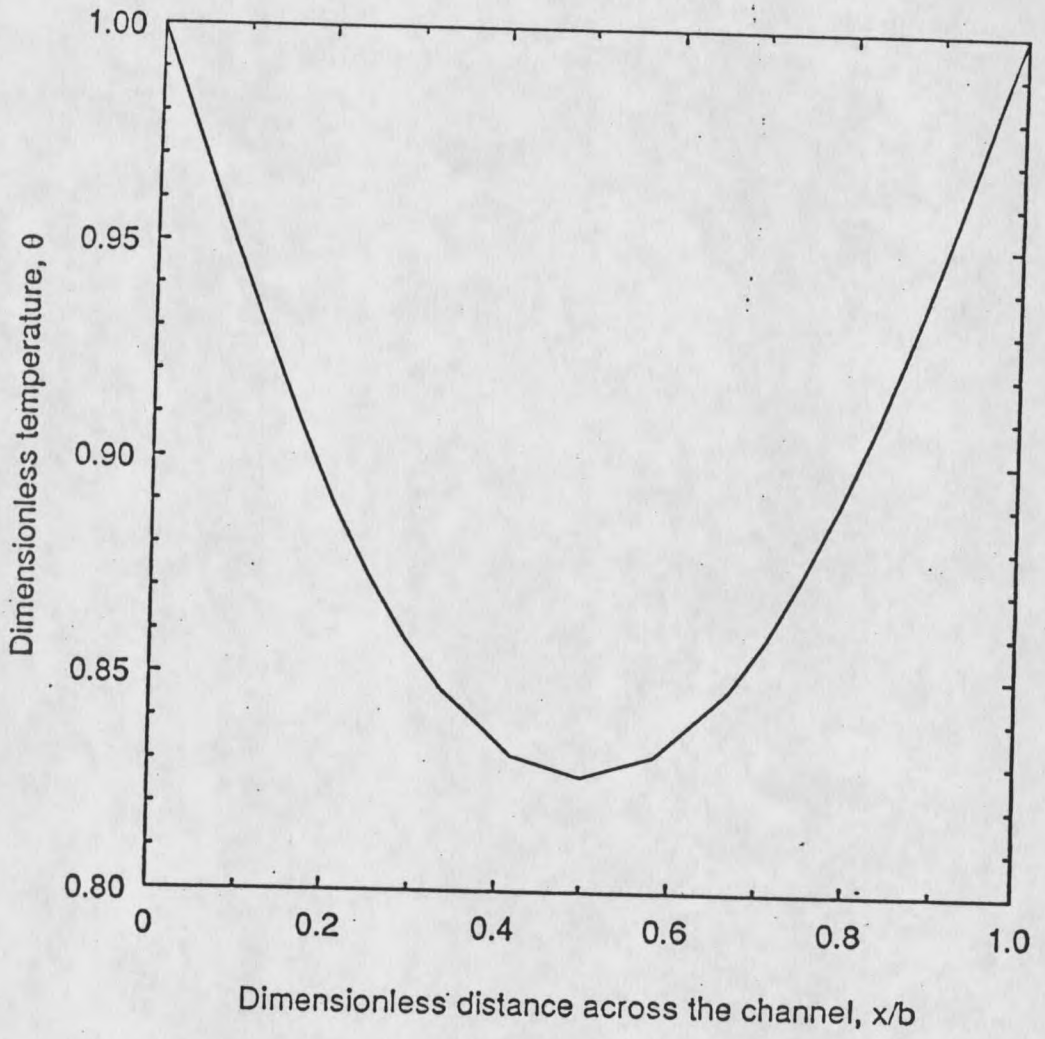


Figure 35. Transverse distribution of temperature at the exit for geometry II with Ra=2×10^4, Ar=0.2

right wall at Ra = 10^4 is shown in Figure 36. It is observed again from this figure that the lowest local Nusselt numbers are at the two intersections between the obstruction and the wall. Same as before, the peak local Nusselt number (Nu_y) occurred at the lower, outside corner (or tip, e.g., point 3 in figure) of the obstruction. In this case, between points 5 and 6, the Nu_y increases first and then decreases. This is different than the case shown in Figure 27, where the local Nusselt number, Nu_y, continuously increases between points 5 and 6. This is due to the effect of the obstruction location on the fluid velocity and thereby the film coefficient. In the case of geometry I (Fig. 27), there was a continuous increase in the velocity of the fluid from the location of the obstruction to the channel exit. In contrast, the velocity of the fluid increased first and then decreased, in the case of geometry II (Fig. 36). Also, for geometry II, because of the higher channel length beyond the obstruction, the fluid remains longer in the channel. This heats up the fluid more and decreases the temperature difference between the fluid and channel wall and hence lower Nusselt number. The local Nusselt number distribution for the left wall was found to be similar to the right wall. This is because of the symmetry of the geometry.

In order to study the effect of multiple obstructions on the heat transfer rate, the computed average Nusselt numbers from the numerical solutions for both obstructed and

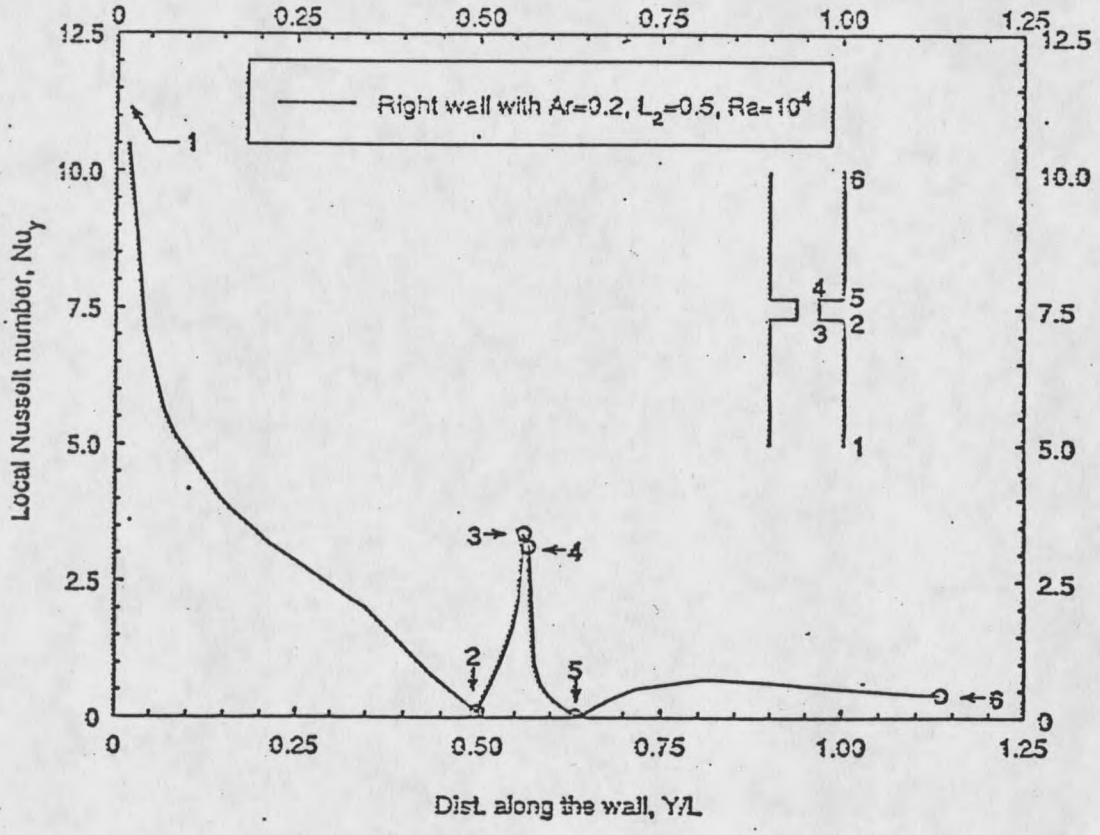


Figure 36. Variation of Nu (right wall) with the elevation for geometry II with $Ra=10^4$, Ar=0.2

unobstructed channels are plotted against the Rayleigh number, Ra. This comparison is shown in Figure 37. The average Nusselt numbers for geometry I are higher than those of geometry II. It is clear from this figure that the obstructions reduced the heat transfer as can be seen from the curve corresponding to the smooth channel. To obtain the amount of reduction in heat transfer due to obstructions, ratio of Nusselt numbers of the obstructed and smooth channels (Nu_o/Nu_s) is plotted against Rayleigh number, Ra. This is shown in Figure 38, for the geometries I and II. At any particular Rayleigh number, the percentage reduction was more for geometry II than geometry I. The maximum reduction in heat transfer for geometry I was approximately 16% and occurred at a Rayleigh number of $5x10^2$. The minimum reduction for this geometry was approximately 5% and occurred at the highest Rayleigh number, i.e., Ra = $5x10^4$. For geometry II, the maximum reduction in heat transfer was approximately 31% at Ra = $5x10^2$, and the minimum reduction in heat transfer was approximately 7.5% at Ra = $2x10^4$.

The above reduction in heat transfer can be explained from the streamline plots of Figures 22 and 31. First of all, the possible mechanisms for altering the heat transfer rates in the channels are: (i) increase in heat transfer due to the increased surface area, (ii) increase in the local heat transfer coefficient due to locally accelerated flow around the obstruction region, and (iii) reduction in

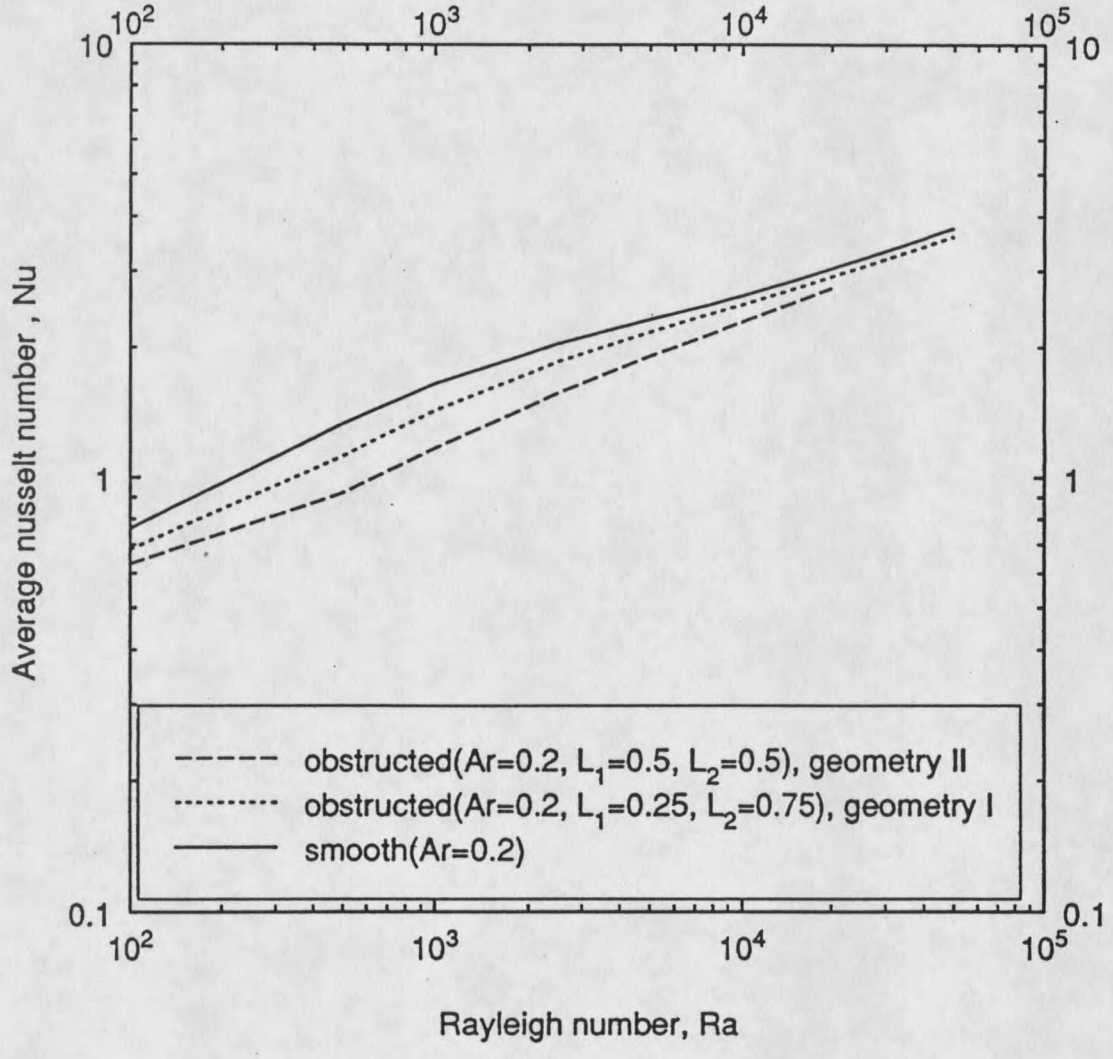


Figure 37. Comparison of the computed average Nusselt numbers for the obstructed and unobstructed channel flows with Ar=0.2

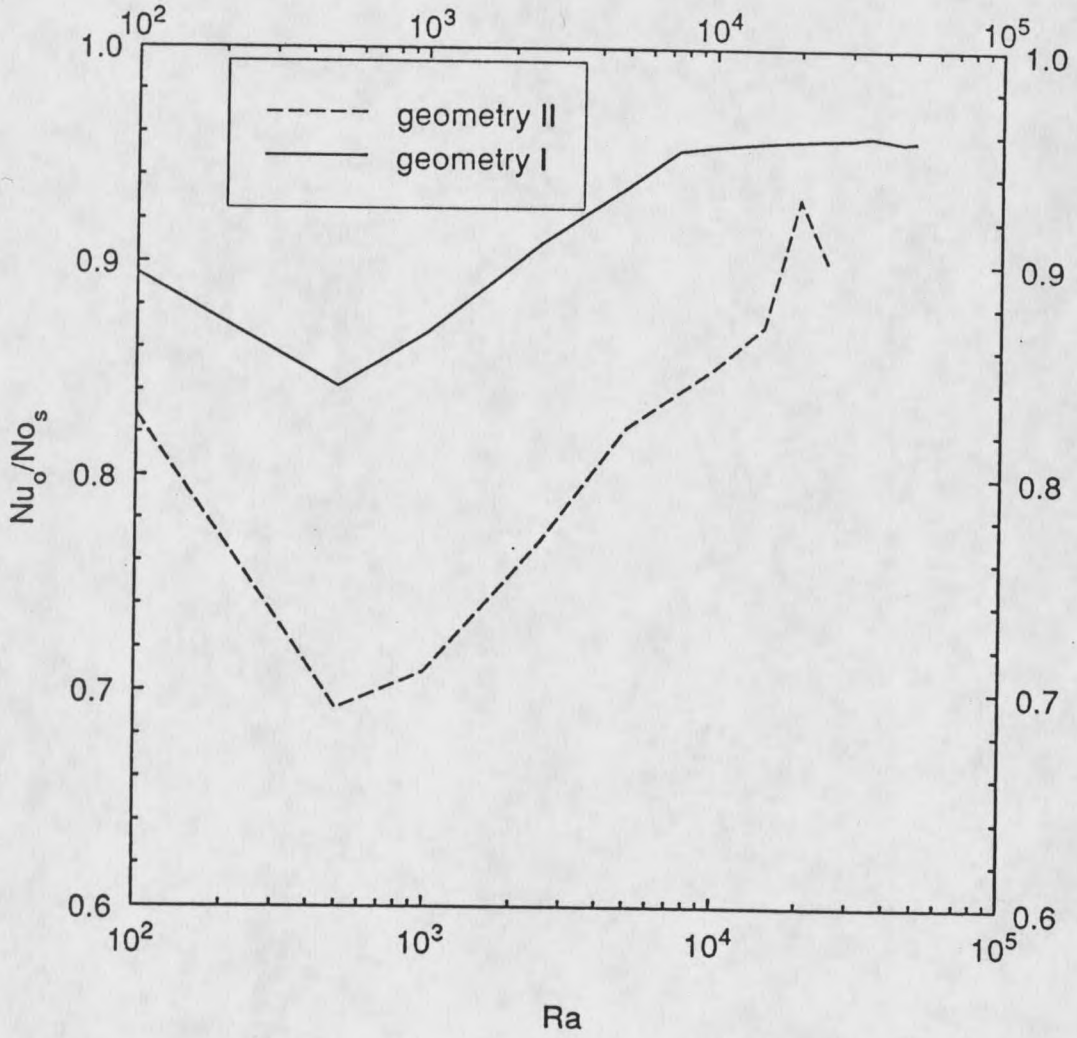
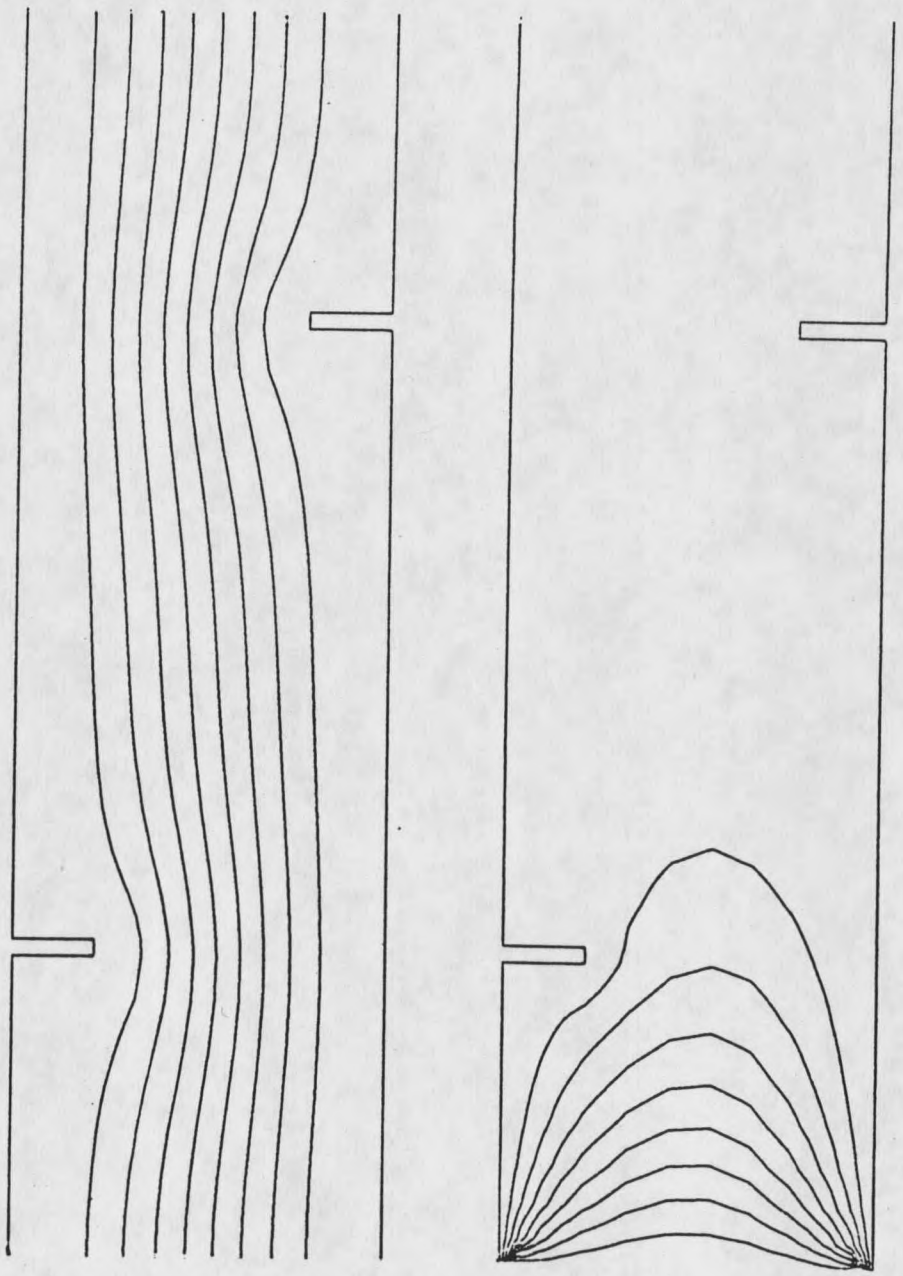


Figure 38. Variation of ratio of Nusselt numbers with Rayleigh number (Ar=0.2)

heat transfer due to the presence of recirculating zones. Recirculating zones reduce the heat transfer as the heat transfer mechanism in these regions is conduction dominated. Therefore, the overall effect of multiple obstructions on heat transfer is a combination of all the above mechanisms. The heat transfer in the obstructed channels increases or decreases depending on the cumulative effect of the above three mechanisms. The increase in the surface area due to the obstructions is the same in both the geometries I and II. This means more heat transfer in both the cases due to mechanism (i). From the velocity field, the velocity around the tip of the obstructions in geometry II was observed to be higher than the corresponding velocity in geometry I. This means higher local heat transfer due to the accelerated flow near the obstructions in geometry II as compared to geometry I [mechanism (ii)]. Considering only these two mechanisms, average Nusselt numbers of geometry II need to be higher than those of geometry I. But, the average Nusselt numbers of geometry II are observed to be lower than those of geometry I. This is because of the predominant effect of mechanism (iii) in geometry II. That is, the recirculating flow regions substantially reduce the overall heat transfer rate for this geometry.

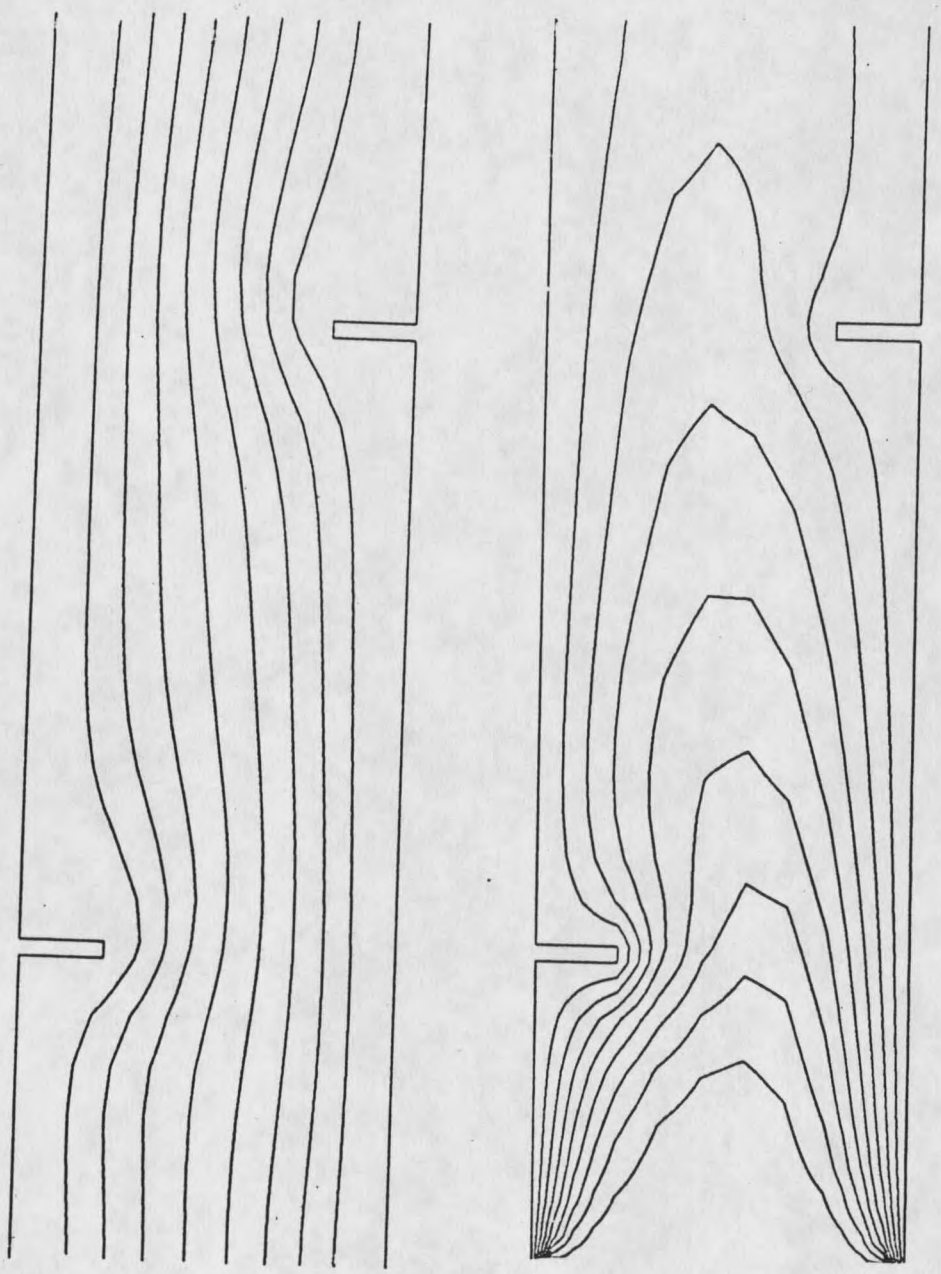
Results for Geometry III

The geometries III and IV were studied in order to investigate the effect of the channel aspect ratio (Ar = b/L) on heat transfer by keeping the location and size of the obstructions as before (i.e., as in geometries I and II). Figures 39 through 42 represent the computed streamlines and isotherms for geometry III. The qualitative pattern of these streamlines and isotherms is observed to be similar to those of geometry I. The observations a, b, c, and d of geometry I were found to apply to this case. This is the only case for which the recirculating zone can not be obtained graphically. However, the velocity field indicate that very small recirculating zones are present above and below the obstructions. Figures 43 and 44 represent the computed vertical velocity profiles with Ra = 5×10^4 at y/L = 0, 1 respectively. Effect of the obstruction on the vertical velocity at the exit plane can be clearly seen from Figure 44. Figure 45 is the computed temperature profile with Ra = 5×10^4 at y/L = 1. Like the previous two geometries, the minimum temperature occurred on the center line of the channel and this minimum temperature decreased as Ra increased.



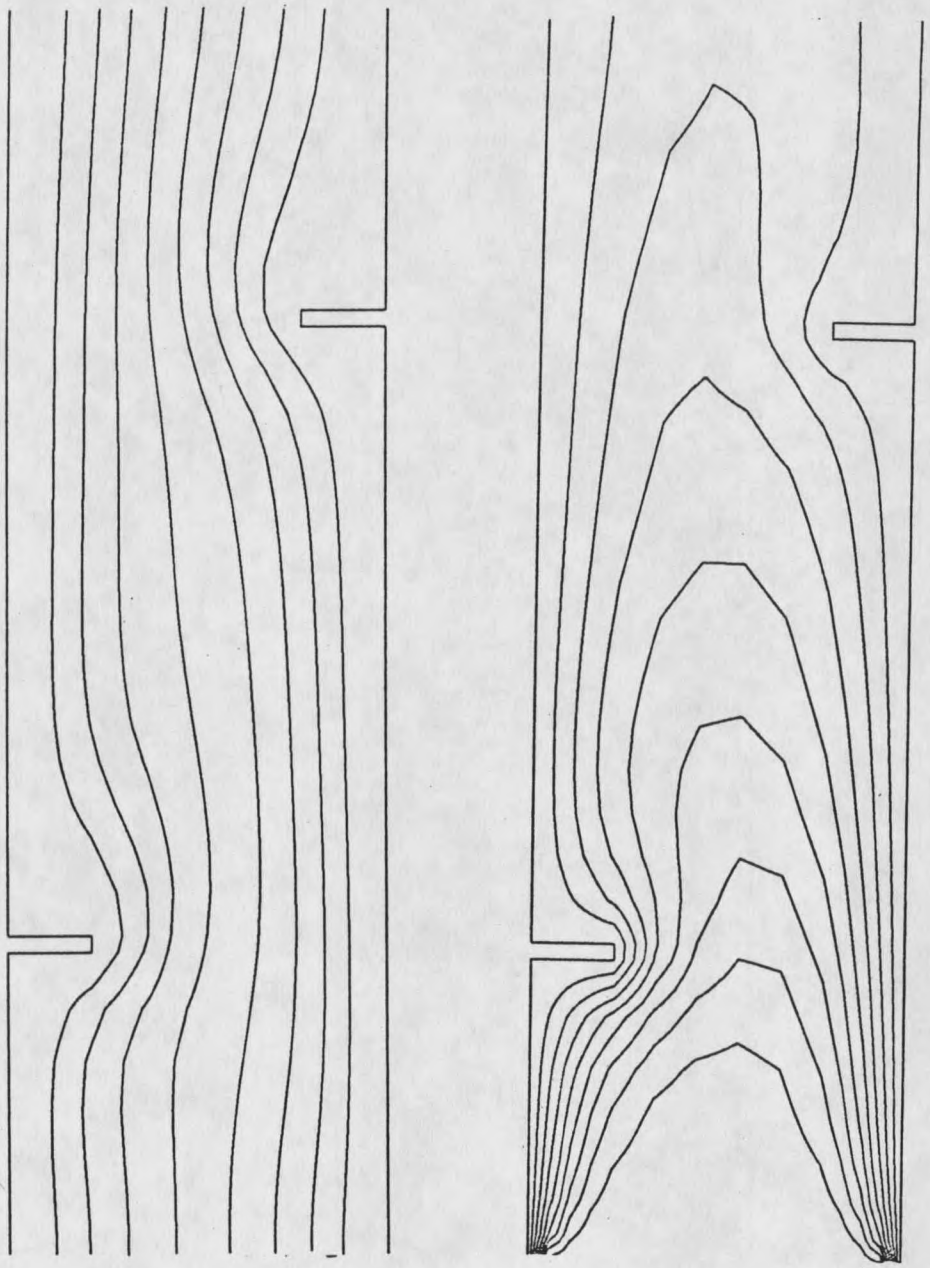
(a) Streamlines (b) Isotherms

Figure 39. Computed streamlines and isotherms for geometry III with $Ra=10^2$, Ar=0.3



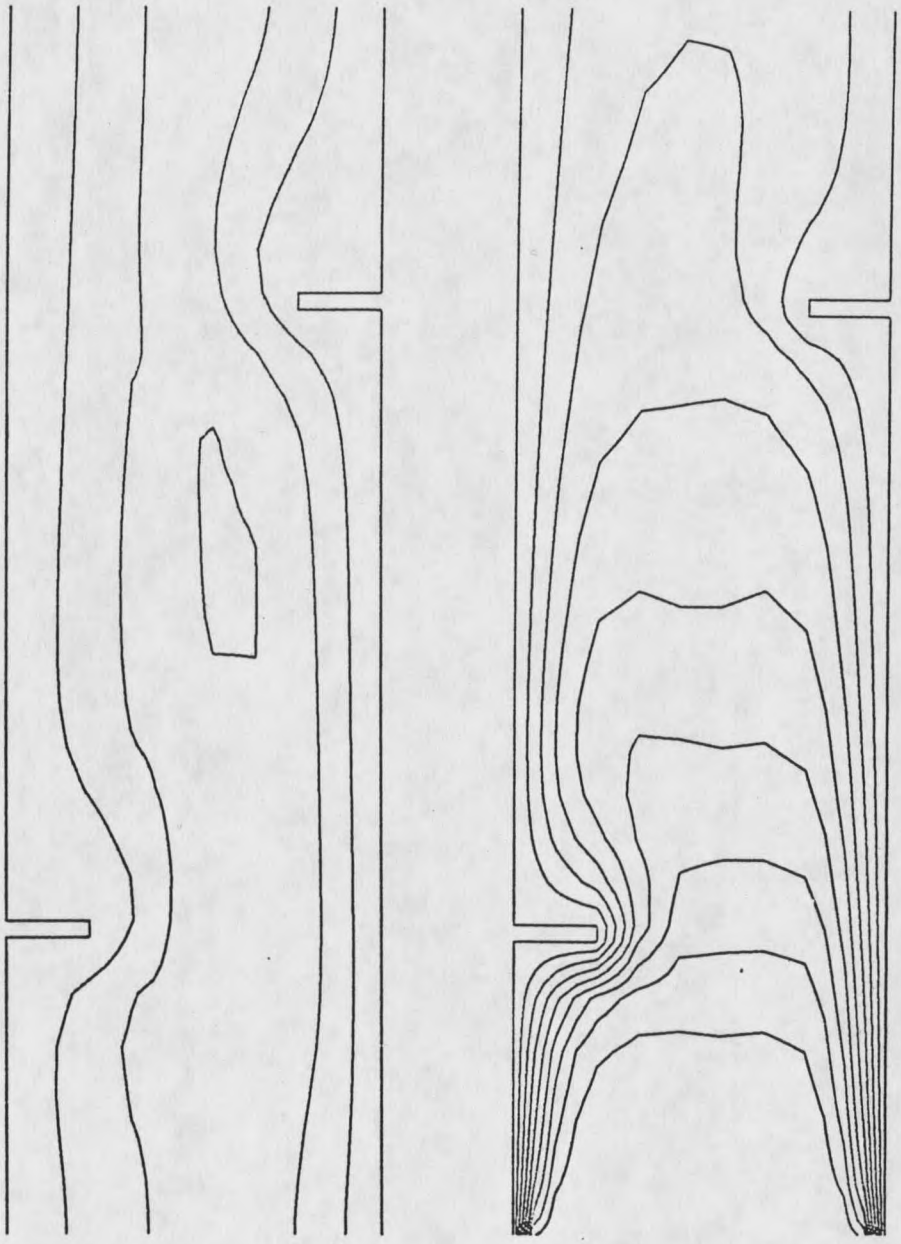
(a) Streamlines (b) Isotherms

Figure 40. Computed streamlines and isotherms for geometry III with $Ra=5x10^3$, Ar=0.3



(a) Streamlines (b) Isotherms

Figure 41. Computed streamlines and isotherms for geometry III with $Ra=10^4$, Ar=0.3



(a) Streamlines (b) Isotherms

Figure 42. Computed streamlines and isotherms for geometry III with $Ra=5x10^4$, Ar=0.3

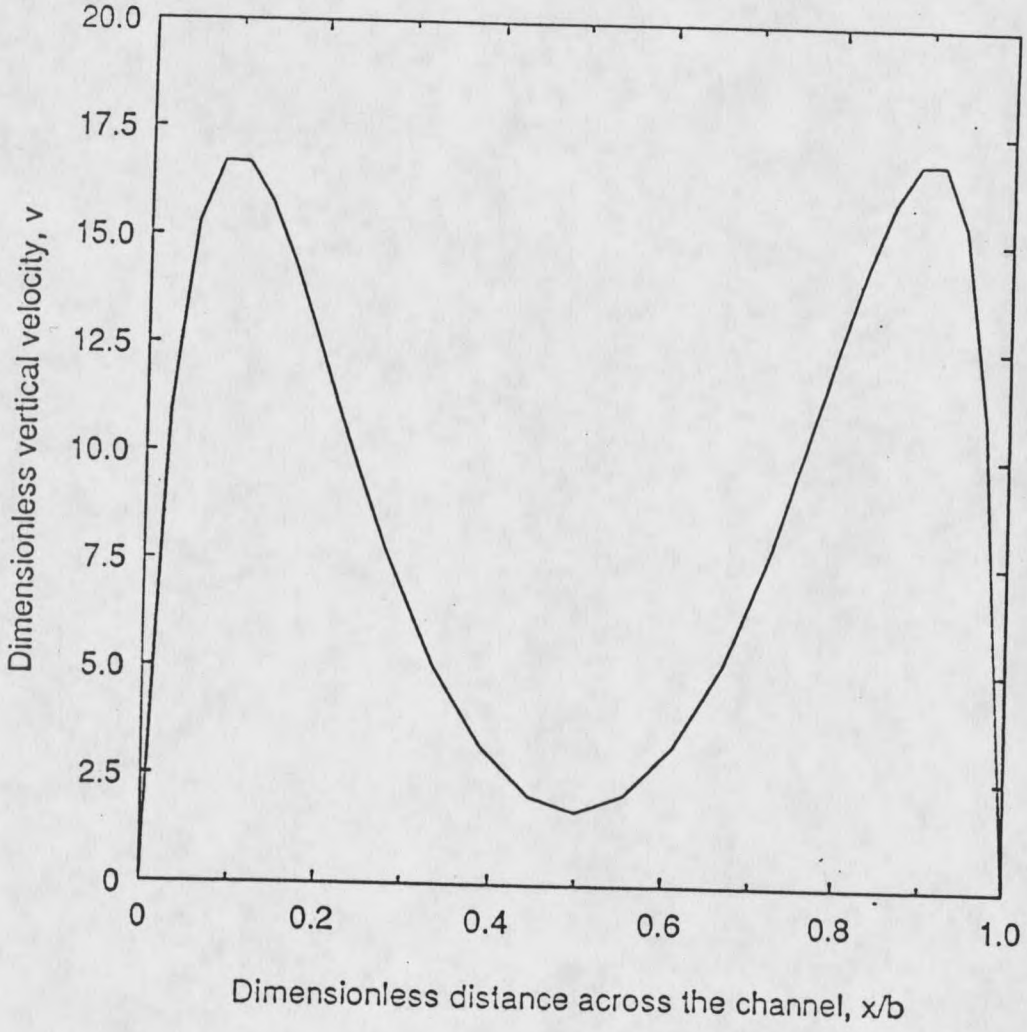


Figure 43. Transverse distribution of inlet velocity for geometry III with $Ra=5x10^4$, Ar=0.3

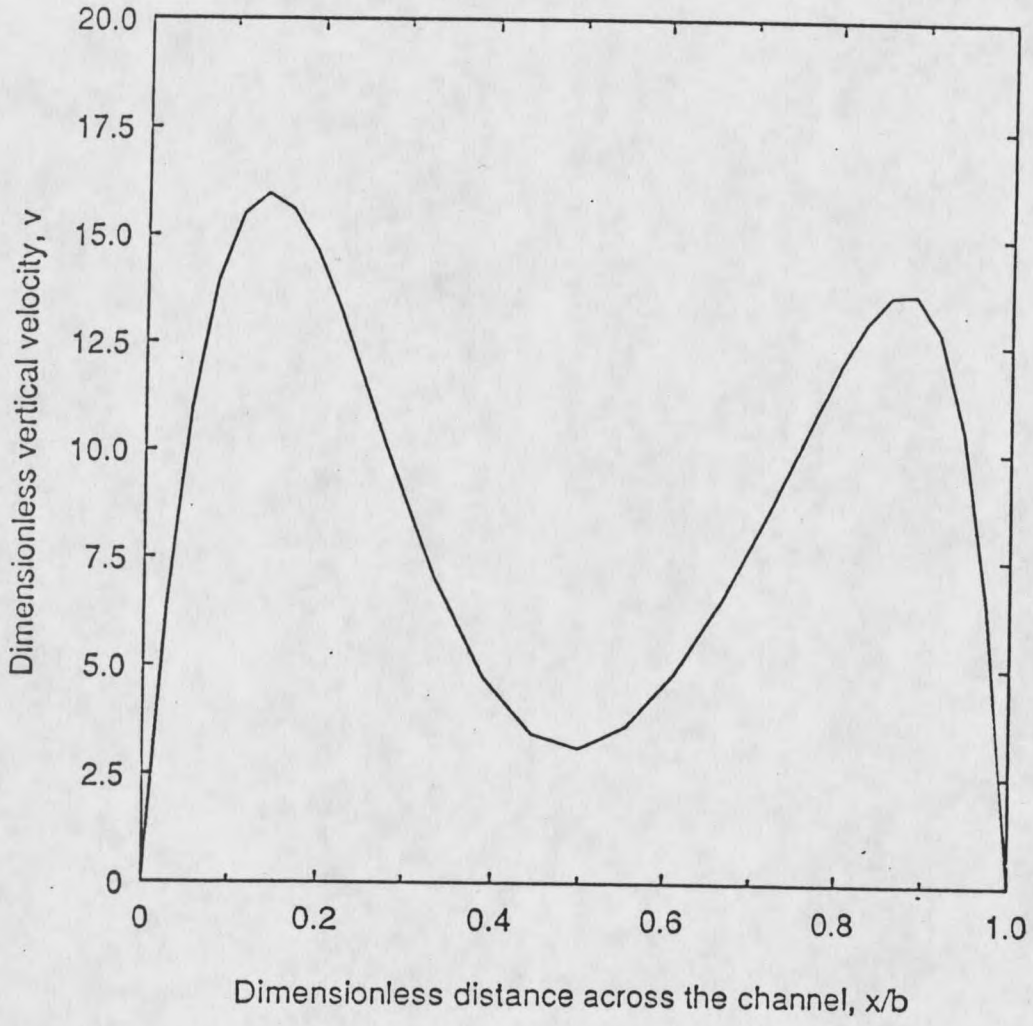


Figure 44. Transverse distribution of exit velocity for geometry III with $Ra=5x10^4$, Ar=0.3

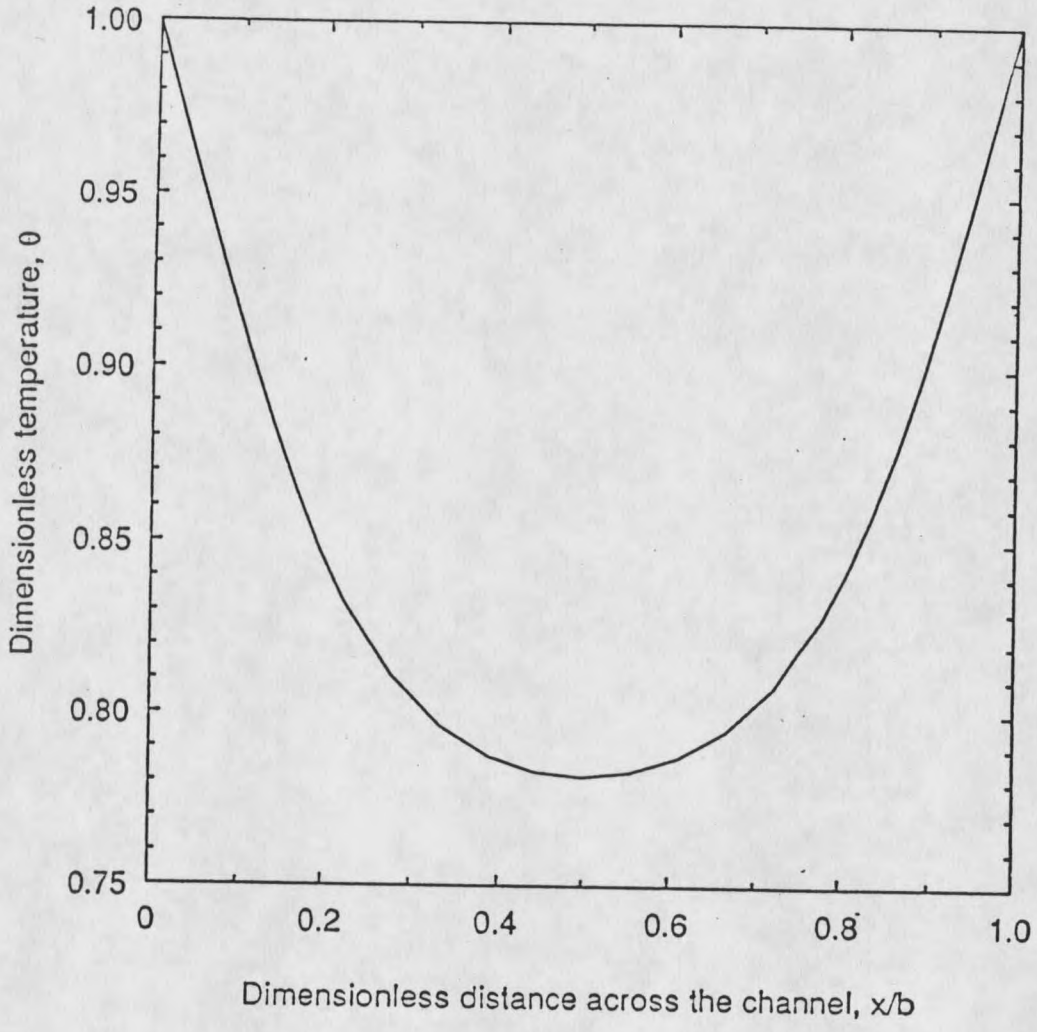
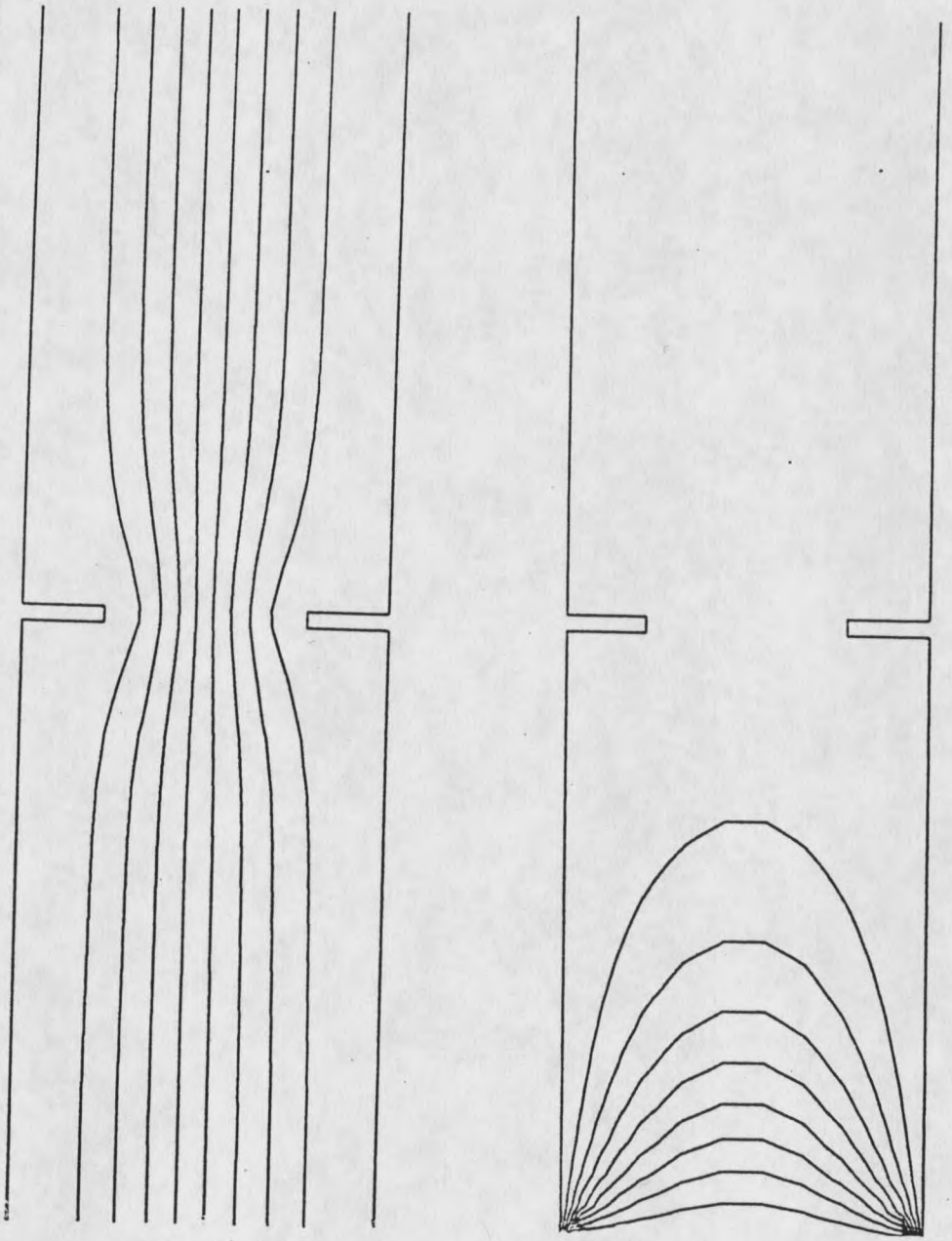


Figure 45. Transverse distribution of temperature at the exit for geometry III with $Ra=5x10^4$, Ar=0.3

Results for Geometry IV

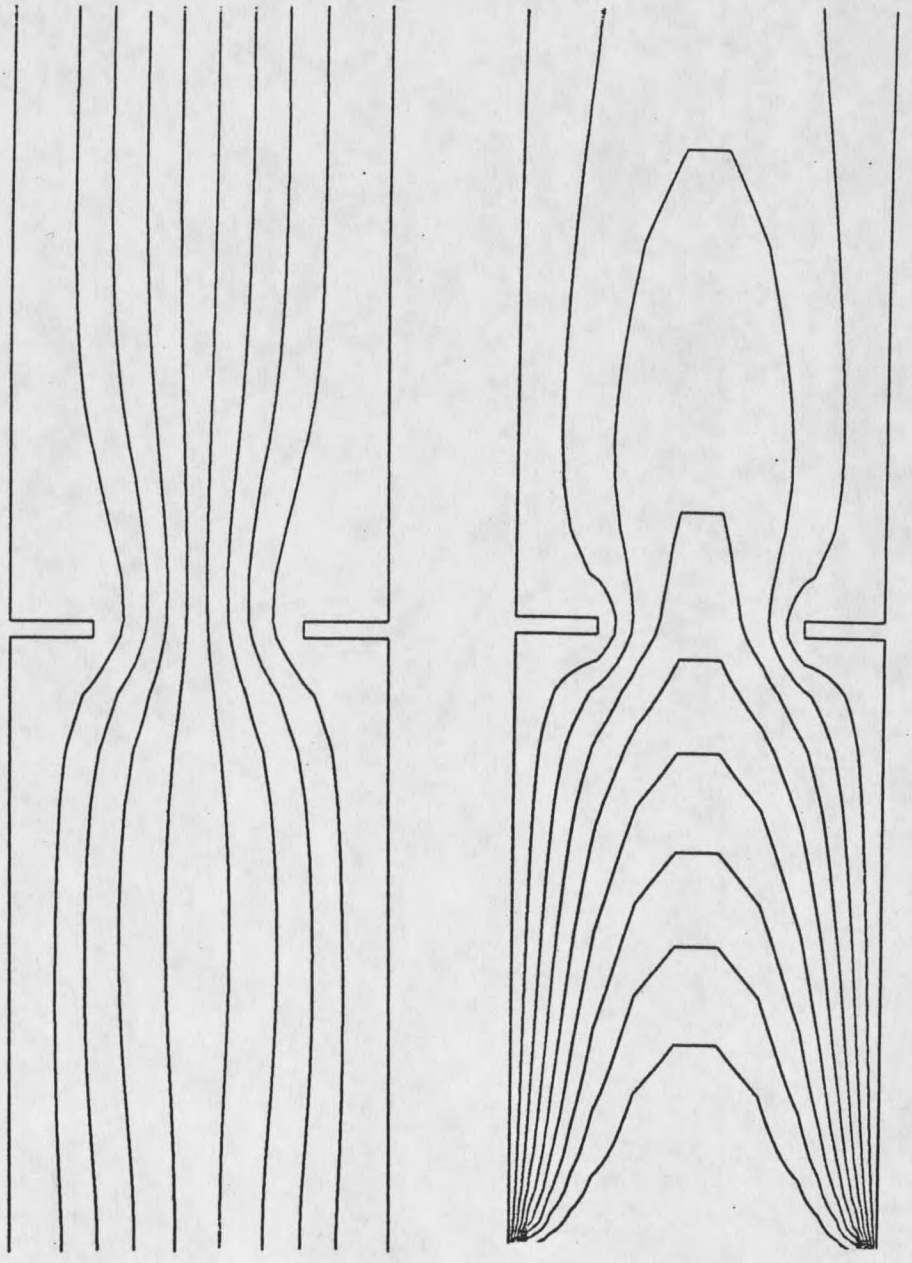
The computed streamlines and isotherms for this geometry are shown in Figures 46 through 49. The pattern of the streamlines and isotherms for this particular geometry is observed to be similar to that of geometry II. Again, the observations a, c, d, and e of geometry I can also be made from this case. Two recirculating zones are observed above the two obstructions at higher values of Ra, and can be seen in Figure 48.

For all the above cases, it can be stated that at high Rayleigh numbers, a boundary layer is formed on each plate. This is similar to the thermal behavior of a smooth channel at high Rayleigh numbers. In other words, the two walls of the channel become thermally independent of each other. Figures 50 and 51 are the computed velocity profiles for this geometry with $Ra = 5 \times 10^4$ at $y/L = 0, 1$ respectively. It is observed from the velocity profiles at different Rayleigh numbers that increasing the Rayleigh number induces a higher vertical velocity at the exit. This was found to be true for all the geometries investigated. This high vertical velocity at the exit does not allow the fluid to be present in the channel for long enough time to be heated up to a temperature approaching the wall temperature. Figure 52 is the computed



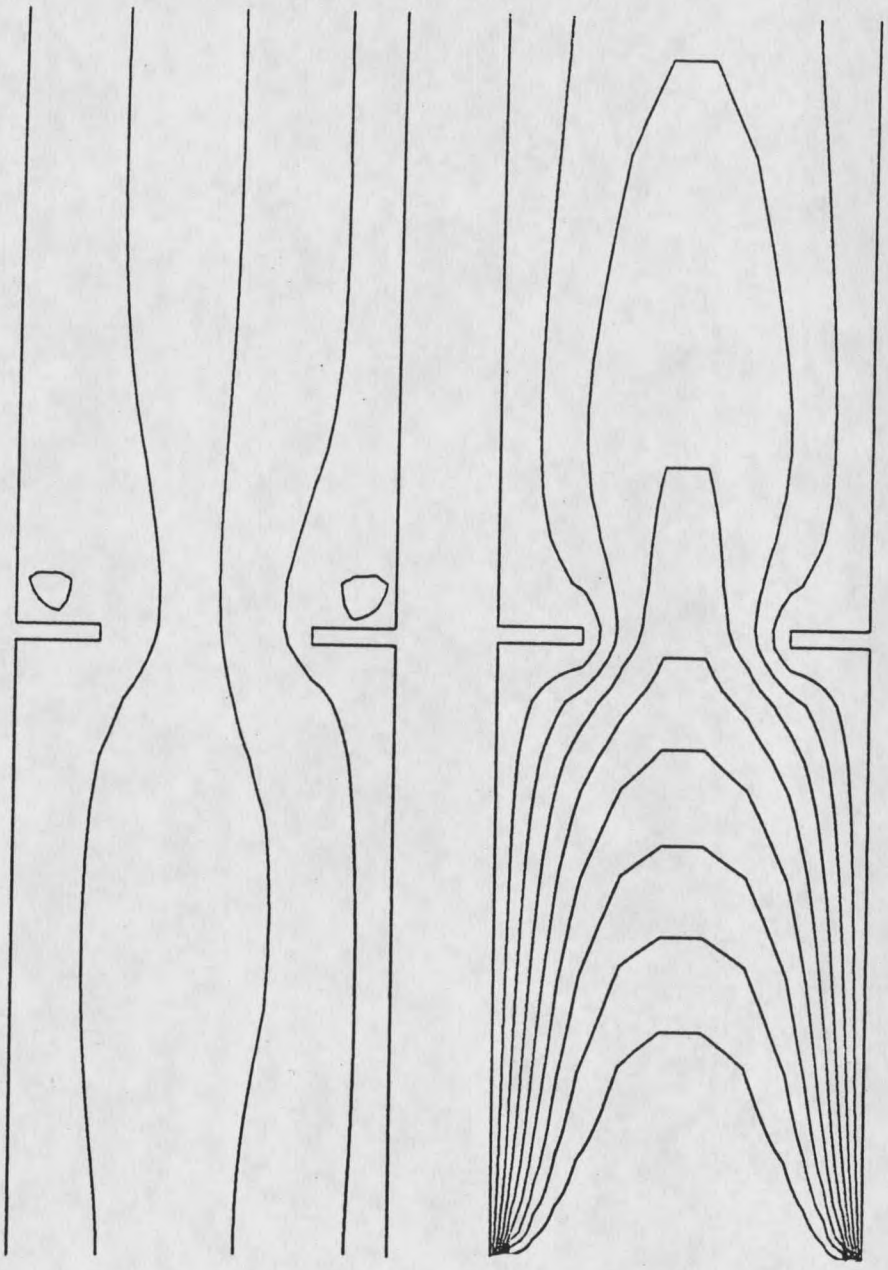
(a) Streamlines (b) Isotherms

Figure 46. Computed streamlines and isotherms for geometry IV with $Ra=10^2$, Ar=0.3



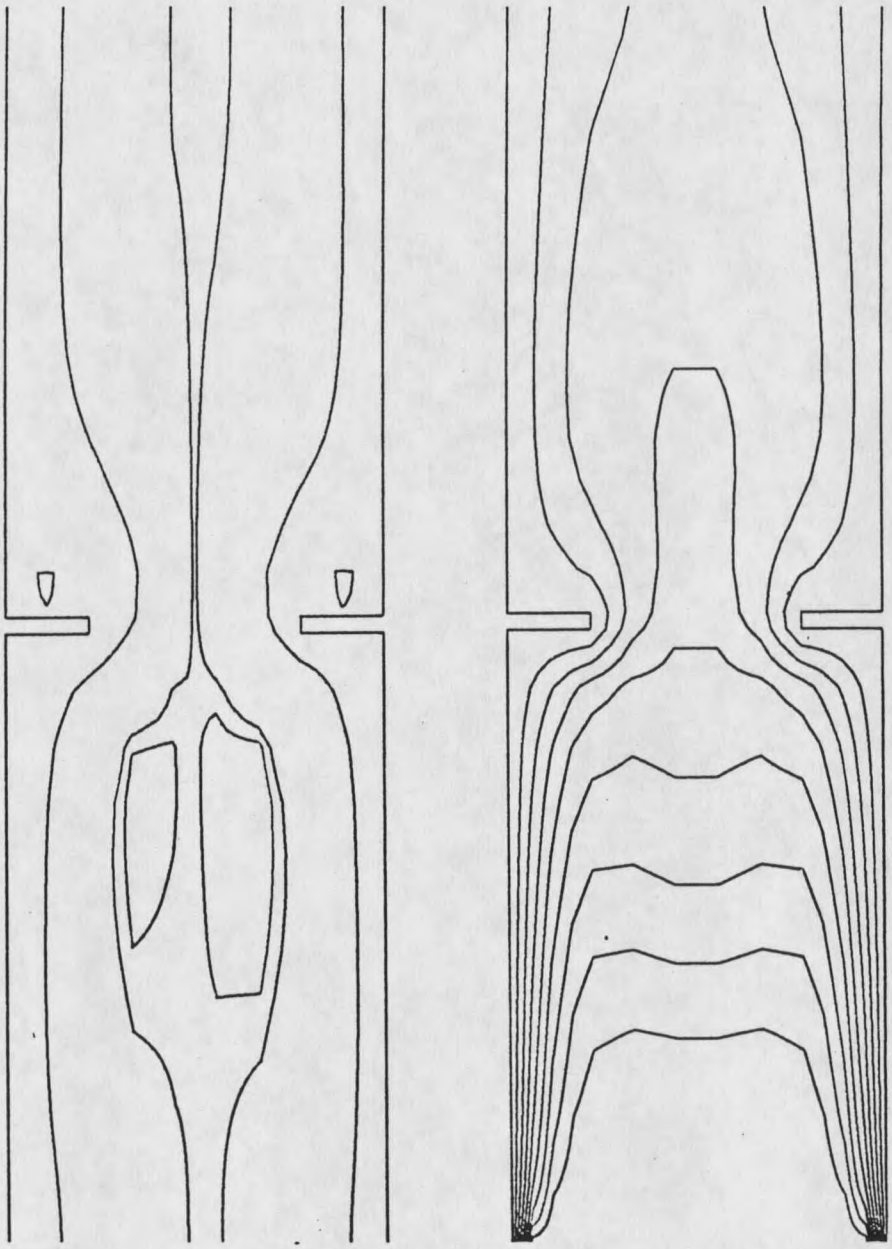
(a) Streamlines (b) Isotherms

Figure 47. Computed streamlines and isotherms for geometry IV with $Ra=5x10^3$, Ar=0.3



(a) Streamlines (b) Isotherms

Figure 48. Computed streamlines and isotherms for geometry IV with $Ra=10^4$, Ar=0.3



(a) Streamlines (b) Isotherms

Figure 49. Computed streamlines and isotherms for geometry IV with $Ra=5x10^4$, Ar=0.3

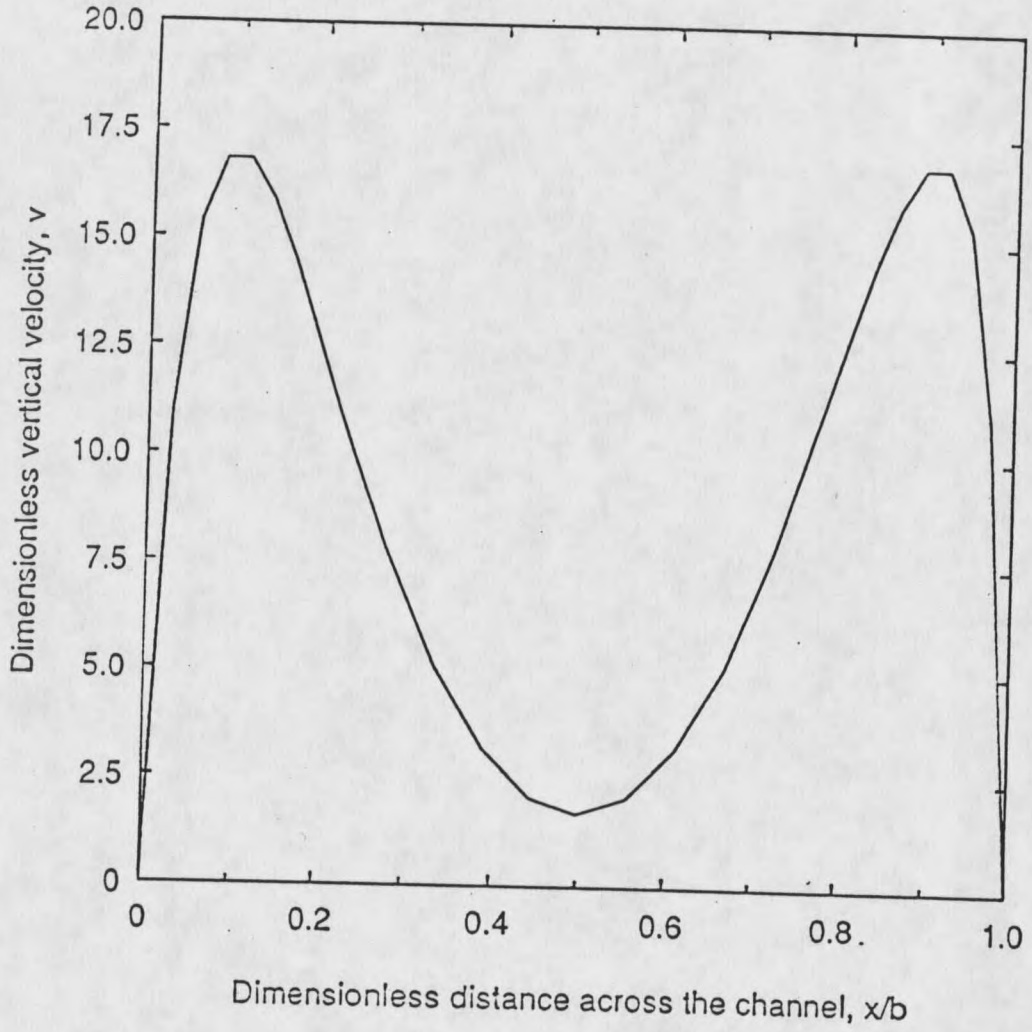


Figure 50. Transverse distribution of inlet velocity for geometry IV with $Ra=5x10^4$, Ar=0.3

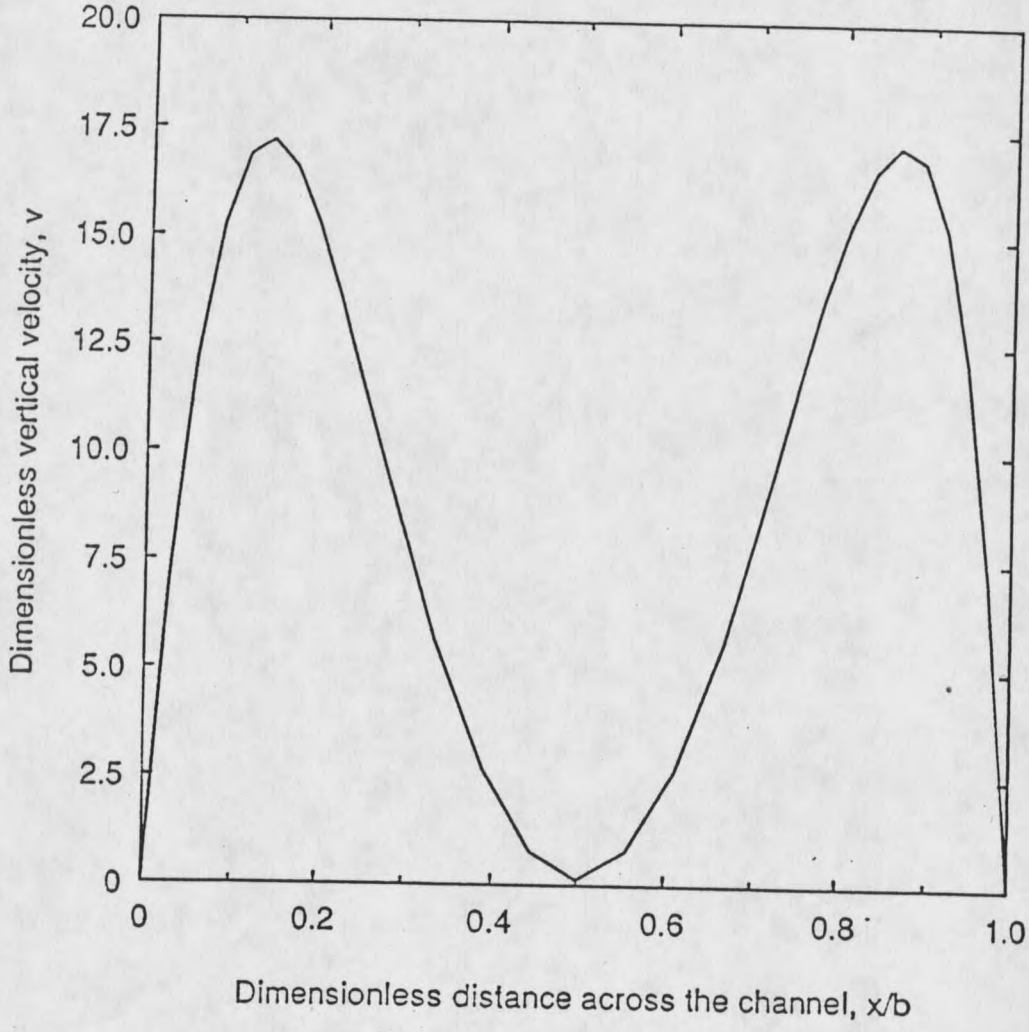


Figure 51. Transverse distribution of exit velocity for geometry IV with Ra=5x10^4, Ar=0.3

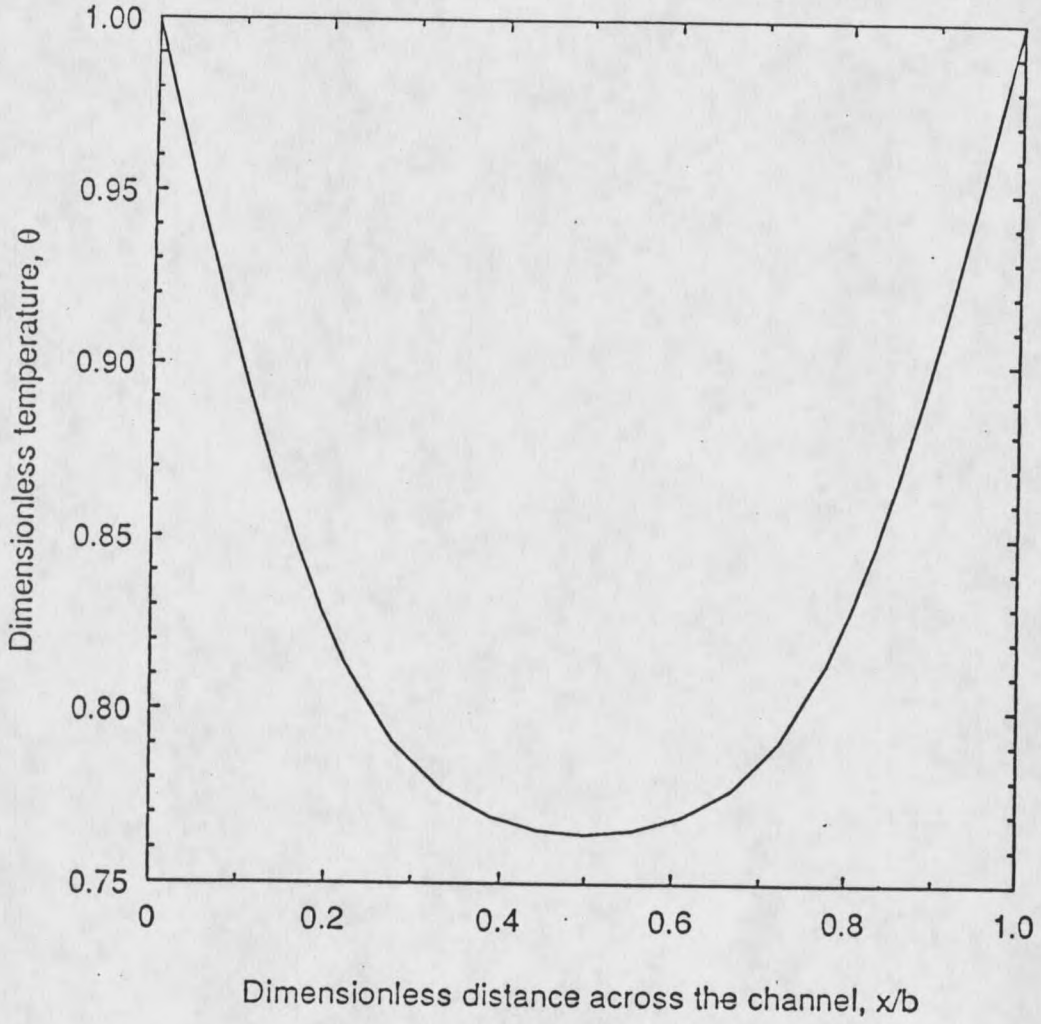


Figure 52. Transverse distribution of temperature at the exit for geometry IV with $Ra=5x10^4$, Ar=0.3

nondimensional temperature profile with $Ra=5 \times 10^4$ at $y/L = 1$. Like other three geometries, the minimum temperature was on the center line of the channel and this minimum temperature decreased with increasing Rayleigh number.

The computed average Nusselt numbers for both the obstructed and smooth channels (with Ar = 0.3) are compared in Figure 53. Similar trend as that of Figure 37 is observed for the variation of average Nusselt number with Rayleigh number. In this case, at high Ra values, the average Nusselt numbers of both the geometries III and IV are found to be almost equal. In contrast, at low Ra values, the average Nusselt numbers of geometry IV are less than those of geometry III. For geometry IV, at low Rayleigh numbers, the mechanism (ii) dominates the mechanism (iii). In contrast, the mechanism (iii) dominates the mechanism (ii) at high Rayleigh numbers and hence the average Nusselt numbers are equal to those of geometry III. As discussed earlier, mechanism (i) is the increase in heat transfer due to the increased surface area, mechanism (ii) is the increase in heat transfer due to locally accelerated flow around the obstruction region, and mechanism (iii) is the reduction in heat transfer due to recirculating zones.

Figure 54 shows the variation of the ratio of Nusselt numbers with Rayleigh number for the geometries III and IV. The percentage reduction in heat transfer at low Ra values was more than the corresponding reduction at high Ra values. The

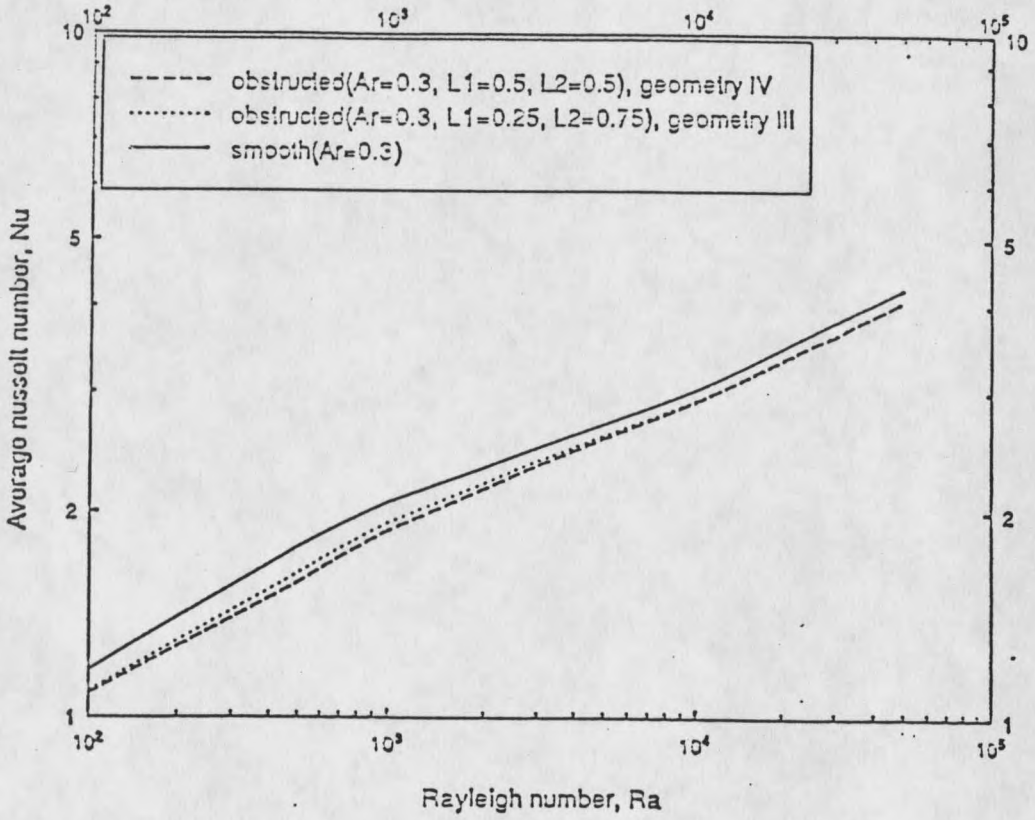


Figure 53. Comparison of the computed average Nusselt numbers for the obstructed and unobstructed channel flows with Ar=0.3

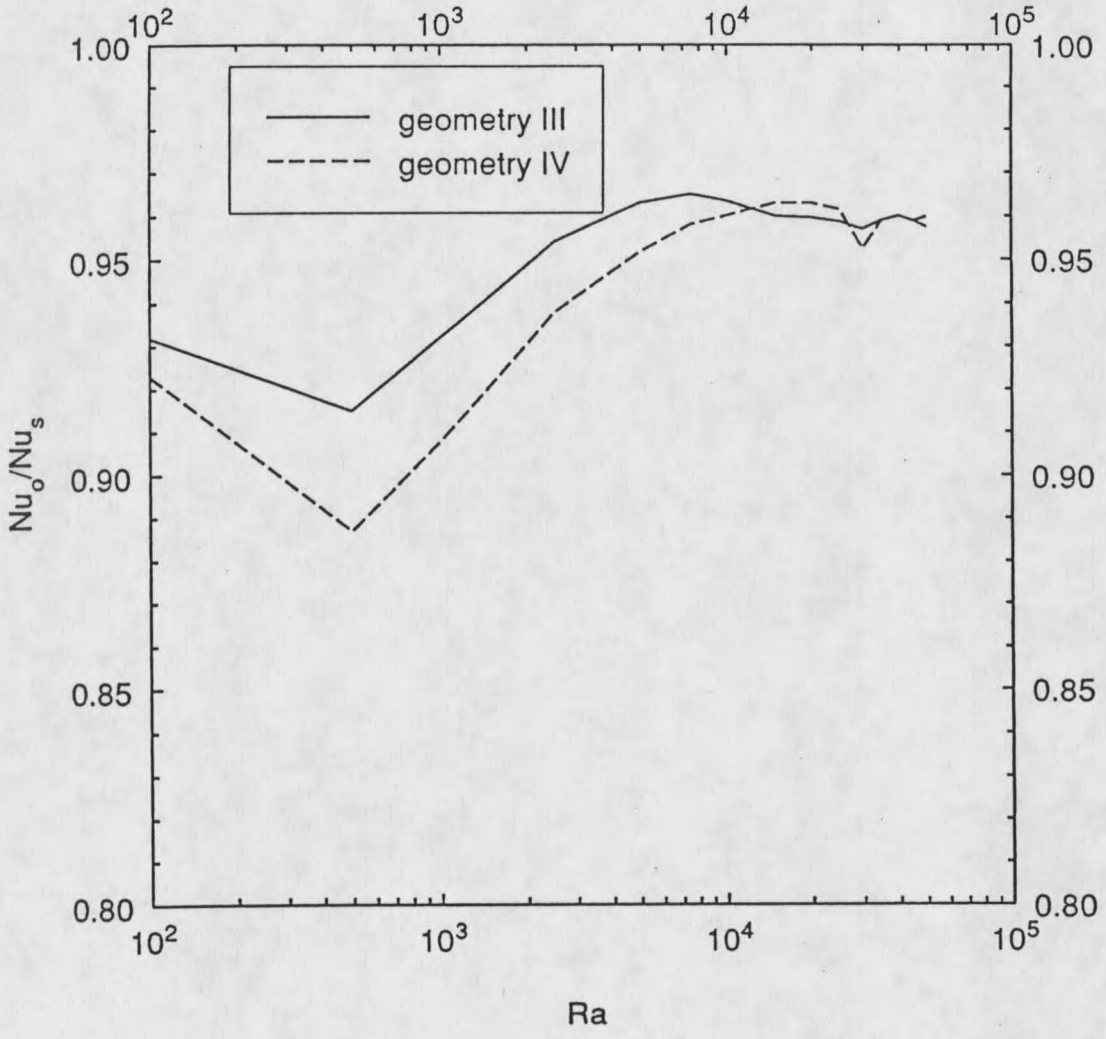


Figure 54. Variation of ratio of Nusselt numbers with Rayleigh number (Ar=0.3)

maximum reduction in heat transfer for geometry III was approximately 8.5% at Ra = $5x10^2$ and the minimum reduction in heat transfer was approximately 3% at Ra = 10^4. The maximum reduction for geometry IV was roughly 11% at Ra = $5x10^2$ and the minimum reduction was nearly 4% at Ra = $2x10^4$.

It is clear from a comparison of Figures 37 and 53 that the average Nusselt number of either the obstructed or unobstructed channel increases with the aspect ratio. From the definition used in this study (shown in Appendix B), Nusselt number is directly proportional to the channel width, b. Therefore, as the aspect ratio (=b/L) is increased by increasing b, the Nusselt number also increases.

To study the effect of aspect ratio on the heat transfer, the average Nusselt numbers of all the four geometries are plotted in Figure 55. From this figure, it can be clearly seen that the effect of aspect ratio decreases as Rayleigh number increases. At a Rayleigh number of 10^2, there is a difference of nearly 61% in the average Nusselt numbers between the geometries I (Ar = 0.2) and III (Ar = 0.3). This percentage difference decreased with increasing Rayleigh number, with the lowest difference being 13% at Ra = $5x10^4$. Similarly, the maximum difference between the geometries II (Ar = 0.2) and IV (Ar = 0.3) is approximately 72% at Ra = 10^2 and the minimum difference is 22% at Ra = $2x10^4$. The percentage difference decreased again with increasing Rayleigh number. These numerical values indicate that for the same

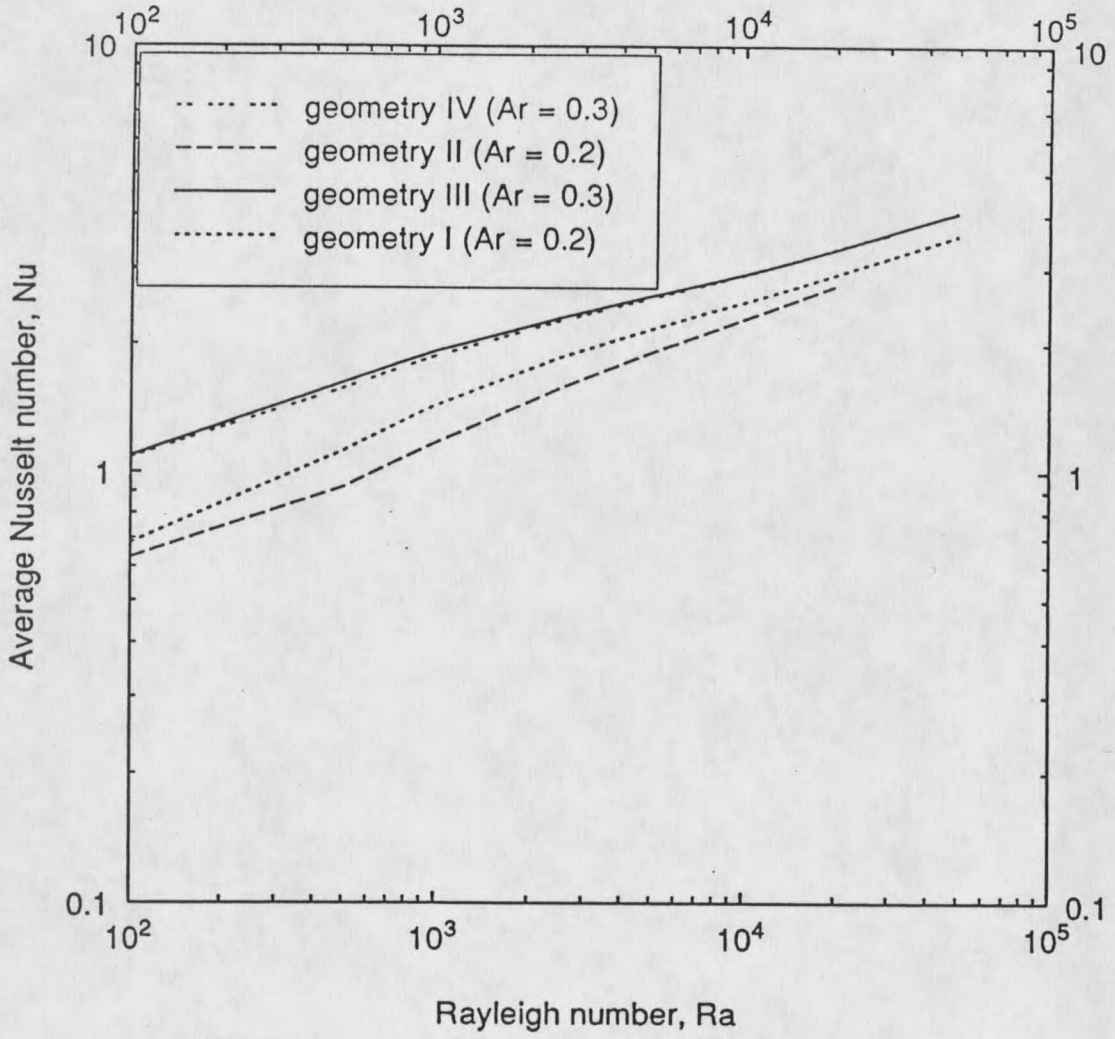


Figure 55. Effect of aspect ratio on the rate of heat transfer

type of geometry, the gap between the two curves corresponding to two aspect ratios narrows down as Ra increases. Here, same type of geometry means that either the obstructions are facing each other or are separated by a fixed distance. This effect of aspect ratio can be understood by examining the nondimensional governing equation. It can be seen from the nondimensional energy equation that the term aspect ratio multiplies (e.g. the conduction term in the streamwise y direction) is expected to be reasonably small. On the other hand, at lower values of Rayleigh number, the flow approaches a fully developed channel flow. This mechanism increases the effect of aspect ratio at low values of Rayleigh number.

CHAPTER 5

CONCLUSIONS AND RECOMMENDATIONS

Conclusions

Steady, two-dimensional, laminar, natural convection of air in vertical channels with and without multiple obstructions was studied numerically. Rayleigh number was varied from 10^2 to 5×10^4. The following conclusions can be made concerning the unobstructed channel:

(i) Average Nusselt number (Nu) of the channel increases as the Rayleigh number (Ra) increases.

(ii) The effect of aspect ratio on average Nusselt number (Nu) decreases with increasing Rayleigh number.

(iii) Local Nusselt number is maximum at the entrance of the channel.

(iv) Local Nusselt number decreases from the entrance to the exit of the channel.

(v) Increasing Rayleigh number induces a large vertical velocity which in turn causes an increase in the energy transport by convection.

(vi) The maximum velocity at the exit increases with increasing Rayleigh number.

(vii) Increasing Ra decreases the exit center line temperature.

(viii) The minimum temperature is on the center line due to the symmetry of the problem (i.e., the geometry of the channel is symmetric about the y-axis).

(ix) At high Rayleigh numbers, due to the large induced vertical velocity, the fluid does not remain in the channel long enough to be heated up to a temperature equal to that of the wall (i.e., Θ is never equal to one).

(x) The mass flow rate increases with the increase of Rayleigh number.

From the four different geometries employed for the obstructed channel, the following conclusions can be drawn regarding the channels with obstruction on both walls:

For all the cases run for the obstructed channel,

(i) The average Nusselt number increases as the Rayleigh number increases.

(ii) The mass flow rate increases as the Rayleigh number increases.

(iii) The maximum velocity at the exit increases as the Rayleigh number increases.

(iv) The minimum temperature at the exit decreases as the Rayleigh number increases. This trend is similar to that observed for the smooth channel.

(v) From Figures 25 and 44, it can be observed that the obstruction at $L_2 = 0.75$ decreased the second peak value of

the exit velocity profile.

(vi) The velocities at the tips of the obstructions at Ra = 10^4 are compared in all the cases. It is found that for the same Rayleigh number, the velocity is more for the geometries II and IV (obstructions facing each other) as compared to the geometries I and III.

(vii) The computed average Nusselt numbers of the obstructed channel are compared to those of the smooth channel and it is found that the average Nusselt numbers for obstructed channel are less than those of the smooth channel. Thus, the presence of the obstructions reduces the heat transfer.

(viii) Local Nusselt number is maximum at the entrance of the channel.

(ix) In the case of the obstructed walls, it can be said that (a) initially, the local Nusselt number decreases from the channel entrance to the lower intersection of obstruction with the wall, (b) then reaches its maximum at the lower, outer corner or tip of the obstruction, (c) then decreases up to the upper intersection of the obstruction with the wall.

(x) Effect of the aspect ratio decreases as the Rayleigh number increases.

(xi) At any particular Rayleigh number, the percentage reduction is more for geometry II than geometry I. The maximum reduction in heat transfer for geometry II is approximately 31% and occurred at Ra=5×10^2.

The minimum reduction in heat transfer is approximately 7.5% and occurred at $Ra=2x10^4$. The maximum reduction in heat transfer for geometry III is roughly 8.5% at $Ra=5x10^2$ and the minimum reduction is 3% at $Ra=10^4$.

Recommendations

The present study is done with a UWT type of boundary condition for the channel walls as well as the obstruction. However, in the real electronic systems, the component cards are subjected to different thermal boundary conditions such as uniform heat flux (UHF), thermal insulation (or adiabatic), wall conduction etc. Hence, there is a need for the analysis of channels with the walls and obstructions subjected to different thermal boundary conditions.

In the present study, both the obstructions on the channel walls are of rectangular shape. Further research can be done using repeating obstructions with different shapes for the obstructions.

REFERENCES

REFERENCES

Anand, N. K., Kim, S.H., and Fletcher, L.S., 1990, "The effect of plate spacing on free convection between heated parallel plates", In Thermal Modeling And Design Of Electronic Systems And Devices, HTD-Vol. 153, (ASME), pp. 81-87.

Aung, W., Beith, K.I., and Kessler, T.J., November 1972a, "Natural convection cooling of electronic cabinets containing arrays of vertical circuit cards", ASME Paper No. 72-WA/HT-40, presented at the ASME Winter Annual Meeting, New York, pp. 26-30.

Aung, W., 1972b, "Fully developed laminar free convection between vertical plates heated asymmetrically", International Journal Of Heat Mass Transfer, Vol. 15, pp. 1577-1580.

Aung, W., Fletcher, L.S., and Sernas, V., 1972c, "Developing laminar free convection between vertical flat plates with asymmetric heating", Int. J. Heat Mass Transfer, Vol. 15, pp. 2293-2328.

Bar-Cohen. A., and Rohsenow, W.M., 1984, "Thermally optimum spacing of vertical, natural convection cooled, parallel plates", ASME J. Heat Transfer, Vol. 106, pp. 116-123.

Bejan, A., 1984, Convection heat transfer, John-Wiley and sons.

Bodoia, J.R., and Osterle, J.F., 1962, "The development of free convection between heated vertical plates", ASME J Heat Transfer, Vol. 84, pp. 40-44.

Burnette, D.S., 1988, Finite element analysis, Addison-Wesley publishing Co.

Carpenter, J.R., Briggs, D.G., and Sernas, V., 1976, "Combined radiation and devoloping laminar free convection between vertical flat plates with asymmetric heating", ASME J. Heat Transfer, Vol. 98, pp. 95-100.

Cha, W., Lloyd, J.R., and Yang, K.T., Dec 10-15, 1989, "Numerical study of natural convection between two vertical parallel plates with one oscillating surface temperature", presented at the winter annual meeting of the **ASME**, pp. 31-38.

Chung, T.J., 1978, Finite element analysis in fluid dynamics, McGraw-Hill International Book Co.

Churchill, S. W., 1977, "A comprehensive correlating equation for buoyancy induced flow in channels", Letters In Heat And Mass Transfer, Vol. 4, pp. 193-199.

De Vahl Davis, G., and Jones, I.P., 1983, "Natural convection in a square cavity: a comparison exercise", International Journal Of Numerical Methods In Fluids, Vol. 3, pp. 227-248.

Eckert, E.R.G., and Drake, R.M., 1959, Heat and mass transfer, McGraw-Hill Book Co, Inc.

Elenbass, W., 1942, "Heat Dissipation of parallel plates by free convection", Physica, Holland, Vol. 9, No. 1, pp. 1-23.

Gartling, D.K., 1978a, "NACHOS II-A finite element computer program for incompressible flow problems, part I-theoritical background", **SAND** 77-1333, Sandia laboratories, Albuquereque, New Mexico.

Gartling, D.K., 1978b, "NACHOS II- A finite element computer program for incompressible flow problems, part II- user's manual", **SAND** 77-1333, Sandia laboratories, Albuquereque, New Mexico.

Gray D.D., and Giorgini, A., 1976, "The validity of the Boussinesq approximation for liquids and gases", International Jounal of Heat And Mass Transfer, Vol. 19, pp. 545-551.

Habchi, S., and Acharya, S., 1986, "Laminar mixed convection in a partially blocked, vertical channel", International Jounal Of Heat And Mass Transfer, Vol. 29, No. 11, pp. 1711-1722.

Kakac, S., and Yener, Y., 1984, Convective heat transfer, Hemisphere publishing corporation, New York.

Kays, W.M., and Crawford, M.E., 1980, Convective heat and mass transfer, 2 nd Ed., McGraw-Hill Book Co.

Kim, S.H., Anand, N.K., and Fletcher, L.S., 1989, "Free convection between series of vertical parallel plates with embedded line heat sources", In Numerical Simulation Of Convection In Electronic Equipment, HTD-Vol. 121 (ASME), pp. 7-16.

Kim, S.H., Anand, N.K., and Aung, W., 1990, "Effect of wall conduction on free convection between asymmetrically heated vertical plates: uniform wall heat flux", Int. J. Heat Mass Transfer, pp. 1013-1022

Kim, W., and Boehm, R.F., 1990, "Combined free and forced convective heat transfer from multiple rectangular wall blocks in vertical channels", In Mixed Convection And Environmental Flows, HTD-Vol. 152 (ASME), pp. 1-8.

Kraus, A.D., and Bar-Cohen, A., 1983, Thermal analysis and control of electronic equipment, McGraw-Hill, New York.

Levy, E.K., 1971, "Optimum plate spacings for laminar natural convection heat transfer from parallel vertical isothermal flat plates", ASME J. Heat Transfer, pp. 463-465.

Levy, E.K., Eichen, P.A., Cintani, W.R., and Shaw, R.R., 1975, "Optimum plate spacings for laminar natural convection heat transfer from parallel vertical isothermal flat plates: experimental verification", ASME J. Heat Transfer, Vol. 97, pp. 474-476.

Mehrotra A., and Acharya, S., 1993, "Natural convection heat transfer in smooth and ribbed vertical channels", Int. J. Heat Mass Transfer, Vol. 36, No. 1, pp. 236-241.

Miyatake, O., and Fujii, T., 1972, "Free convection heat transfer between vertical parallel plates, one plate isothermally heated and the other thermally insulated", Heat Transfer-Japanese Research, Vol. 3, pp. 30-38.

Miyatake, O., Fujii, M., and Tanaka, T., 1973, "Natural convection heat transfer between vertical parallel plates, one plate with a uniform heat flux and the other thermally insulated", Heat Transfer-Japanese Research, Vol. 4, pp. 25-33.

Ostrach, S., 1988, "Natural convection in enclosures", ASME J. Heat Transfer, Vol. 110, pp. 1175-1190.

Patankar, S.V., 1980, Numerical heat transfer and fluid flow, Hemisphere publishing corporation, McGraw-Hill Book Co.

Rheault S., and Bigen, E., 1990, "Mixed convective developing flow with flow reversal in open-ended inclined channels", In Mixed Convection And Environmental Flows, HTD-Vol. 152 (ASME), pp. 9-14.

Said, S.A.M., and Krane, R.J., 1990, "An analytical and experimental investigation of natural convection heat transfer in vertical channels with a single obstruction", International Journal For Heat Mass Transfer, pp. 1121-1133.

Said, S.A.M., and Muhanna, A., 1990, "Investigation of natural convection in a vertical parallel-walled channel with a single square obstruction", In Simulation And Numerical Methods In Heat Transfer, HTD-Vol. 153, pp. 73-80.

Scott, A.W., 1974, Cooling of electronic quipment, John-Wiley and sons.

Sloan, J.L., 1985, Design and packaging of electronic equipment, Van Nostrand Reinhold Company

Seraphim, P., Lasky, R.C., and Li Che-yu, 1989, Principles of electronic packaging, McGraw-Hill Book Company.

Sparrow E.M., and Gregg, J.L., 1958, "The variable fluid property problem in free convection", Transactions Of The ASME, pp. 879-886.

Sparrow E.M., and Bahrami, P.A., 1980, "Experiments on natural convection from vertical parallel plates with either open or closed edges", ASME J. Heat Transfer, Vol. 102, pp. 221-227.

Starner K.E., and Mcnamus, H.N., Jr., 1963, "An experimental investigation of free-convection heat transfer from rectangular fin-arrays", ASME J. Heat Transfer, pp. 273-278.

Webb, B.W.,and Hill, D.P., 1989, "High rayleigh number laminar natural convection in an asymmetrically heated vertical channel", ASME J. Heat Transfer, Vol. 111, pp. 649-656.

Wirtz, R.A.,and Stutzman, R.J., 1982, "Experiments on natural convection between vertical plates with symmetric heating", ASME J. Heat Transfer, Vol. 104, pp. 501-507.

Zhong, Z.Y., Yang, K.T., and Lloyd, J.R., 1985, "variable property effects in laminar natural convection in a square enclosure", ASME Jounal Of Heat Transfer, Vol. 107, pp. 133-138.

APPENDICES

APPENDIX A

THE FINITE ELEMENT ALGORITHM OF NACHOS II

APPENDIX A

THE FINITE ELEMENT ALGORITHM OF NACHOS II

Formulation of the finite element equations

Let the governing equation of the fluid flow be $A(q)=0$ and the corresponding boundary equation be $a(q)=0$. The finite element algorithm for the conservation of convective energy expressed in terms of the method of weighted residuals (MWR) is concerned with the above equations. Initially, it is assumed that an approximate solution, q^h, exists for the above governing equation. Then, $A(q^h)$ and $a(q^h)$ are the residuals in the solution approximation and are obtained by the direct substitution of the approximate solution in the governing equation and the corresponding boundary condition.

The first step in the derivation of the finite element equations is the division or discretization of the continuum domain into a number of simply-shaped regions called "finite elements". The finite element approximation for each dependent variable, $q_e(x_i)$, is evaluated at the nodal points of each element.

Hence, the semi-discrete approximation, $q^h(x_i)$ is defined as

$$q^h(x_i) \equiv \sum_1^j q_e(x_i)$$

where, $q_e(x_i)$ is defined in terms of the cardinal basis as

$$q_e(x_i) \equiv \{N_m(x_i)\}^T \{Q(t)\}_e$$

The elements of $\{Q(t)\}_e$ are the nodal values of $q_e(x_i)$. N_m is the cardinal basis and m is the degree of basis.

The approximation errors in $A(q^h)$ and $a(q^h)$ are to be orthogonal to the cardinal basis $\{N_s\}$ from the concept of the finite element algorithm as defined in the context of the method of weighted residuals. This orthogonality condition when expressed as a combination of linearly independent constraints by using an arbitrary constant multiplier, λ, yields the finite element solution algorithm for the governing equations and associated boundary conditions as follows:

$$\int_{R^2} \{N_m\} A(q^h)\, d\tau - \lambda \int_{\partial R} \{N_m\} a(q^h)\, d\sigma \equiv [0] \qquad \text{(A.1)}$$

Independent of the degree, m, of the basis $\{N_s\}$ equation A.1 represents a system of ordinary differential(and algebraic) equations written on the unknown $q^h(x_i)$ of the form

$$B(\{Q(t)\}) = [C]\{Q(t)\}' + [D+E]\{Q(t)\} + \{f\} = \{0\} \qquad \text{(A.2)}$$

where the square matrices, C, D, and E represent thermal capacity, convection, and diffusion terms respectively. The elements of the column matrix, f, are all the nonhomogeneous terms. The prime (') denotes the first ordinary derivative with respect to time (t). For steady-state conditions, the above equation can be rewritten as

$$\{G(Q)\} = [D+E]\{Q\} + \{d\} = \{0\} \qquad (A.3)$$

The differential equations governing the two dimensional natural convection flow in obstructed channels can be written in the tensor notation as follows:

Conservation of mass $$\frac{\partial u_i}{\partial x_i}=0 \qquad (A.4a)$$

Conservation of momentum $$\rho\frac{Du_i}{Dt}=\frac{\partial \tau_{ij}}{\partial \alpha_j}+\rho g_i \qquad (A.4b)$$

Conservation of energy $$\rho c\frac{DT}{Dt}=-\frac{\partial q_i}{\partial x_i} \qquad (A.4c)$$

where the stress tensor is

$$\tau_{ij}=P\delta_{ij}+\mu\left(\frac{\partial u_i}{\partial x_j}+\frac{\partial u_j}{\partial x_i}\right) \qquad (A.5a)$$

and the heat flux vector is

$$q_i=-k\frac{\partial T}{\partial x_i} \qquad (A.5b)$$

The equation of state is given by

$$\rho=\rho_0[1-\beta(T-T_\infty)] \qquad (A.6)$$

In the above equations, u_i is the velocity component in the x_i coordinate direction, t is the time, T is the temperature, ρ is the density, τ_{ij} is the stress tensor, q_i is the heat flux vector, μ is the viscosity, C_p is the specific heat, k is the thermal conductivity and ß is the coefficient of volumetric expansion. D/Dt is the substantial derivative and δ_{ij} is the kronecker delta.

The dependent variables(u_i, P, T) can be expressed in the following forms within each element after carrying out the general algorithm outlined above:

$$u_i(x_i,t) = \{N_m(x_i)\}^T \{u(t)\}_i \qquad (A.7a)$$

$$P(x_i,t) = \{N_m(x_i)\}_T \{P(t)\} \qquad (A.7b)$$

$$T(x_i,t) = \{N_m(x_i)\}^T \{T(t)\} \qquad (A.7c)$$

In equations (A.7) the u_i, P, T are vectors of unknown nodal point variables and N_m are vectors of interpolation or basis functions. m is the degree of basis and is equal to unity for a linear basis and two for a quadratic basis. The velocity components and temperature are approximated by quadratic basis functions and the pressure by a linear basis function within each element. Element continuity is to be maintained for all the dependent variables. This requirement is satisfied through the appropriate summation of equations for nodes which are common to adjacent elements. The superscript "T" represents a vector transpose and the subscript "i" represents the coordinate directions, x and y.

The set of residuals, R_i, or error equations can be obtained by substituting the approximate forms for the dependent variables (equations A.7) into the field equations (equations A.4), as shown below.

Conservation of mass:

$$f_1(N_2, u_i) = R_1 \qquad (A.8a)$$

Conservation of momentum:

$$f_2(N_2, N_1, N_2, P, T) = R_2 \qquad (A.8b)$$

Conservation of energy:

$$f_3(N_2, N_2, T, u_i) = R_3 \qquad (A.8c)$$

Using the concept of MWR (discussed earlier), the residuals are to be made orthogonal to the basis in order to reduce the residuals R_i, to zero over each element i.e.,

$$< f_1, N_1 > = < R_1, N_1 > = 0 \qquad \text{(A.9a)}$$

$$< f_2, N_2 > = < R_2, N_2 > = 0 \qquad \text{(A.9b)}$$

and,

$$< f_3, N_3 > = < R_3, N_3 > = 0 \qquad \text{(A.9c)}$$

where <, > is the inner product defined by

$$\langle a, b \rangle = \int_v abdv \qquad \text{(A.10)}$$

where v is the volume of the element.

The following set of coupled matrix equations are obtained when the above integrals are carried out:

Momentum and Continuity:

$$[M]\, V' + [C(u)]\, V + [K(T)]\, V = F(T) \qquad \text{(A.11a)}$$

where $V^T = (u_1^T, u_2^T, P^T)$

and, $u^T = (u_1^T, u_2^T)$

Energy:

$$[N]T' + [D(u)]T + [L(T)]T = G(T) \qquad \text{(A.11b)}$$

In the above equations M and N matrices represent the mass and capacitance terms respectively. The C and D matrices represent the convection of momentum and energy, respectively; while the K and L matrices represent the diffusion of momentum and energy. The F and G vectors provide the forcing functions for the system. For steady-state problems, the above matrix equations can be rewritten as follows:

$$[C(u)] + [K(T)] = F(T) \qquad \text{(A.12a)}$$

$$[D(u)] + [L(T)] = G(T) \qquad \text{(A.12b)}$$

The above matrix equations are the conservation equations for an individual finite element. Assembling of these equations results in a large set of strongly coupled, nonlinear equations and the solution procedure to solve these equations is discussed later.

Element Construction

NACHOS II element library consists of six-node isoparametric triangles and eight-node isoparametric quadrilaterals. Quadrilateral elements were employed for the discretization of the channels in the present study. The quadratic basis, or interpolation functions for the velocity components (u_i) and the temperature (T) for the quadrilateral element are given by the vectors,

$$N_2 = \frac{1}{2} \begin{Bmatrix} \frac{1}{2}(1-e)(1-f)(-e-f-1) \\ \frac{1}{2}(1+e)(1-f)(e-f-1) \\ \frac{1}{2}(1+e)(1+f)(e+f-1) \\ \frac{1}{2}(1-e)(1+f)(-e+f-1) \\ (1-e^2)(1-f) \\ (1+e)(1-f^2) \\ (1-e^2)(1+f) \\ (1-e)(1-f^2) \end{Bmatrix} \qquad \text{(A.13)}$$

while the linear basis,or interpolation functions for the

pressure for this element are given by the vector:

$$\frac{1}{4}\begin{Bmatrix}(1-e)(1-f)\\(1+e)(1-f)\\(1+e)(1+f)\\(1-e)(1+f)\end{Bmatrix} \qquad (A.14)$$

where, e and f are the normalized or natural coordinates for the elements.

Outline of the solution procedure:

While dealing with steady-state problems, NACHOS II uses an algorithm that alternately solves equations (A.12) while continually updating the variable coefficient matrices to reflect the most recently computed values for the dependent variables. The alternating procedure used by this algorithm works as follows:

Initially, the energy equation is advanced first using

$$[D(u^n)]T^{n+1} + [L(T^n)]T^{n+1} = G(T^n) \qquad (A.15a)$$

Then, the momentum equation is advanced using

$$[C(u^n)]V^{n+1} + [k(T^{n+1})]V^{n+1} = F(T^{n+1}) \qquad (A.15b)$$

Thus, the solution algorithm keeps alternating between the energy and momentum equations, using updated values of temperature and velocity, as follows:

$$[D(u^{n+1})]T^{n+2} + [L(T^{n+1})]T^{n+2} = G(T^{n+1})$$

$$\cdot \quad \cdot \quad \cdot \qquad (A.16)$$

$$\cdot \quad \cdot \quad \cdot$$

. . .

etc.

where the superscript n represents the number of iterations. The above basic iteration scheme can be accelerated by suitable choice of an interpolation procedure for the dependent variables used to evaluate the coefficient matrices. As an example, the [k] or [L] matrices can be evaluated at $T^{*(n+1)}$ using

$$T^{*(n+1)} = \alpha T^{(n+1)} + (1-\alpha)T^{n} \qquad (0<\alpha<1) \qquad (A.17)$$

For the above interpolation procedure, NACHOS II uses $\alpha=1/2$ for the temperature field whereas no interpolation is used for the velocity field.

APPENDIX B

MATHEMATICAL DEFINITION OF NUSSELT NUMBER

APPENDIX B

Mathematical Definition of Nusselt Number

The local Nusselt number Nu_y for an obstructed channel can be defined by

$$Nu_y = h_{f,y}b/k \qquad (B.1)$$

where,

b = channel width,

k = thermal conductivity of the fluid,

$h_{f,y}$ = local heat transfer coefficient, and is given by

$$h_{f,y} = \frac{q_y''}{\Delta T} \qquad (B.2)$$

where,

q_y'' = local heat flux at a point on the obstructed wall,

$\Delta T = T_w - T_\infty$,

In the present study, the average quantity $\overline{m}$ of any local quantity m_s is defined as

$$\overline{m} = \frac{1}{\Delta s}\int_{s}^{s+\Delta s} m_s ds \qquad (B.3)$$

By definition, the average Nusselt number, Nu is given by

$$Nu = h_f b/k \qquad (B.4)$$

where,

h_f = average heat transfer coefficient.

Then,

$$h_f = Q/(A\Delta T) \qquad (B.5)$$

where,

Q = total heat transfer from the channel walls to the fluid,

A = total wetted area of the channel.

$$Q = Q_1+Q_2 \qquad (B.6)$$

$$A = A_1+A_2 \qquad (B.7)$$

Here, the subscripts 1 and 2 refer to the left obstructed wall and the right obstructed wall, respectively.

From Newton's law of cooling,

$$Q_1 = h_{f,1}A_1\Delta T \qquad (B.8)$$

$$Q_2 = h_{f,2}A_2\Delta T \qquad (B.9)$$

where, the average quantities $h_{f,1}$, $h_{f,2}$ are defined by equation (B.3).

Considering unit depth of the channel walls into the plane of the paper,

$$A_1 = L_1 \qquad (B.10)$$

$$A_2 = L_2 \qquad (B.11)$$

where, L = length of the obstructed wall.

Now, substituting the equations (B.6) through (B.11) in the equation (B.5),

$$h_f = \frac{h_{f,1}A_1\Delta T+h_{f,2}A_2\Delta T}{(A_1+A_2)\Delta T}$$

or,

$$h_f = \frac{h_{f,1}L_1+h_{f,2}L_2}{L_1+L_2} \qquad (B.12)$$

Substituting this h_f into equation (B.4), we obtain

$$Nu = \left(\frac{h_{f,1}L_1+h_{f,2}L_2}{L_1+L_2}\right)\frac{b}{k} \qquad \text{(B.13)}$$

APPENDIX C

CHANEL.FOR: CODE TO CALCULATE THE AVERAGE NUSSELT NUMBER OF THE SMOOTH CHANNEL

Figure 56:

```
C*************************************************************
      PROGRAM CHANEL
C*************************************************************
C          THIS PROGRAM IS TO CALCULATE THE AVERAGE NUSELT
C     NUMBER FOR ISOTHERMAL WALLS OF THE VERTICAL CHANNEL AND
C     ALSO TO CALCULATE THE AVERAGE NUSSELT NUMBER ACROSS THE
C     CHANNEL USING THE SIMPSON'S RULE.  EXTREME BOTTOM AND TOP
C     VALUES OF THE LOCAL FILM COEFFICIENTS ARE EXTRAPOLATED
C     USING LAGRANGES INTERPOLATION METHOD AS NACHOS DOES NOT
C     CALCULATE THE LOCAL HEAT FLUX VALUES AT THOSE POINTS.
C     THIS PROGRAM SHOULD BE USED WHEN THE ELEMENTS IN THE
C     NACHOS CODE ARE NUMBERED FROM BOTTOM TOWARD TOP. THAT IS
C     THE LEFT BOTTOM MOST ELEMENT IS ELEMENT NUMBER ONE AND AS
C     IT GOES VERTICALLY UP THE ELEMENT NUMBER INCREASES.
C
C*************************************************************
C                      T H E    F I L E S    U S E D    A R E :
C*************************************************************
C      'HTFLUXC.DAT' : HEAT FLUX DATA FILE FOR THE COLD WALL
C      'HTFLUXH.DAT' : HEAT FLUX DATA FILE FOR THE HOT WALL
C      'CORDN.DAT' : COORDINATE DATA FILE
C      'CHANEL.OUT' : CALCULATED NUSSELT NUMBERS
C      'CHANEL.DAT' : INPUT DATA FILE
C
C*************************************************************
C           THE  PARAMETERS  USED  ARE  THE  FOLLOWING:
C-------------------------------------------------------------
C     NELMT : TOTAL NUMBER OF ELEMENTS
C     NELMC : NUMBER OF ELEMENTS ON THE HORIZONTAL WALL (COLD
C     WALL)
C     NELMH : NUMBER OF ELEMENTS ON THE HOT HORIZONTAL WALL
C     NELM : ARRAY OF ELEMENTS NUMBERS FOR WHICH HEAT FLUX WAS
C     CALCULATED
C     QC : LOCAL HEAT FLUX ALONG THE ENCLOSURE WALL
C     S : MULTIPLIER TO CALCULATE THE LOCAL FILM COEFFICIENT
C     XNU : LOCAL NUSSELT NUMBER
C     XH: LOCAL FILM COEFFICIENT
C     SNUC : AVERAGE FILM COEFFICIENT ALONG A WALL
C    SSNUC: STORED AVERAGE FILM COEFFICIENT FOR THE RIGHT WALL
C     XL : LENGTH SCALE
C     XK : THERMAL CONDUCTIVITY OF THE FLUID
C     IDEG : DEGREE OF PLYNOMIAL FOR LAGRANGES INTERPOLATION
C
      DIMENSION NELM(900),Y(900),QC(900),XNU(900),XH(900)
```

```
      DIMENSION TY(900),TQC(900)
C^^^
```

```
                    READ(8,520)NELM(I)
                    READ(8,521)TQC(K),TQC(KK)
                    QC1=TQC(K)
                    QC2=TQC(KK)
                    TQC(K)=QC2
                    TQC(KK)=QC1
                510   CONTINUE
C#################################################################
     520   FORMAT(/////22X,I3)
     521   FORMAT(//100X,2E15.7)
           NP=NPH
           NTP=NTPH
           NNELM=NELMH
     502   CONTINUE
C*****************************************************************
           DO 509 I=1,NP
           QC(I)=TQC(I)
     509   CONTINUE
C*****************************************************************
           WRITE (22,301)(NELM(I),I=1,NNELM)
           WRITE (22,300)(QC(I),I=1,NP)
     301   FORMAT(1X,6I5/)
     300   FORMAT(1X,4E18.7/)
C*****************************************************************
C          READING THE VALUE OF THE CORDINATES OF THE POINTS OF
C    HEAT FLUXES
C*****************************************************************
      CALL YVALUE(NELMT,NELM,TY,NP,Y,NIT,NNELM,YL,YYH)
C@@@@@@@@@@@@@@@@@@@@@@@@@@@@@@@@@@@@@@@@@@@@@@@@@@@@@@@@@@@@@@@@@@@
C     RENUMBER THE POINTS
C@@@@@@@@@@@@@@@@@@@@@@@@@@@@@@@@@@@@@@@@@@@@@@@@@@@@@@@@@@@@@@@@@@@
           DO 700 I=1,NP
           TY(I+1)=Y(I)
           TQC(I+1)=QC(I)
     700   CONTINUE
               Y(1)=YL
               Y(NTP)=YYH
           DO 701 I=2,NTP-1
           Y(I)=TY(I)
           QC(I)=TQC(I)
     701   CONTINUE
C-----------------------------------------------------------------
C          EXTRAPLOLATE THE VALUES OF THE HEAT FLUXES FOR THE
C    FIRST AND LAST POINTS USING LAGRANGIAN METHOD
C-----------------------------------------------------------------
      MIN=2
      XARG=Y(1)
      CALL FLAGR(MIN,XARG,IDEG,Y,QC,RSLT)
      QC(1)=RSLT
      MIN=NP+1-IDEG
      XARG=Y(NTP)
      CALL FLAGR(MIN,XARG,IDEG,Y,QC,RSLT)
```

```
      QC(NTP)=RSLT
C*************************************************************
C                  NONDIMENSIONALIZE   THE   Y   COORDINATES
C*************************************************************
          DO 303 I=1,NTP
          Y(I)=Y(I)/XL
     303   CONTINUE
C*************************************************************
C     CALCULATING THE LOCAL FILM COEFFICIENT
C*************************************************************
               DO 30 I=1,NTP
               XH(I)=QC(I)*S
               XNU(I)=XH(I)*CONST
          30    CONTINUE
C^^^^^^^^^^^^^^^^^^^^^^^^^^^^^^^^^^^^^^^^^^^^^^^^^^^^^^^^^^^^^^^^^
C          CALCULATING THE AVERAGE FILM COEFFICIENT USING THE
C    SIMPON'S RULE (ALL POINTS EXCEPT THE LAST POINT)
C^^^^^^^^^^^^^^^^^^^^^^^^^^^^^^^^^^^^^^^^^^^^^^^^^^^^^^^^^^^^^^^^^
      SNUC=0.0
      NNP=NTP-3
      DO 40 I=1,NNP,2
      A=(Y(I)-Y(I+1))*(Y(I)-Y(I+2))
      B=(Y(I+1)-Y(I))*(Y(I+1)-Y(I+2))
      C=(Y(I+2)-Y(I))*(Y(I+2)-Y(I+1))
      A1=(XH(I))/A
      B1=(XH(I+1))/B
      C1=(XH(I+2))/C
      AA=A1+B1+C1

BB=-Y(I+2)*A1-Y(I+1)*A1-Y(I+2)*B1-Y(I)*B1-Y(I+1)*C1-Y(I)*C1
      CC=Y(I+1)*Y(I+2)*A1+Y(I)*Y(I+2)*B1+Y(I)*Y(I+1)*C1
      SNUC=SNUC+(AA*(Y(I+2)**3-Y(I)**3))/3.0+0.5*BB*(Y(I+2)**2
     ?     -Y(I)**2)+CC*(Y(I+2)-Y(I))
40    CONTINUE
C*************************************************************
C     CALCULATING THE LAST POINT USING TRAPEZOIDAL RULE
C*************************************************************
      SNUC=SNUC+(XH(NTP)+XH(NTP-1))*(Y(NTP)-Y(NTP-1))*0.5
C%%%%%%%%%%%%%%%%%%%%%%%%%%%%%%%%%%%%%%%%%%%%%%%%%%%%%%%%%%%%%%%%%
C     WRITING THE RESULTS
C%%%%%%%%%%%%%%%%%%%%%%%%%%%%%%%%%%%%%%%%%%%%%%%%%%%%%%%%%%%%%%%%%
       WRITE(22,50)
       WRITE(22,60)(Y(I),XH(I),XNU(I),I=1,NTP)
          IF(NIT.EQ.0) THEN
          WRITE(22,70)SNUC
          WRITE(6,80)SNUC
          ELSE
          WRITE(22,71)SNUC
          WRITE(6,81)SNUC
          END IF
          50     FORMAT(5X,'NONDIMENSIONAL Y',6X,'LOCAL FILM
     COEFFICIENT',4X, 'LOCAL NUSSELT NUMBER')
```

```
60     FORMAT(5X,F9.6,11X,E18.7,5X,F15.6)
70     FORMAT(2X,'AVG H ON THE RIGHT COLD  WALL=',E18.7)
71     FORMAT(2X,'AVG H ON THE LEFT HOT WALL=',E18.7)
80         FORMAT(/2X,'*******  AVG  H  ON  THE  RIGHT  COLD
          WALL=',E18.7,1' *******'/)
81     FORMAT(/2X,'******* AVG H ON LEFT HOT WALL=',E18.7,1'
      *******'/)
       IF(NDE.EQ.1) THEN
       IF(NIT.EQ.0)GO TO 500
       ANU=(SNUC*XL1+SSNUC*XL2)*CONST/SUMOFL
       WRITE(6,75)ANU
       WRITE(22,77)ANU
77     FORMAT(2X,'AVG OF HOT AND COLD WALL NU NO=',F15.6)
75       FORMAT(/2X,'*******  AVG  OF  HOT  AND  COLD  WALL  NU
      NO=',F15.6,1' *******'/)
       END IF
       CLOSE(UNIT=5,STATUS='KEEP')
       CLOSE(UNIT=8,STATUS='KEEP')
       CLOSE(UNIT=9,STATUS='KEEP')
       CLOSE(UNIT=10,STATUS='KEEP')
       CLOSE(UNIT=22,STATUS='KEEP')
       STOP
       END
C*************************************************************
C          SUBROUTINE TO READ/CALCULATE THE COORDINATES OF THE
C     POINTS OF HEAT FLUX
C*************************************************************
       SUBROUTINE YVALUE(NELMT,NELM,TY,NP,Y,NIT,NNELM,YL,YYH)
       DIMENSION NELM(900),TY(900),Y(900),YY(3000),DH(900)
       OPEN(UNIT=7,FILE='CORDN.DAT',STATUS='OLD')
       MX=0
       M1=0
       M=0
       MM=1
       LL=0
       LL1=0
       KT=0
C*************************************************************
       DO 400 I=1,NELMT
       L1=LL1+1
       LL1=L1+1
       M1=M1+1
       MX=MX+1
       IF(MX.EQ.11) GO TO 415
       IF(M1.EQ.12) GO TO 415
       READ(7,422)YY(L1),YY(LL1)
       GO TO 425
415    M1=1
       READ(7,423)YY(L1),YY(LL1)
425    IF(I.EQ.NELM(MM)) GO TO 410
       GO TO 400
410    L=LL+1
```

```
      LL=L+1
      KT=KT+1
      TY(L)=YY(L1)
      TY(LL)=YY(LL1)
        IF(KT.EQ.1) THEN
        YL=TY(L)
        END IF
        IF(KT.EQ.NNELM) THEN
        YYH=TY(LL)
        END IF
      M=M+1
      DH(M)=(TY(L)-TY(LL))/4.0
      TY(L)=TY(L)-DH(M)
      TY(LL)=TY(L)-DH(M)*2.0
      MM=MM+1
400   CONTINUE
422   FORMAT(////24X,F9.3,51X,F9.3)
423   FORMAT(/////////24X,F9.3,51X,F9.3)
      KTY=0
      DO 600 I=1,NP
      Y(I)=TY(I)
600   CONTINUE
      CLOSE(UNIT=7,STATUS='KEEP')
      RETURN
      END
C*****************************************************************
C          SUBROUTINE TO EXTRAPOLATE THE VALUES OF THE FIRST
C     AND LAST POINT FOR THE EXPLANATION OF THE VARIABLES USED
C     IN THIS SUBROUTINE SEE "APPLIED NUMERICAL METHODS",1969,
C     BY B. CARNAHAN, H.A. LUTHER, J.O.WILKES, PAGES-30,31,32.
C*****************************************************************
      SUBROUTINE FLAGR(MIN,XARG,IDEG,Y,QC,RSLT)
C*****************************************************************
      DIMENSION Y(900),QC(900)
      FACTOR=1.0
      MAX=MIN+IDEG
C*****************************************************************
          DO 21 J=MIN,MAX
          IF(XARG.NE.Y(J)) GO TO 21
          RSLT=QC(J)
          RETURN
     21    FACTOR=FACTOR*(XARG-Y(J))
C
      YEST=0.0
      DO 51 I=MIN,MAX
      TERM=QC(I)*FACTOR/(XARG-Y(I))
          DO 41 J=MIN,MAX
     41    IF(I.NE.J) TERM=TERM/(Y(I)-Y(J))
     51    YEST=YEST+TERM
          IF(YEST.LT.0.) THEN
          RSLT=0.0
           ELSE
```

```
RSLT=YEST
END IF
RETURN
END
```

APPENDIX D

OBSNU.FOR: CODE TO CALCULATE THE AVERAGE NUSSELT NUMBER OF THE OBSTRUCTED CHANNEL

Figure 57:

```
C*************************************************************
      PROGRAM OBSNU
C*************************************************************
C          THIS PROGRAM IS TO CALCULATE THE AVERAGE NUSELT
C     NUMBER FOR ISOTHERMAL WALLS OF THE VERTICAL CHANNEL WITH
C     OBSTRUCTIONS AND ALSO TO CALCULATE THE AVERAGE NUSSELT
C     NUMBER ACROSS THE CHANNEL USING THE SIMPSON'S RULE.
C     EXTREME BOTTOM AND TOP VALUES OF THE LOCAL FILM
C     COEFFICIENTS ARE EXTRAPOLATED USING LAGRANGES
C     INTERPOLATION METHOD AS NACHOS DOES NOT CALCULATE THE
C     LOCAL HEAT FLUX VALUES AT THOSE POINTS.  THIS PROGRAM
C     SHOULD BE USED WHEN THE ELEMENTS IN THE NACHOS CODE
C     CODE ARE NUMBERED FROM TOP TOWARD BOTTOM. THAT IS THE
C     LEFT TOP MOST ELEMENT IS ELEMENT NUMBER ONE AND AS IT
C     GOES HORIZONTALLY RIGHT THE ELEMENT NUMBER INCREASES.
C*************************************************************
C                      THE    FILES    USED    ARE:
C*************************************************************
C      'OBSHFR.DAT' : HEAT FLUX DATA FILE FOR THE COLD WALL
C      'OBSHFL.DAT' : HEAT FLUX DATA FILE FOR THE HOT WALL
C      'COORDN.DAT' : COORDINATE DATA FILE
C      'OBSNU.OUT' : CALCULATED NUSSELT NUMBERS
C      'OBSNU.DAT' : INPUT DATA FILE
C
C*************************************************************
C            PARAMETERS  &  VARIABLES  USED  ARE:
C-------------------------------------------------------------
C      NELMT : TOTAL NUMBER OF ELEMENTS
C      NELMC : NUMBER OF ELEMENTS ON THE RIGHT VERTICAL WALL
C      NELMH : NUMBER OF ELEMENTS ON THE LEFT VETICAL WALL
C     NELM : ARRAY OF ELEMENTS NUMBERS FOR WHICH HET FLUX WAS
C      CALCULATED
C      QC : LOCAL HEAT FLUX ALONG THE ENCLOSURE WALL
C      S : MULTIPLIER TO CALCULATE THE LOCAL FILM COEFFICIENT
C      XNU : LOCAL NUSSELT NUMBER
C      XH: LOCAL FILM COEFFICIENT
C      SNUC : AVERAGE FILM COEFFICIENT ALONG A WALL
C       SSNUC: STORED AVERAGE FILM COEFFICIENT FOR THE RIGHT
C      WALL
C      XL : LENGTH SCALE
C      XK : THERMAL CONDUCTIVITY OF THE FLUID
C      IDEG : DEGREE OF PLYNOMIAL FOR LAGRANGES INTERPOLATION
C*************************************************************
C     DIMENSION STATEMENTS FOLLOW:
```

```
C*************************************************************
      DIMENSION NELM(900),Y(900),QC(900),XNU(900),XH(900)
      DIMENSION TY(900),TQC(900)
      DIMENSION TEMPC(900),TEMPH(900),TELM(450)
C*************************************************************
C     OPEN STATEMENTS
C*************************************************************
      OPEN(UNIT=5,FILE='OBSHFR.DAT',STATUS='OLD')
      OPEN(UNIT=8,FILE='OBSHFL.DAT',STATUS='OLD')
      OPEN(UNIT=10,FILE='OBSNU.DAT',STATUS='UNKNOWN')
      OPEN(UNIT=22,FILE='OBSNU.OUT',STATUS='NEW')
      OPEN(UNIT=23,FILE='RW.DAT',STATUS='OLD')
      OPEN(UNIT=24,FILE='LW.DAT',STATUS='OLD')
C*************************************************************
      READ(10,*)NDE,NELMT,NELMC,XL,XK,XL1,XL2,XB,DELT,IDEG,
     +NRC1,NRC2,NRC3,NRC5,NLH1,NLH2,NLH3,NLH5
          IF(NDE.EQ.1)THEN
          READ(10,*)NELMH
          END IF
          NRC4=NRC2
          NLH4=NLH2
          S = 1.0/DELT
          CONST = XB/XK
          SUMOFL = (XL1+XL2)
          NPH=(NELMH+2)*2
          NPC=(NELMC+2)*2
          NTPH=NPH+2
          NTPC=NPC+2
          KK=0
          NIT=0
C*************************************************************
C     READING THE VALUES OF HEAT FLUX ON THE RIGHT WALL
C*************************************************************
      DO 110 I=1,NRC1
      K=KK+1
      KK=K+1
      READ(5,1001)NELM(I)
      READ(5,1002)TQC(K),TQC(KK)
      QC1=ABS(TQC(K))
      QC2=ABS(TQC(KK))
      TQC(K)=QC2
      TQC(KK)=QC1
110   CONTINUE
           NR1=NRC1+1
           NR2=NRC1+NRC2
           DO 111 I=NR1,NR2
          K=KK+1
          KK=K+1
          READ(5,1003)NELM(I)
          READ(5,1004)TQC(K),TQC(KK)
      QC1=TQC(K)
      QC2=TQC(KK)
```

```
      TQC(K)=QC2
      TQC(KK)=QC1
111   CONTINUE
          NR3=NR2+1
          NR4=NR2+NRC3
               DO 121 I=NR3,NR4
                         K=KK+1
                         KK=K+1
               READ(5,1001)NELM(I)
               READ(5,1002)TQC(K),TQC(KK)
                    QC1=ABS(TQC(K))
                    QC2=ABS(TQC(KK))
                    TQC(K)=QC2
                    TQC(KK)=QC1
          121   CONTINUE
                         NR5=NR4+1
                         NR6=NR4+NRC4
                         DO 131 I=NR5,NR6
                         K=KK+1
                         KK=K+1
                    READ(5,1003)NELM(I)
                    READ(5,1008)TQC(K),TQC(KK)
                    QC1=ABS(TQC(K))
                    QC2=ABS(TQC(KK))
                    TQC(K)=QC2
                    TQC(KK)=QC1
               131   CONTINUE
          NR7=NR6+1
          NR8=NR6+NRC5
          DO 141 I=NR7,NR8
          K=KK+1
          KK=K+1
          READ(5,1001)NELM(I)
          READ(5,1002)TQC(K),TQC(KK)
          QC1=ABS(TQC(K))
          QC2=ABS(TQC(KK))
          TQC(K)=QC2
          TQC(KK)=QC1
      141  CONTINUE
          DO 166 L=1,NPC
          TEMPC(L)=TQC(L)
      166  CONTINUE
          JJ=0
               DO 188 LL=1,NPC
               TQC(LL)=TEMPC(NPC-JJ)
               JJ=JJ+1
          188   CONTINUE
                    DO 1 I=1,NELMC+2
                         TELM(I)=NELM(I)
               1     CONTINUE
          II=0
          DO 2 I=1,NELMC+2
```

```
          NELM(I)=TELM(NELMC+2-II)
          II=II+1
     2     CONTINUE
C*****************************************************************
C     FORMAT STATEMENTS
C*****************************************************************
     1001  FORMAT(/////22X,I3)
     1002  FORMAT(//40X,2E15.7)
     1003  FORMAT(////22X,I3)
     1004  FORMAT(///11X,2E15.7)
     1008  FORMAT(///70X,2E15.7)
C*****************************************************************
          NP=NPC
          NTP=NTPC
          NNELM=NELMC
          GO TO 502
C*****************************************************************
C      READING THE VALUES ON THE LEFT WALL
C*****************************************************************
******************
     500   NIT=NIT+1
          SSNUC=SNUC
          KK=0
      DO 511 I=1,NELMC+2
          NELM(I)=0
     511   CONTINUE
          DO 510 I=1,NLH1
               K=KK+1
               KK=K+1
          READ(8,1011)NELM(I)
          READ(8,1012)TQC(K),TQC(KK)
          TQC(K)=ABS(TQC(K))
          TQC(KK)=ABS(TQC(KK))
     510   CONTINUE
          NL1=NLH1+1
          NL2=NLH1+NLH2
          DO 512 I=NL1,NL2
          K=KK+1
          KK=K+1
      READ(8,1013)NELM(I)
      READ(8,1014)TQC(K),TQC(KK)
     512   CONTINUE
      NL3=NL2+1
      NL4=NL2+NLH3
          DO 513 I=NL3,NL4
          K=KK+1
          KK=K+1
          READ(8,1011)NELM(I)
          READ(8,1012)TQC(K),TQC(KK)
          TQC(K)=ABS(TQC(K))
          TQC(KK)=ABS(TQC(KK))
     513   CONTINUE
```

```
                    NL5=NL4+1
                    NL6=NL4+NLH4
                  DO 514 I=NL5,NL6
                         K=KK+1
                         KK=K+1
                  READ(8,1013)NELM(I)
                  READ(8,1018)TQC(K),TQC(KK)
                    TQC(K)=ABS(TQC(K))
                    TQC(KK)=ABS(TQC(KK))
                  514   CONTINUE
                    NL7=NL6+1
                    NL8=NL6+NLH5
          DO 515 I=NL7,NL8
                    K=KK+1
                    KK=K+1
          READ(8,1011)NELM(I)
          READ(8,1012)TQC(K),TQC(KK)
          TQC(K)=ABS(TQC(K))
          TQC(KK)=ABS(TQC(KK))
      515  CONTINUE
          DO 198 LA=1,NPH
          TEMPH(LA)=TQC(LA)
      198  CONTINUE
              LB=0
          DO 208 LC=1,NPH
          TQC(LC)=TEMPH(NPH-LB)
          LB=LB+1
      208  CONTINUE
          DO 3 I=1,NELMH+2
          TELM(I)=NELM(I)
      3    CONTINUE
          II=0
       DO 4 I=1,NELMH+2
          NELM(I)=TELM(NELMH+2-II)
          II=II+1
      4    CONTINUE
          WRITE(*,*)(NELM(I),I=1,NELMH+2)
C*************************************************************
C     FORMAT STATEMENTS
C*************************************************************
      1011  FORMAT(/////22X,I3)
      1012  FORMAT(//100X,2E15.7)
      1013  FORMAT(////22X,I3)
      1014  FORMAT(///12X,2E15.7)
      1018  FORMAT(///70X,2E15.7)
C^^^^^^^^^^^^^^^^^^^^^^^^^^^^^^^^^^^^^^^^^^^^^^^^^^^^^^^^^^^^^^^^
          NP=NPH
          NTP=NTPH
          NNELM=NELMH
      502  CONTINUE
          DO 509 I=1,NP
          QC(I)=TQC(I)
```

```
      509    CONTINUE
             WRITE (22,301)(NELM(I),I=1,NNELM+2)
             WRITE (22,300)(QC(I),I=1,NP)
      301    FORMAT(1X,6I5/)
      300    FORMAT(1X,4E18.7/)
C*************************************************************
C          READING THE VALUE OF THE CORDINATES OF THE POINTS OF
C     HEAT FLUXES
C*************************************************************
C       CALL YVALUE(NELMT,NELM,TY,NP,Y,NIT,NNELM,YL,YYH)
      IF(NIT.EQ.0)THEN
             READ(23,*)(Y(I),I=1,NTP)
      ELSEIF(NIT.EQ.1)THEN
             READ(24,*)(Y(I),I=1,NTP)
      ENDIF
C*************************************************************
C      RENUMBER THE POINTS
C*************************************************************
             DO 700 I=1,NP
             TQC(I+1)=QC(I)
      700    CONTINUE
             DO 701 I=2,NTP-1
             QC(I)=TQC(I)
      701    CONTINUE
C*************************************************************
C      EXTRAPLOLATE THE VALUES OF THE HEAT FLUXES FOR THE FIRST
C     AND LAST POINTS USING LAGRANGIAN METHOD
C*************************************************************
       MIN=2
       XARG=Y(1)
       CALL FLAGR(MIN,XARG,IDEG,Y,QC,RSLT)
       QC(1)=RSLT
       MIN=NP+1-IDEG
       XARG=Y(NTP)
       CALL FLAGR(MIN,XARG,IDEG,Y,QC,RSLT)
       QC(NTP)=RSLT
   ^^^^^^^^^^^^^^^^^^^^^^^^^^^^^^^^^^^^^^^^^^^^^^^^^^^^^^^^^^^^^
C
C                    NONDIMENSIONALIZE    THE    Y-COORDINATES
C*************************************************************
             DO 303 I=1,NTP
             Y(I)=Y(I)/XL
      303    CONTINUE
C*************************************************************
C      CALCULATING THE LOCAL FILM COEFFICIENT
C*************************************************************
             DO 30 I=1,NTP
             XH(I)=QC(I)*S
             XNU(I)=XH(I)*CONST
      30     CONTINUE
C-------------------------------------------------------------
C          CALCULATING THE AVERAGE FILM COEFFICIENT USING THE
C     SIMPON'S RULE (ALL POINTS EXCEPT THE LAST POINT)
```

```
C-------------------------------------------------------------
      SNUC=0.0
      NNP=NTP-3
      DO 40 I=1,NNP,2
      A=(Y(I)-Y(I+1))*(Y(I)-Y(I+2))
      B=(Y(I+1)-Y(I))*(Y(I+1)-Y(I+2))
      C=(Y(I+2)-Y(I))*(Y(I+2)-Y(I+1))
      A1=(XH(I))/A
      B1=(XH(I+1))/B
      C1=(XH(I+2))/C
      AA=A1+B1+C1

BB=-Y(I+2)*A1-Y(I+1)*A1-Y(I+2)*B1-Y(I)*B1-Y(I+1)*C1-Y(I)*C1
      CC=Y(I+1)*Y(I+2)*A1+Y(I)*Y(I+2)*B1+Y(I)*Y(I+1)*C1
      SNUC=SNUC+(AA*(Y(I+2)**3-Y(I)**3))/3.0+0.5*BB*(Y(I+2)**2
     ?     -Y(I)**2)+CC*(Y(I+2)-Y(I))
     40    CONTINUE
C-------------------------------------------------------------
C     CALCULATING THE LAST POINT USING TRAPEZOIDAL RULE
C-------------------------------------------------------------
      SNUC=SNUC+(XH(NTP)+XH(NTP-1))*(Y(NTP)-Y(NTP-1))*0.5
C-------------------------------------------------------------
C     WRITING THE RESULTS
C*************************************************************
       WRITE(22,50)
       WRITE(22,60)(Y(I),XH(I),XNU(I),I=1,NTP)
       IF(NIT.EQ.0) THEN
        WRITE(22,70)SNUC
        WRITE(6,80)SNUC
       ELSE
         WRITE(22,71)SNUC
         WRITE(6,81)SNUC
       END IF
C-------------------------------------------------------------
C     FORMAT STATEMENTS
C-------------------------------------------------------------
     50         FORMAT(5X,'NONDIMENSIONAL  Y',6X,'LOCAL  FILM
          COEFFICIENT',4X,LOCAL NUSSELT NUMBER')
     60     FORMAT(5X,F9.6,11X,E18.7,5X,F15.6)
     70     FORMAT(2X,'AVG H ON THE RIGHT COLD  WALL=',E18.7)
     71     FORMAT(2X,'AVG H ON THE LEFT HOT WALL=',E18.7)
     80       FORMAT(/2X,'*******  AVG  H  ON  THE  RIGHT  COLD
          WALL=',E18.7,1' *******'/)
81    FORMAT(/2X,'******* AVG H ON LEFT HOT WALL=',E18.7,
          1' *******'/)
          IF(NDE.EQ.1) THEN
          IF(NIT.EQ.0)GO TO 500
          ANU=(SNUC*XL1+SSNUC*XL2)*CONST/SUMOFL
          WRITE(6,75)ANU
          WRITE(22,77)ANU
     77    FORMAT(2X,'AVG OF HOT AND COLD WALL NU NO=',F15.6)
     75     FORMAT(/2X,'******* AVG OF HOT AND COLD WALL NU
```

```
                NO=',F15.6,1' *******'/)
            END IF
          CLOSE(UNIT=5,STATUS='KEEP')
          CLOSE(UNIT=8,STATUS='KEEP')
          CLOSE(UNIT=9,STATUS='KEEP')
          CLOSE(UNIT=10,STATUS='KEEP')
          CLOSE(UNIT=22,STATUS='KEEP')
          CLOSE(UNIT=23,STATUS='KEEP')
          CLOSE(UNIT=24,STATUS='KEEP')
          STOP
          END
C
C-------------------------------------------------------------
C          SUBROUTINE TO EXTRAPOLATE THE VALUES OF THE FIRST
C     AND CLAST POINT FOR THE EXPLANATION OF THE VARIABLES USED
C     IN THIS SUBROUTINE SEE "APPLIED NUMERICAL METHODS",1969,
C     BY B. CARNAHAN, H.A. LUTHER, J.O.WILKES, PAGES-30,31,32.
C-------------------------------------------------------------
          SUBROUTINE FLAGR(MIN,XARG,IDEG,Y,QC,RSLT)
          DIMENSION Y(900),QC(900)
          FACTOR=1.0
          MAX=MIN+IDEG
          DO 21 J=MIN,MAX
          IF(XARG.NE.Y(J)) GO TO 21
          RSLT=QC(J)
          RETURN
21        FACTOR=FACTOR*(XARG-Y(J))
          YEST=0.0
          DO 51 I=MIN,MAX
          TERM=QC(I)*FACTOR/(XARG-Y(I))
          DO 41 J=MIN,MAX
41        IF(I.NE.J) TERM=TERM/(Y(I)-Y(J))
51        YEST=YEST+TERM
          IF(YEST.LT.0.) THEN
          RSLT=0.0
          ELSE
          RSLT=YEST
          END IF
          RETURN
          END
```

MONTANA STATE UNIVERSITY LIBRARIES
3 1762 10064726 0